



**Optimization of spatial balancing and storage needs  
for large-scale power system integration of fluctuating  
solar energy**

Von der Fakultät für Mathematik und Naturwissenschaften  
der Carl von Ossietzky Universität Oldenburg zur Erlangung des  
Grades und Titels

*eines Doktors der Naturwissenschaften (Dr. rer. nat.)*

angenommene Dissertation  
von **Frau Kabitri Chattopadhyay**  
geboren am 08.05.1985 in Kolkata

Gutachter: Prof. Dr. Jürgen Parisi

Weitere Gutachterin/Gutachter: Prof. Dr. Hans-Georg Beyer, Prof. Dr. Ulrike Freudel

Tag der Disputation: 11 July, 2017

## Erklärung

Hiermit erkläre ich, dass ich die vorliegende Dissertation selbstständig verfasst und nur die angegebenen Hilfsmittel benutzt habe. Die Dissertation hat weder in ihrer Gesamtheit noch in Teilen einer anderen Hochschule zur Begutachtung in einem Promotionsverfahren vorgelegen.

Kabitri Chattopadhyay



## Acknowledgements

This thesis has become a reality with the kind support of many individuals. I would like to extend my sincere thanks to all of them.

First of all, I would like to thank all the experts in my PhD committee, Prof. Dr. Jürgen Parisi, Prof. Dr. Hans-Georg Beyer, Prof. Dr. Ulrike Feudel, and Dr. Detlev Heinemann for making this dissertation possible and the three anonymous referees of my paper whose inputs have enhanced the quality of my work in several ways. Additionally, a credit is due to the people who made my PhD studies possible with their financial support: Federal Ministry of Education and Research (BMBF). Without them this work could not have been conducted.

My sincere gratitude to my advisor Dr. Detlev Heinemann for giving me the opportunity to work with him, for his unique vision, guidance, and advice during the thesis, and his continuous support during the past four years. I am eternally grateful to Dr. Elke Lorenz, for introducing me to the topic of the renewable energy, her immense patience, motivation, and enthusiasm.

My sincere thanks also goes to Dr. Lüder von Bremen for many stimulating discussions during our project meetings. It was his invaluable insights on the challenges of grid stability with increasing renewable shares that I first got interested in the subject. I would like to extend my gratitude to all our project partners from Next Energy and Wuppertal Institute, not only for those intriguing and extensive discussions, but also for maintaining a fine balance of professional and friendly atmosphere. In this aspect, a special thanks goes to Alexander Kies, for helping me with the algorithm development and model implementation.

I am also grateful to Dr. Jan Kühnert for providing me with the TSO data set and the related scripts. A special thanks goes to Dr. Francisco J. Santos-Alamillos for sharing very useful model code and information on CSP modeling. Also, I would like to mention Dr. Jens Tambke for giving me the opportunity to perform a thorough evaluation of German PV power.

My heartfelt of gratitude to all the current and past members of the solar group of the energy meteorology department of Oldenburg University that I had the opportunity

to work with. They have given me excellent input on diverse fields and constant support. I would like to specially mention Dr. Annette Hammer and Dr. Ontje Lünsdorf for patiently going through my thesis and giving their valuable opinion on the work. The abstract of this thesis is translated to German by Elena Barykina, and later modified by Dr. Annette Hammer, so my sincere thanks to both of them. Also a special thanks to Björn Wolff, for being an excellent office mate and for helping me out so many times whenever I had any trouble, particularly with the local language!

In addition, I would like to thank my tutors from the graduate school, specially Dr. Frank Lauterbach, for many excellent courses and for guiding me in the right direction so that I can successfully complete my dissertation. These courses have not only helped me to improve myself not only in academic excellence, but also on a personal level. A special thanks to Dr. Robin Knecht for giving me the opportunity to tutor the masters students from PPRE. It has been an amazing experience for me.

My sincere thanks to many personalities from the university's administration, who have always been extremely helpful and thoroughly welcoming to me: Elzbieta Chojnowski, Grit Schürmann, Oili Irmeli Tsakmakis, Klaudia Hettwer, Katje Kaboth-Larsen, Petra Rölle, Janny de Wall, Vera Rommel, and many more.

Apart from the official aspects, my sincere thanks to my friends in Oldenburg: Özden Demircioglu, Elena Barykina, Juliane Be, Simone Heinke. I have so many wonderful memories with them and I am going to cherish them for the rest of my life.

Finally, I would like to thank all members of my family for their continuous support and enormous faith in me. Thank you. A very special thanks to my mother, Banani Nag, and my forever interested, encouraging and always enthusiastic late grandmother, Bakul Rani Mitra. Thank you so much for all your sacrifices for me. And last but not the least, to my husband, Siddhartha, for I have no words to express my gratitude to you. Thank you for always being there for me.

## Kurzfassung

Die erneuerbaren Energien wie Solarenergie and Windenergie haben in den vergangenen Jahrzehnten eine enorme Bedeutung als Alternative zu den konventionellen fossilen Brennstoffen wie Kohle, Erdöl und Erdgas gewonnen. Diese alternativen Quellen sind sauber, umweltfreundlich und regenerativ. Jedoch sind sie auch sehr wetterabhängig und nicht direkt von Menschen kontrollierbar. Dadurch verursacht die großmaßstäbliche Integration der erneuerbare Energien eine Netzin stabilität, weil das traditionelle Stromnetz für eine vorhersagbare Last und eine abschaltbare Erzeugung ausgelegt ist. In dieser Arbeit werden die Variabilität der erneuerbaren Quellen und deren Einfluss auf den Ausgleichsbedarf für ein zukünftiges europäisches Energiesystem mit hohen Anteilen an Solar- und Windenergie untersucht. Der Schwerpunkt ist die Analyse der Auswirkungen unterschiedlich geneigter und unterschiedlich orientierter PV-Module auf den Ausgleichsbedarf für Europa. Darüber hinaus wird die Modelldomäne nach Nordafrika erweitert, um den Einfluss des konzentrierten Solarstromimports auf den europäischen Speicher- und Backup-Bedarf abzuschätzen. Es wurde gezeigt, dass die beste Wahl der Modulkonfiguration sehr empfindlich von den jeweiligen Solar- und Windanteilen am Strommix abhängt. Falls ein Speicher mit einer Kapazität von mindestens sechs durchschnittlichen Stundenbelastungen zur Verfügung steht, sollten steil aufgestellte Module mit gering ausgeprägten Jahresgängen bevorzugt werden. In einem winddominierten Szenario sind die niedrig geneigten Ost- und Westmodule am besten geeignet um den Ausgleichsbedarf zu reduzieren. Wenn kein Speicher vorhanden ist, reduziert ein Verbund von stark geneigten Ost- und Westmodulen den Ausgleichsbedarf, solange der Solaranteil hoch genug ist, um zwischen verschiedenen Konfigurationen zu unterscheiden. Einige dieser Modulkonfigurationen können in Bezug auf die installierte Kapazität ziemlich teuer sein. Aber der Umbau alter PV-Systeme zu Konfigurationen die für ein bestimmtes Szenario am besten geeignet sind, kann langfristig vorteilhaft sein.





## Abstract

Over the past decades, renewable energy sources like solar and wind have gained enormous importance as alternative to the conventional fossil fuel based resources, such as coal, petroleum, and natural gas. These alternative sources are clean, environmental friendly, and naturally replenished. However, these renewable sources are largely weather-dependent and their output is not directly controllable by human beings. As a result, their large scale integration causes grid instability as the traditional power grid is designed for somewhat predictable load and dispatchable generation. In this thesis, this variable nature of renewable sources and their influence on balancing needs are studied for a future European power system with high shares of solar and wind generation. The main focus here is the analysis of the impact of differently inclined and differently oriented PV modules on balancing needs for Europe. Additionally, the model domain is expanded to North Africa to estimate the influence of concentrated solar power import on European storage and backup needs. The results show that the favorable choice of module configuration is very sensitive to the shares of solar and wind. For high solar shares, highly inclined modules with less pronounced annual courses are favorable, if a storage is available with a capacity to cover at least 6 hours of average load. In a wind-dominated scenario, lowly inclined East/West facing modules are most suitable to reduce balancing needs. When no storage is present, a combination of highly inclined East and West facing modules reduces the balancing needs as long as solar share is high enough to distinguish between different configurations. Some of these module configurations may be quite expensive in terms of installed capacity, but repowering old PV modules to configurations best suited for a specific scenario, can be advantageous in the long run.



## List of publications

1. **The impact of different PV module configurations on storage and additional balancing needs for a fully renewable European power system,** **K. Chattopadhyay**, A. Kies, E. Lorenz, L. von Bremen, and D. Heinemann: *Renewable Energy*, (<https://doi.org/10.1016/j.renene.2017.05.069>), 2017.
2. **Investigation of balancing effects in long term renewable energy feed-in with respect to the transmission grid,** A. Kies, **K. Nag**<sup>1</sup>, L. von Bremen, E. Lorenz, and D. Heinemann: *Adv. Sci. Res.*, **12**, 91-95, 2015.

---

<sup>1</sup>Last name changed to Chattopadhyay from Nag in 2014



# Table of contents

<b>List of figures</b>	<b>xvii</b>
<b>List of tables</b>	<b>xxi</b>
<b>Nomenclature</b>	<b>xxv</b>
<b>1 Introduction</b>	<b>1</b>
1.1 Challenges with variable resources . . . . .	2
1.1.1 Issues on non-dispatchable nature . . . . .	2
1.1.2 Balancing over- and under-production . . . . .	2
1.1.3 Disrupting thermal units . . . . .	3
1.1.4 Problems due to site-specific abundance . . . . .	3
1.1.5 Challenges during meteorological events . . . . .	3
1.1.6 Power drop during solar eclipse . . . . .	4
1.2 State of knowledge . . . . .	4
1.3 Scope of this work . . . . .	6
<b>2 Data description and model overview</b>	<b>9</b>
2.1 Data description . . . . .	9
2.2 Model overview . . . . .	11
2.2.1 Module-Ia: Submodel for meteorological data . . . . .	11
2.2.2 Module-Ib: Submodel for capacity distribution . . . . .	16
2.2.3 Module-Ic: Submodel for power calculation . . . . .	21
2.2.4 Module-IIa: Mismatch and residual load . . . . .	23
2.2.5 Module-IIb: Backup model . . . . .	25
2.2.6 Module-IIc: Storage model . . . . .	25
<b>3 Evaluation of regionally averaged PV power</b>	<b>29</b>
3.1 Evaluation on country level . . . . .	31

3.2	Evaluation of control zones . . . . .	33
3.3	Evaluation of selected German federal states . . . . .	36
3.4	Summary . . . . .	40
<b>4</b>	<b>Variability analysis of VRE sources</b>	<b>41</b>
4.1	Spatial variability of resources . . . . .	42
4.2	Diurnal variability . . . . .	45
4.3	Seasonal variability . . . . .	49
4.4	Summary . . . . .	54
<b>5</b>	<b>Impact of PV module configurations on European balancing needs</b>	<b>55</b>
5.1	Estimation of backup needs . . . . .	56
5.1.1	Backup in absence of storage . . . . .	56
5.1.2	Backup in presence of storage . . . . .	60
5.2	Estimation of storage needs . . . . .	63
5.2.1	Unconstrained lossless storage . . . . .	65
5.2.2	Using a two-storage system . . . . .	68
5.3	Summary . . . . .	71
<b>6</b>	<b>CSP import from North Africa</b>	<b>73</b>
6.1	Data set for North Africa . . . . .	73
6.1.1	Meteorological data . . . . .	73
6.1.2	CSP capacity . . . . .	74
6.2	Cloud index data base . . . . .	74
6.2.1	Quality control (QC) . . . . .	75
6.2.2	Removing the effects of Bidirectional reflection . . . . .	75
6.3	Impact of CSP import on European balancing needs . . . . .	77
6.3.1	Balancing in absence of storage . . . . .	79
6.3.2	Balancing combined with storage . . . . .	80
6.4	Summary . . . . .	81
<b>7</b>	<b>Summary and conclusion</b>	<b>83</b>
	<b>References</b>	<b>87</b>
	<b>Appendix A Overview of simulated European countries</b>	<b>95</b>
	<b>Appendix B Additional investigation for PV modules with different configurations</b>	<b>97</b>

Table of contents	xv
-------------------	----

---

Appendix C Statistical error measures	99
---------------------------------------	----





# List of figures

2.1	Module-I for solar power: Schematic representation of different components of Module-I. All three sub-models, which are used for both PV and CSP, are considerably modified to be applicable for each technology. All images shown here are examples of deriving the PV power. . . . .	12
2.2	Schematic representation of different steps to derive global horizontal irradiance using the Heliosat method. . . . .	13
2.3	Optimum inclination of the PV modules for a maximum annual yield ©IES, JRC. . . . .	15
2.4	Resource-dependent capacity distribution functions for Germany. . . . .	18
2.5	Average DNI map for Spain (2003-2012) in kWh/m <sup>2</sup> /y. Black dots mark the CSP plants operational in 2012 (top) and modelled for 2050 (bottom). . . . .	20
2.6	Balancing module: Schematic representation of different components of Module-II and their interplay. . . . .	23
2.7	An excerpt of load, wind and PV time series during 10-16 June, 2012 for Europe in the top panel. The bottom panel shows the corresponding mismatch time series calculated for $\alpha = 1$ and $\beta = 0.4$ and using PV power generation from South facing optimally inclined modules. . . . .	24
3.1	Regional coverage of four TSOs from Germany © Wikipedia: Tennet ( <a href="https://de.wikipedia.org/wiki/Tennet_TSO">https://de.wikipedia.org/wiki/Tennet_TSO</a> ), [accessed on: 24. 03. 2017]	30
3.2	Comparison of simulated and upscaled measured regionally averaged normalized PV power for Germany. . . . .	32
3.3	Comparison of simulated and upscaled measured normalized PV power for Germany, 2012. The time series is shown for daily mean values while the scatter plot in the inset is given on the hourly scale. . . . .	33
3.4	Comparison of simulated and upscaled measured regionally averaged normalized PV power for the control zone of Tennet. . . . .	34

3.5	Comparison of simulated daily PV power with upscaled measurements for four TSOs in Germany, 2012. All time series are normalized to their respective installed capacities. In the inset is the scatter plot of normalized hourly time series. . . . .	35
3.6	Comparison of simulated and upscaled measured regionally averaged normalized PV power for the German federal state of Schleswig-Holstein.	37
3.7	Comparison of simulated daily PV power with upscaled measurements for two federal states of Germany, 2012. All time series are normalized to their respective installed capacities. In the inset is the scatter plot of normalized hourly time series. . . . .	38
3.8	Tennet . . . . .	39
4.1	Annual average (4.1a) and annual standard deviation (4.1b) maps of PV capacity factor for Europe calculated over ten years (2003-2012). . . .	43
4.2	Comparison between GHI and DNI in Spain for two days with different cloud cover. . . . .	46
4.3	The diurnal variation of European load, wind, and PV power from different module configurations averaged over the simulation period in a power system with $\alpha = 1.0$ and $\beta = 0.4$ . . . . .	47
4.4	Hourly standard deviation of 55 different module configurations. This standard deviation is normalized to the mean PV power. . . . .	47
4.5	Cumulated distribution of hourly incremental power generation and mismatch. . . . .	49
4.6	Weekly time series depicting the annual course of load, wind, and different module configurations for 2011. . . . .	51
4.7	Weekly standard deviation of 55 different module configurations. This standard deviation is normalized to the mean PV power. . . . .	52
5.1	Additional average balancing $E_b^{add}$ as a function of average VRE generation factor $\alpha$ in absence of any storage for highly (optimal+25°) inclined PV modules with different orientations for different shares of PV and wind. . . . .	56
5.2	Average additional balancing needs ( $E_b^{add}$ ) for different module configurations for $\alpha = 1.25$ . . . . .	57

5.3	Variation of average additional balancing $E_b^{add}$ as a function of small storage size $C_s$ for South facing modules with different inclinations for different solar and wind shares for $\alpha = 1$ . No storage loss is considered here. . . . .	60
5.4	Excerpt of storage filling with charging (pink), discharging (light blue), curtailment (red) and balancing needs (dark blue) for a few days in winter. This example compares different module configurations for $\alpha = 1.0$ , $\beta = 0.4$ , and $C_s = 6$ av.h.l. . . . .	62
5.5	Reduction in average additional balancing $E_b^{add}$ up on using a lossless storage shown for South facing modules with different inclinations over a wide range of $\alpha$ values. Example shown for $\beta = 0.6$ . . . . .	63
5.6	Lossless storage filling for different shares of solar (and wind) and for different module configurations at $\alpha = 1$ . (a)-(b) compare optimally inclined modules with different orientations while (c)-(d) compare South-facing modules with different inclinations. . . . .	64
5.7	Storage capacity ( $C_s$ ) in average annual load (av.a.l) at $\alpha = 1$ for different module configurations for (a) solar share ( $\beta$ ) 0.2 and for (b) solar share ( $\beta$ ) 0.8. . . . .	65
5.8	Storage capacity ( $C_s$ ) for unconstrained lossless storage shown for different module configurations and for different shares of PV and wind. (a) compares optimally inclined modules with different orientations while (b) compares South-facing modules with different inclinations. . . . .	67
5.9	Storage capacity as a function of $\alpha$ and solar shares $\beta$ . The dashed line indicates the optimal mix ( $\beta_{opt}$ ) that minimizes the storage capacity without introducing any average additional balancing. . . . .	69
5.10	Changes in relative reduction in backup needs for different shares of PV and wind up on introducing a lossless 6 hour storage. The remaining mismatch is then used to quantify the storage needs for a seasonal storage ( $\eta_{in} = \eta_{out} = 0.6$ ) for different shares of PV and wind and for different module configurations. . . . .	70
6.1	Improvement of DNI time series upon quality control. . . . .	76
6.2	Removing the effects of Bidirectional reflection shown for a few days in Fall. . . . .	77
B.1	PV installed capacity adjustment with respect to a reference time series for different PV module configurations to have equal average yield. . .	98



# List of tables

2.1	A combination of different module configurations as taken from the work of Pfluger et al. [67]. . . . .	16
2.2	Projected installed capacity values (GW) of different renewable energy sources for Europe from the meta-studies after inclusion of the Balkan countries. . . . .	17
2.3	Country level CSP capacities (GW) taken from EWI energynautics report [28] and scaled to the ISI scenario [67]. . . . .	18
2.4	Numerical values of variables used in power calculation of CSP plants are taken from [94]. . . . .	22
3.1	Comparison of statistical measures of normalized PV power time series of Germany for 2012 (rounded to 3 digits after decimal). . . . .	33
3.2	Comparison of statistical measures of normalized PV power time series for four TSO controlled zones for 2012 (rounded to 3 digits after decimal). . . . .	36
3.3	List of capacity factors (%) of each control zone calculated for simulations and upscaled measurements. . . . .	36
3.4	Comparison of statistical measures of normalized PV power time series for two German federal states which are partly/fully covered by Tennet for 2012 (rounded to 3 digits after decimal). . . . .	39
4.1	Mean, standard deviation (Std.), and correlation coefficients of PV capacity factors computed over the ten years of simulation period for five selected countries. . . . .	44
4.2	Mean, maxima (Max.), and standard deviation (Std.) of hourly power ramps for different shares of PV and wind. All values are expressed as the share of peak load. . . . .	48

4.3	Statistical dispersion of hourly mismatch ramps [share of peak load] calculated for different degrees of renewable penetration ( $\alpha$ ) and different shares of PV and wind ( $\beta$ ). . . . .	50
4.4	Statistical measures of power and ramp of demand and generation. All values are expressed as the share of the peak load of the corresponding temporal resolution. The PV and wind generation are shown for PV-only and wind-only scenarios, respectively. Here, Std. stands for standard deviation. The values in the parenthesis denote the corresponding numbers of the absolute values of ramps. . . . .	53
5.1	Comparison of $E_b^{add}$ between different module configurations with changing solar shares. These values are computed for $\alpha = 1.5$ in the scenario without any storage. . . . .	58
5.2	Reduction in balancing potential with the accompanying capacity increase shown for different module configurations compared to the optimally inclined South facing ones in a scenario with $\alpha = 1.0$ and $\beta = 0.4$ . All values are given in %. . . . .	59
5.3	Average additional balancing needs in presence of lossless storages for South facing modules with different inclinations. All values are calculated for high solar shares ( $\beta = 0.8$ ) to distinguish between different configurations. . . . .	61
5.4	Storage capacity needs ( $C_s$ ) for different values of $\alpha$ and $\beta$ shown for different module configurations. $C_s$ is expressed as average annual load (av.a.l.). . . . .	68
6.1	Statistical measures of DNI time series of 2005 from MSG satellite against the same retrieved from MFG. For the correlation coefficient, the night time values are filtered out. . . . .	78
6.2	Statistical measures of CSP time series of North Africa for 2005. . . . .	78
6.3	Annual CSP capacity factors (%) of Europe and North Africa for each simulated year. . . . .	79

---

6.4	A table summarizing the impact of CSP import from North Africa on European balancing needs in absence of any storage. The first column states the chosen scenario, the second column gives the percentage of total CSP that is imported to Europe. As CSP generation capacity is very different in the two scenarios, their respective shares on load coverage is also significantly different (column four), even for the same share of CSP import. The remaining columns show the changes in the balancing parameter due to CSP import. . . . .	80
6.5	A table summarizing the impact of CSP import from North Africa on European balancing needs in presence of a storage with efficiency ( $\eta_{in}=\eta_{out}=0.6$ ). For the detailed description of each column, please see the caption of Table. 6.4 that has the same structure as this one. . . .	81
A.1	List of capacity factors calculated over ten years (2003-2012) for each country simulated in this work. Additionally, the chosen optimal angle of PV module inclination to maximize average annual yield is included here. These angles are taken from Fig. 2.3 according to [86]. . . . .	96
B.1	A list of module configurations analyzed in this work . . . . .	98





# Nomenclature

## Acronyms / Abbreviations

av.a.l. average annual load

av.h.l. average hourly load

BDSG Bundesdatenschutzgesetz

BMBF Federal Ministry of Education and Research

$CO_2$  carbon dioxide

COSMO-EU COnsortium for Small-scale MOdeling - Europe

CSI clear sky irradiance

CSP Concentrated Solar Power

DHI diffuse horizontal irradiance

DNI direct normal irradiance

DSM demand-side management

EEG Erneuerbare Energien Gesetz

EEX European Energy Exchange

EU European Union

GHG greenhouse gas

GHI global horizontal irradiance

HRV high resolution visible channel

MERRA Modern-Era Retrospective analysis for Research and Applications

MFG Meteosat First Generation

MPP maximum power point

MSG Meteosat Second Generation

NERC North American Electric Reliability Corporation

NWP Numerical Weather Prediction

PV photovoltaics

QC Quality control

RES Renewable Energy Sources Act

RMSE<sub>rel</sub> relative root mean square error

RMSE root mean square error

SAM Solar Advisor Model

SFOI South facing optimally inclined

STC standard test condition

STDERR standard deviation of error

Std. standard deviation

TPES total primary energy supply

TSO transmission system operator

VIS visible channel

VRE variable renewable energy

### **Mathematical symbols from Module I**

$a_1$  device specific parameter 1

$a_2$  device specific parameter 2

$a_3$  device specific parameter 3

---

$\rho$	apparent albedo
$\alpha_T$	temperature coefficient
$A_{sf}$	solar field area
$C_0$	instrument offset of digital counts
$\eta_{MPP}$	efficiency at maximum power point
$\eta_{opt}$	optical efficiency
$\eta_{Turbine}$	Design turbine gross efficiency
$f$	earth-sun distance
$\rho_g$	ground albedo
$\gamma$	mounting type dependent system parameter
$I_{POA}$	irradiance on the plane of array
$k^*$	clear sky index
$Loss_{HCE}$	HCE thermal losses
$Loss_{parasitic}$	Electric parasitic loss
$Loss_{SFP}$	solar field piping heat losses
$n$	cloud index
$\rho_o$	overcast cloud albedo
$P_{CSP}$	Power generation from CSP
$P_{inst}$	Installed capacity
$P_{PV}$	PV power
$T_a$	ambient temperature
$\theta$	solar zenith angle
$T'_m$	temperature difference between the $T_m$ and 25°C
$T_m$	module temperature in °C

**Mathematical symbols from Module II**

$\alpha$	average VRE generation factor
$\beta$	solar share
$C_s$	storage capacity
$\Delta$	mismatch
$E_b$	average balancing parameter
$E_b^{add}$	average additional balancing parameter
$\eta$	storage efficiency
$\eta_{in}$	efficiency to put energy in storage
$\eta_{out}$	efficiency to take energy out of storage
$\tilde{\Delta}$	modified mismatch due to storage interaction
$F$	storage filling level
$G$	variable renewable generation
$L$	load
$\Delta_-$	negative component of mismatch
$\Delta_+$	positive component of mismatch

# Chapter 1

## Introduction

The energy debate has identified itself as one of the most discussed topics of the world's social, political, economic, and environmental issues. Today fossil fuels are the dominant sources of world energy supply. Of the 13,147.3 Mtoe<sup>1</sup> of world's total primary energy supply (TPES) in 2015, oil, coal and natural gas had the shares of 32.9%, 29.2%, and 23.8%, respectively [23]. However, climate impacts and rapid depletion of these fuels are continuously raising questions on their future reliability. Combustion of fossil fuels results in the emission of several gases like carbon dioxide ( $CO_2$ ), methane ( $CH_4$ ) and others, collectively known as the greenhouse gases (GHG), which can potentially trap the long wave (infrared) radiation causing temperature increase of earth's atmosphere. To prevent dangerous consequences of climate change, the European Council has endorsed the objective of reducing the GHG emissions to 80 – 90% below the 1990 levels by 2050. However, climate risks are not the only problem, fossil fuels also pose the threat of scarcity of resources. As of today, fossil fuels are being extracted at an exorbitant rate to meet the demand. Since the reserves are only finite, large amounts of fuel consumption leads to their rapid depletion. The ratios of world consumption to reserves for fossil fuels show that if the world continues to consume fossil fuels at today's rates, the reserves of oil, coal, and gas will last a further 35, 107 and 37 years, respectively [80]. This problem of limited resource also translates into the increase of fuel price. Depleting resources will drive us to explore increasingly remote places, which indicates a significant rise in fuel price due to the additional transport and infrastructure costs.

The combined effects of climate threats, scarcity of resources, increasing fossil fuel price, and growing public aversion towards nuclear energy have motivated the world to

---

<sup>1</sup>Mtoe: Million Tonnes of Oil Equivalent

deploy the renewable resources as alternatives to the conventional power plants. Major renewable energy sources include solar, wind, hydro, tidal, biomass, and geothermal, the sources that are clean and are naturally replenished. Due to these benefits, the share of renewable energy sources to the world electric power generation mix is growing rapidly. In most European countries today, solar photovoltaics (PV) and wind have established themselves as technologically mature and economically affordable. However, solar and wind power supply substantially differ from the conventional, dispatchable generations in one key aspect: The highly variable nature of these two renewable energy sources.

## **1.1 Challenges with variable resources**

Power systems have always dealt with the variable demand and over the course of time have adopted themselves with some flexibility built-in for load following purposes. In fact, at relatively low levels of renewable penetration, power output from solar and wind resources can essentially be absorbed into the traditional system operations without degrading system reliability. However, with increasing level of penetration, these resources require more advanced and sophisticated mechanisms to maintain proper system performance. The transition to a renewable-based power system brings along certain challenges and disrupts traditional power system operation. To allow large shares of generation from these variable renewable energy (VRE) sources, it is important to understand the challenges they pose to the operational power grid.

### **1.1.1 Issues on non-dispatchable nature**

The electricity network, in contrast to other supply networks, such as the gas network, is virtually incapable of storing energy. Hence, it is absolutely necessary to balance supply and consumption at every time step. Introducing very large shares of uncontrollable generation to the power grid makes system operation quite difficult. As solar and wind power fluctuates over a wide range of time horizons (from seconds to beyond several decades), the grid operators are forced to repeatedly adjust the output to match the power demand.

### **1.1.2 Balancing over- and under-production**

Any imbalance between demand and generation in the power system is a direct consequence of either over- or under-production, that must be resolved immediately to

maintain acceptable quality of power supply. The highly variable weather-dependent nature of solar and wind power casts a doubt on the reliability and stability of power supply from these resources. When generation fails to meet the demand, serious consequences may follow, including the phenomena of forced load-shedding (i.e., power outage in one or more areas) or even worse, the blackouts. In situations of surplus generation, the excess energy produced is practically wasted unless a storage of adequate size is used.

### **1.1.3 Disrupting thermal units**

With increasing level of VRE penetration, the operation of thermal units need to change in order to follow the new profile of residual load, resulting in increased cycling of thermal generation (start-ups and shut-downs). This cycling is expensive because it requires fuel consumption and increased operational and maintenance cost. Additionally, in certain hours, base load operation of the inflexible power plants (such as, nuclear) are either restricted or bid to zero or even negative prices to avoid expensive shut-down and restarts.

### **1.1.4 Problems due to site-specific abundance**

The average power generation from solar and wind resources exhibits highly variable geographic distribution. Very often sites, that can provide abundant resources throughout the year, are located away from the demand centers. For example, southern Europe receives enough solar irradiance to promote solar infrastructure whereas northern Europe is suitable for offshore and onshore wind farms. However, the primary demand in Europe mainly comes from its central part. In such cases, reinforcement of existing transmission infrastructure is required along with adequate planning and system-wide upgrade.

### **1.1.5 Challenges during meteorological events**

Apart from the major challenges discussed above, there are several important events like severe storms, dust storms, snowfall etc, that can potentially disrupt power production from VRE sources. During severe storms, when wind intensity is as high as 8 on the Beaufort scale (i.e., wind speed of above 75 km/hour), most of the wind turbines are powered down for safety reasons. During large meteorological events, such as cyclones, the incoming solar radiation can also be diminished significantly. Moreover,

their influence on solar power generation can be severe as the life time of typical extra-tropical cyclones may vary from a few days to beyond a week. Snow is another potential obstruction of PV power production during winter. But it is to be noted here that between the scant sunlight during short winter days and the occasional snowfall, energy yield from PV panels during the cold months is significantly low compared to the other months of the year. So, the additional reduction in power generation due to snowfall doesn't affect the power supply much.

### **1.1.6 Power drop during solar eclipse**

Another interesting event that can strongly influence changes in solar power is the occurrence of a solar eclipse [26]. For countries with large shares of solar PV, the impact of solar eclipse (specially on clear-sky days) can be very critical on the national grid. Unlike clouds, that can rarely affect an entire nation exactly at the same time, the influence of eclipse can be realized over large geographic area. Depending on how much the moon blocks the sun disk, there can be sharp changes in PV power that can potentially disrupt the grid stability. For example, the German national grid with 38 GW PV capacity experienced a partial solar eclipse (73% coverage of the sun disk) on 20<sup>th</sup> March, 2015 which changed PV power output from an estimated 13 to 4.8 GW, and the grid frequency from 50.2 to 49.97 Hz within 75 minutes. The drop in low price PV power during solar eclipses is usually compensated by relatively expensive generators like nuclear power plants. As a result, a very precise forecast of the event is not only crucial for the grid operators, it is also indispensable in terms of energy trading.

## **1.2 State of knowledge**

To ensure stable and sustainable electricity supply from renewable-based power systems, several strategies like optimizing the mix of different renewable sources [55, 27, 33, 42, 45], demand side management (DSM) [29, 59, 44], reinforcement of the transmission grid [16, 74, 93, 78, 77, 50, 51], usage of storage [33, 88], balancing through dispatchable generation [34, 52, 38, 79] have been proposed. To avoid wastage of energy from surplus generation, the peak load can be shifted to hours of highest generation. Also, if the period of increased generation is anticipated ahead of time, the grid operators can decrease the power feed-in from dispatchable plants to allow proper usage of each technology. These strategies allow system flexibility that is highly desirable for any



operational power grid. System flexibility can act on the supply side (i.e., generation technologies that can quickly adjust power production without causing major impact on the equipment's lifetime) as well as on the demand side (for example, promoting incentives to allow load shifting, deploying smart grid) or on both supply and demand sides using storage technologies. Plessmann et al. [68] have investigated the global storage demand of a sustainable electricity supply based on wind, PV and concentrated solar power (CSP) and found such system to be feasible with decent cost. Additionally, Brown et al. [20] have shown that coupling of electricity, transport, and heat sectors can be beneficial for a highly renewable power system. It is also possible to envision a global renewable energy grid consisting of renewable harvesters connected to the load centers by long distance transmission as discussed by Chatzivasileiadis et al. [22].

Multiple studies have quantified the storage and backup needs in highly renewable power systems around the globe: Lise et al. [52] have quantified balancing needs as a function of the share of variable generation in mid-term (2030) and long-term (2050) European power market. Heide et al. have estimated the storage requirement for a 100% solar and wind power generation scenario of Europe: Depending on the round-trip storage technology, a mix of 40% PV and 60% wind results in storage needs of 400 TWh (without storage losses) to 480 TWh (for hydrogen storage) [33], which is around 12-15% of the annual European consumption nowadays. These storage needs double if shifted to a solar-only or a wind-only scenario. The influence of the degree of variable renewable penetration to the power system and their mix on the ramping flexibility needs is assessed by Huber et al. [38]. These two factors also play very important roles in determining how much storage and balancing are required [69, 34]. However, the estimated storage and balancing needs can also be influenced by the choice of PV module configurations (tilt angle and orientation given by azimuth). Existing studies on PV module configurations have either focused on how module performance is affected by the mounting types, properties of the material, sensitivity to temperature (and solar irradiance) [64] or on optimizing average yield [39] and the economic aspects of PV installations [95]. In this work, the influence of different PV module configurations on storage and balancing needs for Europe is analyzed. Solar PV has been the primary focus throughout this thesis. Since wind will also have a dominant share in a future European power system [40], the model is expanded to include it alongside PV.

### 1.3 Scope of this work

Through all the advantages and challenges discussed above, it is established that the renewable energy sources like wind and solar PV are indeed the alternate to the conventional fossil fuels, but implementing them to the operational power system requires proper planning, correct estimation of balancing needs and DSM, and continuous monitoring to ensure stable and reliable power supply. Favorable policies with high incentives to renewable energy sources can promote the ongoing transformation towards a wind- and solar-dominated power system. However, government policies alone are not enough to develop such path ways, detailed knowledge of the system behavior under varying conditions is also of fundamental importance. The research work presented in this thesis aims to focus on the assessment of the variable nature of wind and solar technologies over multiple time horizons. It includes estimation of balancing needs through backup and/or storage for different shares of solar and wind energy as well as for different degrees of VRE penetration to the power system. The interplay between all these factors have been studied and analyzed for a wide variety of scenarios. An extensive work has been included to identify how different PV module configurations can influence storage and backup needs for different shares of wind and solar for different extents of VRE penetration.

**Major research questions discussed in this thesis:**

- how does the weather-dependent nature of solar and wind power influence grid operation
- how well does the model reproduce the regionally averaged PV power from real world
- how does the variable nature of solar and wind affect balancing needs over short time period (such as a few hours) as well as on longer time horizon (seasonal)
- what are the factors that determine the ability of a module configuration to best match the load curve
- how does power ramp vary on supply side as well as on the demand side
- what are the synergies between storage and backup supplies
- to what extent can storage/backup alone be the answer to grid balancing
- to what extent can storage reduce the backup needs
- what influence does the integration of the controllable feed-in of North Africa have on the balancing needs of Europe
- what is the impact of the parallel expansion of renewable energies in countries inside and outside (here North Africa) of the European Union

In this work, the variable nature of solar and wind is addressed in the context of balancing requirements in a renewable-based power system. The entire investigation presented here can be understood under the aspect of system-friendly renewables [36]. In Chapter. 2, a short description of the data sources is given with an overview of the model components. The model is designed for the assessment of balancing needs in future energy supply scenarios based on a system representation in high spatial and temporal resolution. The quality of the power output from this model is next evaluated in Chapter. 3 for Germany. Since this thesis is focused mainly on the characteristics of solar power, only the evaluation of PV power is included here. The key essence of this work is the analysis of the variability characteristics of VRE generation and their effect on European balancing needs. These are discussed in Chapter. 4 and Chapter. 5, respectively. Given the variety in temporal fluctuations of demand and VRE power generation on the one hand, and restrictions in technology potentials on the other, different balancing means, such as storage and backup power supply, are included here. The synergies between these balancing options are also evaluated along with the

optimal mix of solar and wind in each scenario. Furthermore, the power generation potential of different PV module configurations are analyzed in the context of balancing and variability reduction on relevant scales. Next, the impact of CSP import from North Africa on European power system is quantified in Chapter. 6 for scenarios with different shares of power import. Finally, the key findings of this work and the critical areas of future research are summarized and concluded in Chapter. 7.

# Chapter 2

## Data description and model overview

A dynamically growing power system with increasing shares of VRE sources require high resolution long term data analysis to quantify multi-scale fluctuations and to estimate possible balancing needs to ensure reliability of such systems. This section is comprised of the dataset description and an overview of the model layout used in this work. The data description includes information on different features of the input data, such as data sources, data resolution, model domain, duration of simulation period etc. The model is designed for a future European power system with increased installed capacity and improved capacity distribution of all renewable energy sources. The entire database is derived as part of the project RESTORE 2050<sup>1</sup>. In this work, only solar and wind power have been considered as the VRE sources. Among other major renewable sources is the hydro power, which is omitted here due to its limited scope of future growth. Other forms of renewable generation like biomass energy, which are dispatchable in nature, are implicitly included in the model as backup sources to ensure balancing.

### 2.1 Data description

A large database of solar power generation is developed in this work with high spatio-temporal resolutions. To understand the intra-day power ramps, the temporal resolution

---

<sup>1</sup>The project RESTORE 2050 (grant number: 03SFF0439A) has investigated the issues of power grid expansion, storage, and DSM needs for a VRE-dominated European power system for the year 2050. It was funded by the Federal Ministry of Education and Research (BMBF).

of the model is chosen to be an hour. To resolve the meso-scale features, such as developing convective complexes, the spatial resolution of the model is made  $7 \times 7 \text{ km}^2$ . Model grid points in this high resolution are taken from the COnsortium for Small-scale MOdelling - EUrope (COSMO-EU) model. The simulation period for this work is ten years (2003 - 2012). Analysis over such long period of time gives the advantage to obtain representative statistical measures of possible anomalies and extreme events. The model domain primarily<sup>2</sup> covers a total of 33 countries (see Table. A.1).

**Wind and load data:**

Both wind and load data used in this work are originally computed for the project RESTORE-2050. Wind power time series is derived using wind speed from Modern-Era Retrospective analysis for Research and Applications (MERRA) reanalysis with horizontal interpolation to the COSMO-EU model resolution. Since this reanalysis only provides wind speeds at 10m and 50m heights, they are logarithmically extrapolated to the hub height of 140m. Model details on the wind power are given in Ref. [43].

Load data of each country in the model domain is taken from ENTSO-E. The load curve of a randomly chosen year (2011) is used here as the base data. Using a temperature fitting function on this base data, the synthetic load curves for the remaining years are computed. For the ten year simulation period, the average hourly load (av.h.l.) and average annual load (av.a.l.) for Europe are 404.2 GWh and 3543.3 TWh, respectively. For details on the methods of deriving load data, please see the second annual report of the project RESTORE 2050 [11].

This study focuses on the solar power data derived from satellite measurements. Solar irradiance data is used to compute solar power for PV and CSP technologies and is retrieved from Meteosat satellites. Two generations of satellites with different spatio-temporal resolutions were operational over the simulation period. For the first two years (2003 - 2004), solar irradiance data are retrieved from the broadband visible channel (VIS) of Meteosat First Generation (MFG) satellites. This broadband visible channel has a spectral range of 0.5 - 0.9  $\mu\text{m}$  and is very suitable for cloud detection. This channel has a spatial resolution of  $2.5 \times 2.5 \text{ km}^2$  at the sub-satellite point and collects data every 30 minutes. For the remaining years (2005 - 2012), solar irradiance is retrieved from the Meteosat Second Generation (MSG) satellites. MSG has one high

---

<sup>2</sup>It is to be noted that only for one specific section of this work (Chapter. 6), the model domain is extended to North Africa.

resolution visible (HRV) channel with an improved sampling interval of 15 minutes and a  $1 \times 1 \text{ km}^2$  spatial resolution at the sub-satellite point. It operates over the spectral range of 0.6 - 0.9  $\mu\text{m}$ . This broadband HRV of MSG satellites is used to retrieve solar irradiance from 2005 - 2012. To maintain uniformity with the wind and the load data, solar irradiance retrieved from both generations of satellites are regridded to  $7 \times 7 \text{ km}^2$  and averaged to hourly resolution. The 2 m temperature data used for calculating the PV module efficiency are derived from the MERRA reanalysis [72].

## 2.2 Model overview

The model developed here is composed of two major components: Module-I (Fig. 2.1) and Module-II (Fig. 2.6). Module-I focuses on the development of long term solar power time series using three sub-models. Each of these sub-models are significantly different in design for PV and CSP due to strong contrasts in their characteristics. Derivation of wind power is not discussed here. But wind power time series is taken from the project RESTORE 2050 to analyze and to use in Module-II .

Module-II is designed to estimate balancing needs for European countries and uses the PV power output from Module-I as one of its input data. For Module-II, only PV and wind power are used as feed-in time series. As CSP industry needs guaranteed high solar irradiance throughout the year, only a hand full of European countries are projected to invest in such plants in future [28]. So, CSP is not included here in Module-II.

### 2.2.1 Module-Ia: Submodel for meteorological data

Due to the weather-dependent nature of solar and wind, it is very important to thoroughly analyze the meteorological conditions when computing their respective power. This sub-model of Module-I takes raw meteorological data (wind speed for wind power, global horizontal irradiance and temperature for PV power, direct normal irradiance for CSP) and converts them in specific forms usable for their power calculations.

#### Solar irradiance retrieval from satellite images

The Heliosat method is a technique to convert the observations made by geostationary satellites to determine solar irradiance at the ground level [17, 32]. In this work, the Heliosat method is used in combination with a clear sky model [60] to compute global horizontal irradiance (GHI), diffuse horizontal irradiance (DHI), and direct normal

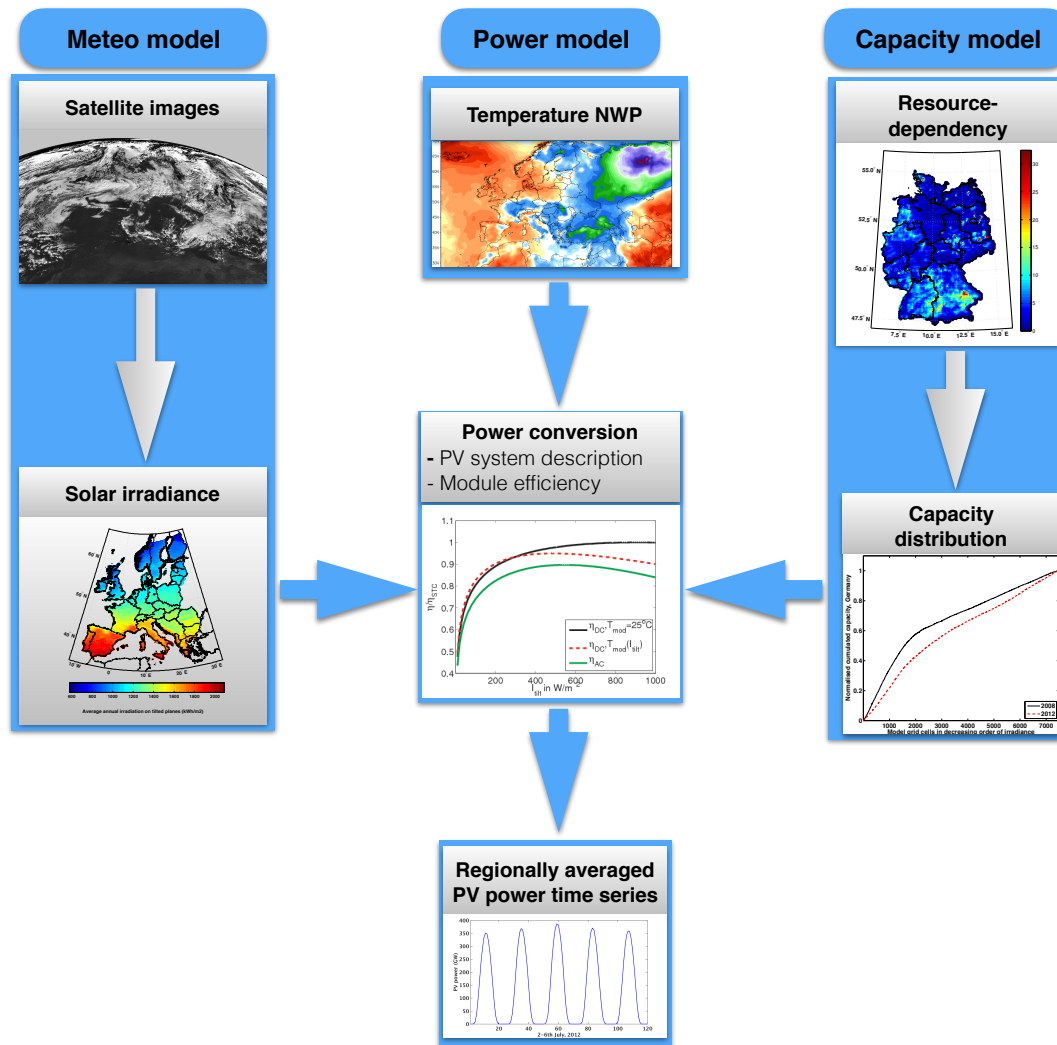


Fig. 2.1: Module-I for solar power: Schematic representation of different components of Module-I. All three sub-models, which are used for both PV and CSP, are considerably modified to be applicable for each technology. All images shown here are examples of deriving the PV power.



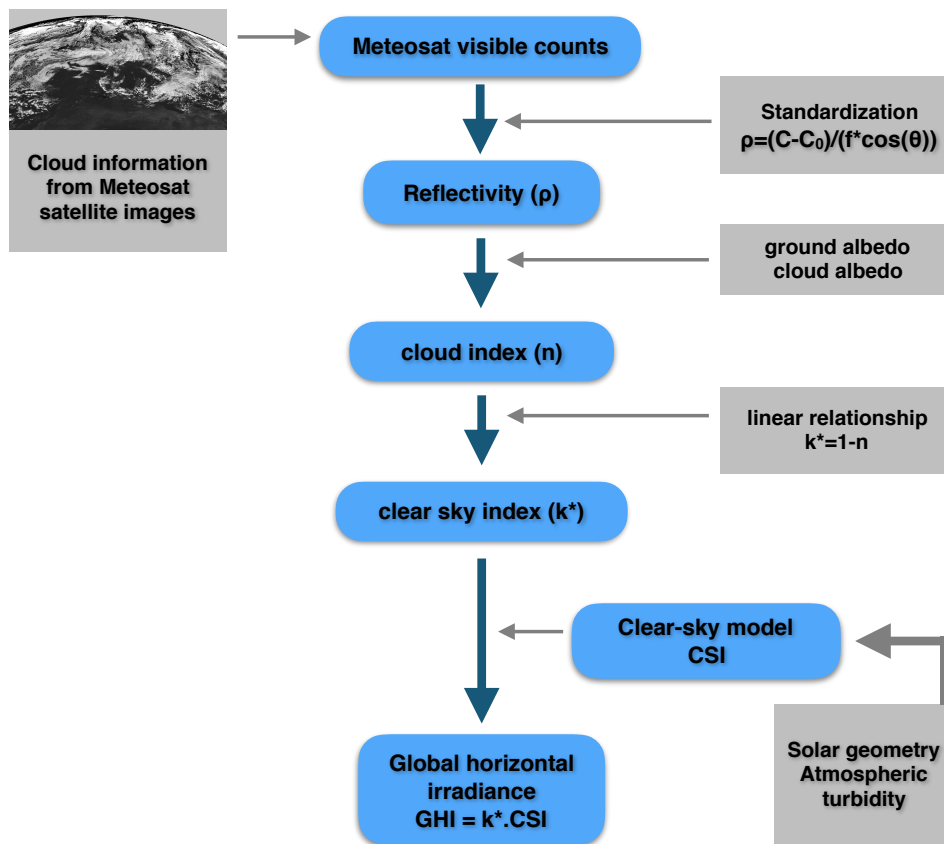


Fig. 2.2: Schematic representation of different steps to derive global horizontal irradiance using the Heliosat method.

irradiance (DNI). The clear-sky model computes clear sky irradiance (CSI) using solar elevation, surface topography, and atmospheric turbidity as the input parameters. There are two turbidity data sets used here. For simulation over Europe, the data base of Bourges with yearly patterns of turbidity is used [24] while for North Africa, the high resolution data base of Remund et al. [71] is applied.

The Heliosat method relies on the fact that usually the albedo of clouds is larger than that from earth's land and ocean surfaces<sup>3</sup>. The main steps of the Heliosat method are shown in Fig. 2.2. The first step is to determine the reflectance values (correcting for the instrument offset of the digital counts ( $C_0$ ), the solar zenith angle

<sup>3</sup>As the albedo from snow covered surfaces can be even larger than that of the clouds, Heliosat method can result in misinterpretation in presence of the snow.

( $\theta$ ), and the variations of the earth-sun distance ( $f$ ) to identify clear sky time slots and the ground albedo for individual pixel. The second step is to compute the cloud index ( $n$ ) from the apparent albedo ( $\rho$ ), ground albedo ( $\rho_g$ ) and the overcast cloud albedo ( $\rho_o$ ):

$$n = \frac{\rho - \rho_g}{\rho_o - \rho_g}, \quad (2.1)$$

The cloud index is the key parameter of the Heliosat method and it relates to the atmospheric transmission via an empirical linear relationship with the clear sky index ( $k^*$ ) which is defined as the ratio of GHI and the CSI.

$$k^* = \frac{\text{GHI}}{\text{CSI}}, \quad (2.2)$$

Knowing  $k^*$  from the cloud index and CSI from the clear-sky model, it is possible to determine global horizontal irradiance from Eq. (2.2).

### Conversion of solar irradiance

Depending on the solar technology, the conversion of solar irradiance to power can be very different. While PV power is computed from irradiance on tilted surface ( $I_{\text{POA}}$ ), CSP is deduced from DNI. The conversion of GHI onto inclined surfaces used here is based on the Klucher model [47]. In 1979, Klucher found that the traditional isotropic models underestimate irradiance under clear sky or partly cloudy conditions and he modified the isotropic model to incorporate the effects horizon brightening and increased intensity in the circumsolar region of the sky. Hence, this model not only functions well for overcast conditions (isotropic atmosphere), but also yields satisfactory results when the diffuse component of solar irradiance is not uniformly distributed.

In order to convert global irradiance to  $I_{\text{POA}}$ , it is mandatory to get the information on the angle of inclination of the PV module plane. The optimum module inclination of a certain location under clear sky condition resembles its local latitude. Hence, with increasing latitude, the power production for clear sky conditions can be optimized by increasing module inclinations. During cloudy conditions, however, most of the radiation comes from the diffuse component of solar irradiance as optically thick clouds can strongly diminish the direct component of sunlight. Hence, using modules with high inclinations causes a substantial portion of the diffuse radiation to be lost behind

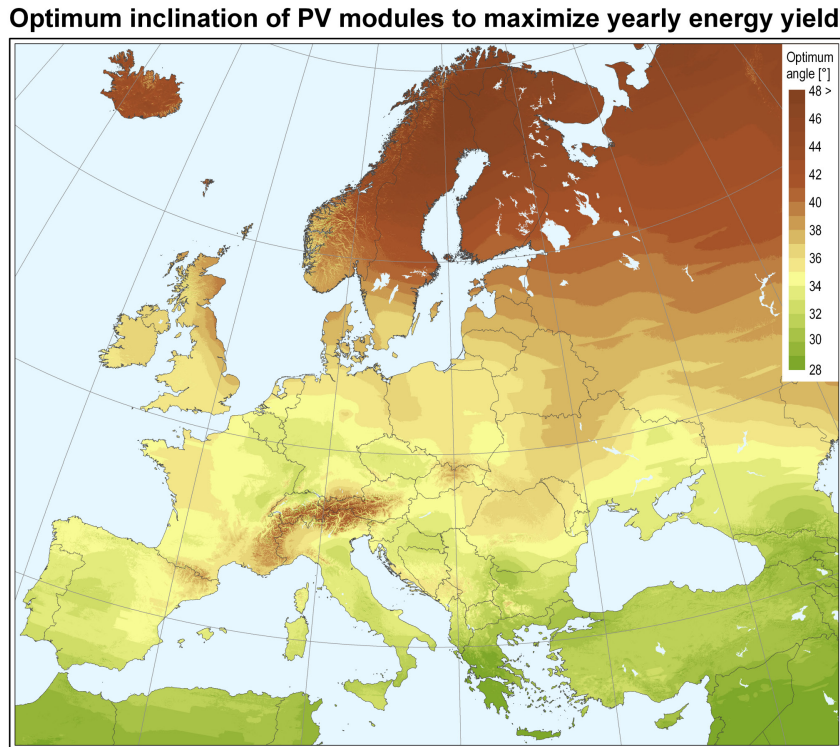


Fig. 2.3: Optimum inclination of the PV modules for a maximum annual yield ©IES, JRC.

the modules during overcast conditions. So, for all practical purposes, the optimum tilt angles are kept at a lower angle than the local latitude. For this study, the optimum tilt angles for each country are chosen from the map (shown in Fig. 2.3) provided by IES [86]. The exact values are given in Table. A.1.

PV systems are often not configured optimally, specially the small stand-alone ones (e.g., roof-top PV). So, to keep the assumptions realistic, a combination of three different module orientations and five different tilt angles are used (Table.2.1). The relative contributions of these configurations to the final power production are substantially different from each other and are taken from the work of Pfluger et al. [67].

For CSP calculations, GHI is converted to the DNI as the mirrors and other concentrating optics require abundant direct solar radiation to be able to effectively focus solar irradiance to the temperatures needed for electricity generation. DNI is given by the direct solar irradiance received by a surface oriented perpendicular to the direction of the sun and is given by:

parameters	configurations	shares
inclinations	$\pm 10^\circ$	5%
	$\pm 5^\circ$	20%
	Optimal	50%
orientations	South-East	20%
	South	60%
	South-west	20%

Table 2.1: A combination of different module configurations as taken from the work of Pfluger et al. [67].

$$\text{DNI} = \frac{\text{GHI} - \text{DHI}}{\cos\theta}, \quad (2.3)$$

where DHI is the diffuse component of irradiance on horizontal plane and  $\theta$  is the solar zenith angle. Since CSP output is exclusively dependent on the direct sunlight (unlike PV, which can also utilize the diffuse component of solar irradiance), its performance is extremely sensitive to cloud conditions.

**Investigation of different PV module configurations:**

The orientations and inclinations of PV modules can significantly influence their gross power production as well as variabilities. In this research work, a substantial part of the analysis is focused on the behavior of different PV module configurations to quantify their impact on storage and balancing needs. It is shown that the South facing optimally inclined (SFOI) may not always be the best to reduce balancing needs, given the average output from all configurations are scaled to match each other. A detailed description on the chosen configurations is presented in Appendix. B.

### 2.2.2 Module-Ib: Submodel for capacity distribution

With a model to analyze the prospects of VRE generation in the future European power system, solar and wind installed capacities and their distributions are expected to improve significantly. In the following section, installed capacities of different renewables and their distribution within single countries is discussed briefly.

### Country level capacity distribution

Country level installed capacities for different renewable generations are taken from two existing studies, hereafter referred to as the ISI [67] and the EREC [82] studies. For the work, scenario B of the ISI study and the energy [r]evolution scenario of the EREC study are used. With the assumption of renewable penetration close to 100% for the year 2050, both studies give projected installed capacities of different VRE generations in Europe. Additionally, the capacity values of individual European countries is given in the ISI study. These values are used to derive the country level capacity values for the EREC scenario. Since both studies exclude the Balkan countries, it is assumed that the area weighted capacity values of the surrounding countries like Greece, Bulgaria, Romania, Slovenia, and Hungary also hold true for the Balkan countries. The projected installed capacities of different VRE sources for Europe after including the Balkan countries are given in Table. 2.2. Although the offshore wind capacity is very similar in both scenarios, the ratio of PV and onshore wind is very different from each other (roughly 1:2 for the ISI scenario while 2:1 for the EREC scenario).

Scenarios	PV	CSP	Onshore wind	Offshore wind
ISI	339.4	18.0	618.8	212.2
EREC	612.3	81.0	317.0	206.7

Table 2.2: Projected installed capacity values (GW) of different renewable energy sources for Europe from the meta-studies after inclusion of the Balkan countries.

For CSP, the ISI and the EREC scenarios project 18 GW and 81 GW installed capacities for Europe, respectively. However, country level capacity values of CSP are not given in these two studies. In the ISI scenario, country level CSP capacity values are given in combination with other renewables like wave, geothermal, tidal etc. Therefore, CSP capacity values for different countries are taken from the EWI Energynautics report [28] and scaled-up to match the value given for Europe in the ISI and the EREC studies. The results of this scaling is summarized in Table. 2.3.

According to the EWI report, only Spain, Italy, and Greece will have operational CSP plants by 2050. These countries are located in Southern Europe where there is sufficient direct sunlight available throughout the year and are quite suitable for CSP plants that operate exclusively on the DNI component of solar irradiance. Hence, only these three countries are investigated here for CSP feed-in.

Countries	EWI	Scaled with ISI	Cumulative with other renewables
Spain	108.9	9.9	15.0
Italy	70.2	6.4	7.5
Greece	19.0	1.7	2.2

Table 2.3: Country level CSP capacities (GW) taken from EWI energynautics report [28] and scaled to the ISI scenario [67].

### Capacity distribution within each country

The capacity distribution of centralized technologies like CSP are inherently different from those of PV and wind which mostly operate as distributed generations. In this section, the capacity distribution within single country is discussed separately for the PV and the CSP plants<sup>4</sup>.

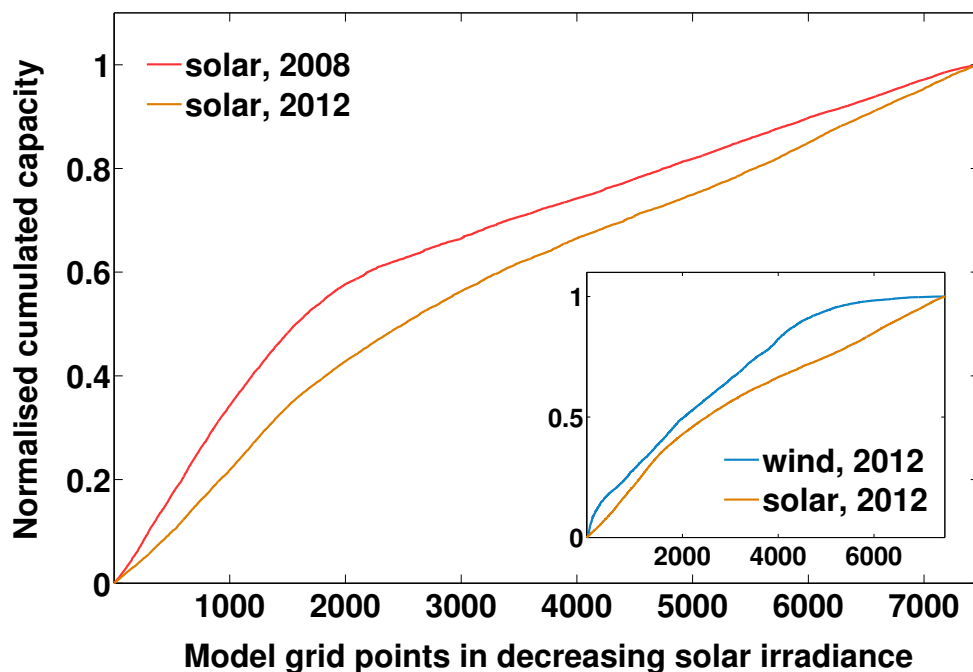


Fig. 2.4: Resource-dependent capacity distribution functions for Germany.

<sup>4</sup>The capacity distribution of wind follows similar methodology as of PV and is discussed in [43]

In this work, an empirical resource-dependent distribution is used for the capacity distribution of solar PV within single countries. Detailed information on the capacity distributions within countries is not available for all investigated countries. Also, it seems unlikely that the distribution will stay similar until 2050. Germany is as of now one of the countries with highest installed PV capacities in Europe. Therefore, it is assumed that Germany's installations might be representative for Europe in the midterm-future (2050). Hence, its resource-dependent distribution should be a realistic way to model the future European PV power generation facilities. The resource-dependent distribution function used here is based on the real distribution in Germany for one of the recent years (2012).

The empirically derived distribution functions modelled for Germany is shown in Fig. 2.4. This function is then applied to all countries to derive their resource-dependent capacity distributions. The distributions show that although installed capacity of wind is significantly high for regions with high average wind speed, its distribution function soon creates a plateau indicating very weak resources for  $\sim 30\%$  of the grid points in Germany (regions which are furthest away from the coasts). The inset of Fig. 2.4 represents the irradiance-dependent PV capacity distribution functions for two years, 2008 and 2012. Since the locations with best available irradiance are filled up first, the curve of 2008 is quite steep in the beginning. With time, other locations with comparatively poor resources are also filled up and this effect is reflected in the curve of 2012.

For a resource-dependent distribution of CSP plants, a different approach is taken as CSP is a centralized technology. The CSP plants need at least a minimum of average DNI available for their proper performances, both technically and economically. According to a DLR report (Ref. [83]), this threshold is set to  $1800\text{kWh}/\text{m}^2$  per year for technical potential and  $2000\text{kWh}/\text{m}^2$  per year for economic potential. Hence, a threshold of  $1800\text{kWh}/\text{m}^2$  of average DNI is set to select the best locations for CSP installation in Spain. For Italy and Greece, however, this threshold is quite inadequate to implement a large number of CSP plants. So, a threshold is reduced to  $1750\text{kWh}/\text{m}^2$  per year for these two countries.

Most operational CSP plants in Spain today have 50 MW capacity [91]. There are also a few larger (100 MW) operational CSP plants in Spain. Assuming reasonable development in CSP technology and the expanded market by 2050, each CSP plant is modelled with 100 MW capacity in the simulations. The distribution of CSP plants as of today and as implemented in the model for 2050 within Spain with average DNI from 2003-2012 is shown in Fig. 2.5.

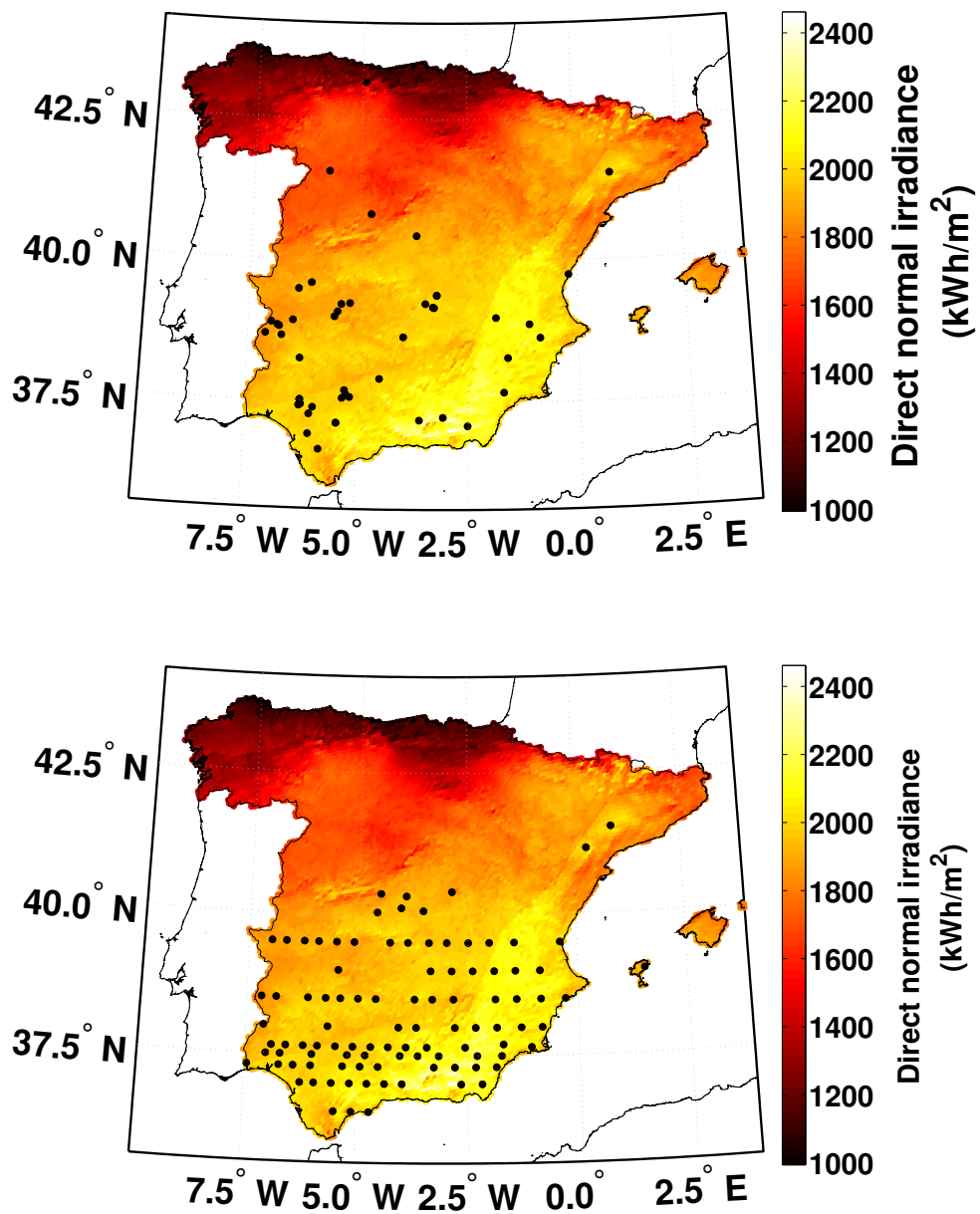


Fig. 2.5: Average DNI map for Spain (2003-2012) in kWh/m<sup>2</sup>/y. Black dots mark the CSP plants operational in 2012 (top) and modelled for 2050 (bottom).



### 2.2.3 Module-Ic: Submodel for power calculation

To estimate how much power is produced, the corresponding meteorological data base is combined with the future-projected capacities. The power output from each model grid point is aggregated to the country level to produce the final feed-in data that is used as input for Module-II. A brief description of the PV and CSP power models is presented in the following section. For the details on the wind power model, the reader is referred to the annual report of the project RESTORE 2050 [43].

#### PV power model

The power model used here is applicable to a variety of module types, including the classic crystalline silicon and various other thin film technologies. Since realistic simulations over large area require a variety of module types to be considered, the power model used here is very suitable for this purpose. This PV power model uses module efficiency from module temperature which is calculated from:

$$T_m = T_a + \gamma I_{POA} \quad (2.4)$$

where  $T_m$  is the module temperature ( $^{\circ}C$ ),  $T_a$  is the ambient temperature ( $^{\circ}C$ ) and  $I_{POA}$  is the solar irradiance on an inclined surface ( $W/m^2$ ). The parameter  $\gamma$  depends on the mounting type of the system.

The calculation of the module efficiency is a two step process. The first step is to compute module efficiency of the PV generators operated in the maximum power point (MPP) using a parametric model:

$$\eta_{MPP}(I_{POA}, 25^{\circ}C) = a1 + a2I_{POA} + a3\ln I_{POA} \quad (2.5)$$

where  $a1$ ,  $a2$  and  $a3$  are device-specific parameters. The next step is to calculate module efficiency at module temperature using:

$$\eta_{MPP}(I_{POA}, T_m) = \eta_{MPP}(I_{POA}, 25^{\circ}C)(1 + \alpha_T T'_m) \quad (2.6)$$

where  $\alpha_T$  is the temperature coefficient, ( $T'_m$ ) is the temperature difference between the module temperature and  $25^{\circ}C$  which corresponds to the standard test conditions.

The numerical values of all the parameters used here is given in the annual report of RESTORE 2050 project [43]. With all the above information on module efficiency, module temperature, and the incoming solar irradiance on inclined surfaces, it is possible to calculate the PV power ( $P_{PV}$ ) output using the following equation:

$$P_{PV} = \frac{\eta_{MPP}(I_{POA}, T_m)}{\eta_{STC}} \frac{I_{POA}}{1000W/m^2} P_{inst} \quad (2.7)$$

where  $P_{inst}$  is the PV installed capacity and  $\eta_{STC}$  is the module efficiency under standard test condition (STC).

### Power model for CSP

The CSP model used in this work characterizes performance equations from the first principles of heat transfer and thermodynamics. Different factors like duration and intensity of solar irradiance, solar field size, system efficiency etc together determine the potential of a CSP plant. In this work, CSP is computed using the following equation:

$$P_{csp} = (1 - Loss_{parasitic}) \eta_{Turbine} A_{sf} (DNI \eta_{opt} - Loss_{HCE} - Loss_{SFP}) \quad (2.8)$$

This functional form of Eq. 2.8 is derived from the Solar Advisor Model (SAM) developed by NREL, in conjunction with Sandia National Laboratory and in partnership with the U.S. Department of Energy [87]. The numerical values of different parameters in Eq. (2.8) are taken from Ref. [94] and are listed in Table 2.4.

Variable	Meaning (unit)	Value
$Loss_{parasitic}$	Electric parasitic loss (%)	11.1 [41]
$\eta_{Turbine}$	Design turbine gross efficiency (%)	36.4 [41]
$A_{sf}$	Solar Field Area ( $m^2$ )	685,666 [94]
$\eta_{opt}$	Optical efficiency (%)	60.2 [41]
$Loss_{HCE}$	HCE Thermal Losses ( $W/m^2$ )	42.629 [87]
$Loss_{SFP}$	Solar Field Piping Heat Losses ( $W/m^2$ )	10.05 [87]

Table 2.4: Numerical values of variables used in power calculation of CSP plants are taken from [94].

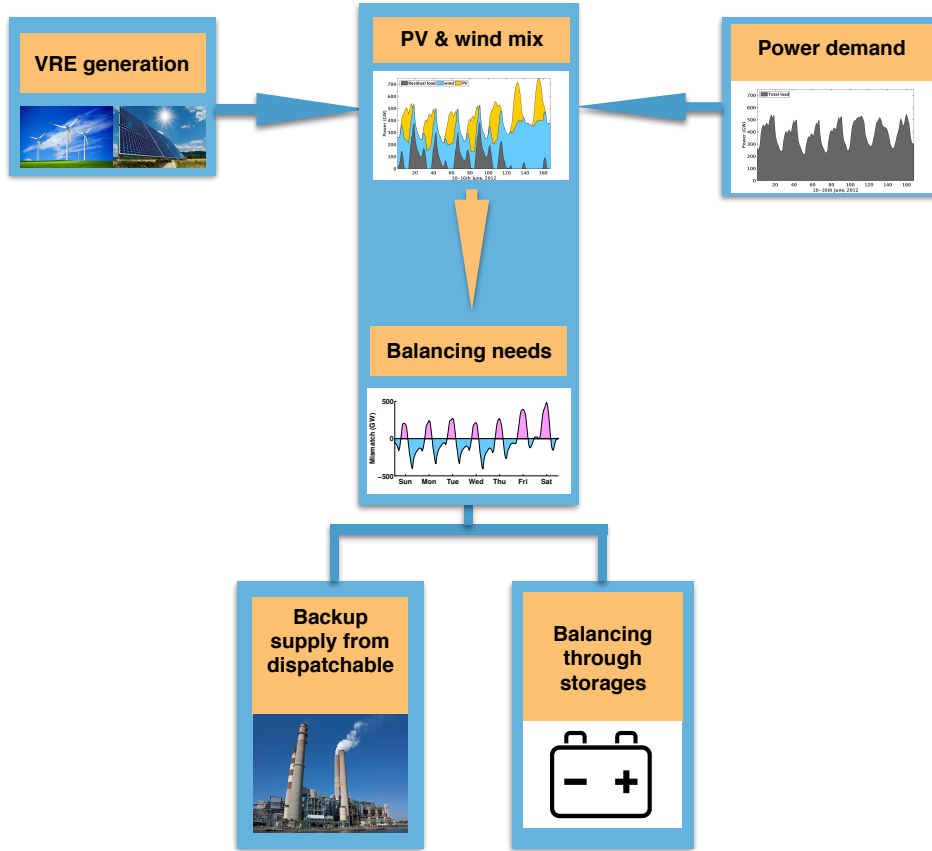


Fig. 2.6: Balancing module: Schematic representation of different components of Module-II and their interplay.

#### 2.2.4 Module-IIa: Mismatch and residual load

The Module-II of this work covers the aspects of mismatch between VRE generation ( $G$ ) and the load ( $L$ ) and by extension the estimation of balancing needs under different scenarios. In Module-II, only PV and wind power are considered in VRE generation. This module is formulated as a 100% renewable-based generation. Other forms of generation from either conventional or dispatchable renewable sources are used here for balancing purposes. The model is developed with the initial condition that over the entire simulation period, average  $G$  exactly matches the average load ( $\langle G \rangle = \langle L \rangle$ ). Under this condition, the mismatch is defined as:

$$\Delta(t) = \alpha G(t) - L(t) \quad (2.9)$$

where  $\alpha$  is a scaling parameter. It indicates situations when average generation is either higher or lower than the average demand.  $\alpha$  values larger than one indicate over-installation while  $\alpha$  less than one denotes under-installation of renewable sources.  $\alpha$  applies a linear scaling on generation at each time step.  $\alpha$  is defined as the average VRE generation factor. It is a measure of how far PV and wind have penetrated into the power system. In this model,  $\alpha$  is not computed, rather a range of pre-determined  $\alpha$  values is used to analyze a variety of scenarios.

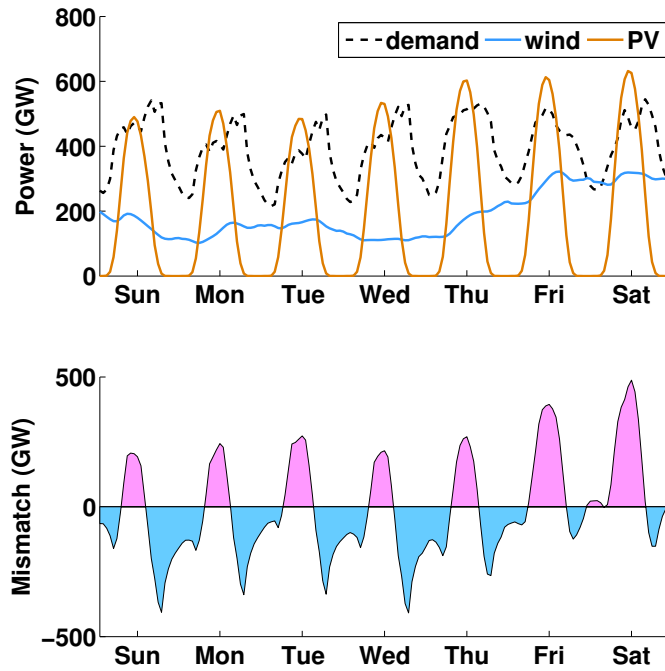


Fig. 2.7: An excerpt of load, wind and PV time series during 10-16 June, 2012 for Europe in the top panel. The bottom panel shows the corresponding mismatch time series calculated for  $\alpha = 1$  and  $\beta = 0.4$  and using PV power generation from South facing optimally inclined modules.

$$\Delta(t) = \Delta_+(t) + \Delta_-(t) \quad (2.10)$$

The estimation of storage and/or backup needs for different combination and penetration level of PV and wind is determined by the different components of mismatch ( $\Delta_+$  and  $\Delta_-$ ). These are further illustrated in Fig. 2.7. Specific combination of PV and wind influence balancing needs on short-term and long-term scales. The PV share

in terms of gross VRE generation is represented as  $\beta$ . Since this model only considers PV and wind as the VRE sources, the wind share is simply given by  $(1 - \beta)$ .

For this work, the term ‘residual load’ is used to indicate any unbalanced demand that is present in the system. In absence of any storage, this directly follows the negative mismatch while in presence of a storage, it refers to the load that still remains uncovered after energy supply from the storage.

### 2.2.5 Module-IIb: Backup model

The variable nature of solar and wind power pose a great challenge on the stability of a power system with high shares of VRE generations. In such systems, power from dispatchable generations often act as backup sources. In this model, backup sources either balance all negative mismatches ( $\Delta_-$ ) present in the system (in absence of any storage) or cover any residual load that remains after energy supply from the storage. Rasmussen et al. [69] formulated a dimensionless parameter ( $E_b$ ) to quantify the backup needs:

$$E_b = \langle \Delta_- \rangle / \langle L \rangle \quad (2.11)$$

The parameter  $E_b$  strongly depends on the share of renewables ( $\alpha$ ) and the mix of PV and wind. Even for very large  $\alpha$  values, it is not possible to completely eliminate all negative mismatches. When average generation is lower than the average load ( $\alpha < 1$ ), the balancing parameter ( $E_b$ ) alone cannot ensure system stability. The authors of Ref. [69] have shown that in such cases, additional balancing is required, which is defined as:

$$E_b^{add} = E_b - (1 - \alpha)_+ \quad (2.12)$$

The average additional balancing ( $E_b^{add}$ ) parameter is a measure of how well the variable resources are integrated into the power system. For  $\alpha$  values greater than or equal to one,  $E_b$  and  $E_b^{add}$  become equivalent.

### 2.2.6 Module-IIc: Storage model

For decades, energy storage has been considered a possibility to avoid expensive standing capacity to meet peak demand. Now with the advent of VRE deployment, the possible services by the storage facilities have acquired new dimension. Storages can play key role in the integration of solar and wind power by decoupling supply

and demand during peak hours of system operations and by providing a bidirectional service both injecting and absorbing energy to and from the grid. By storing energy, curtailment of renewables can be reduced, or even avoided, thus allowing a more efficient use of each infrastructure. In fact, certain storage technologies have faster response rates than traditional thermal generators. Hence, they can provide frequency regulation, voltage control, and load-following services in moments when the system experiences fast and pronounced fluctuations of renewable energy and demand. This model is not restricted to any particular storage technology. Instead of focusing on a specific technology, a rather generic form of ‘storage’ is used here to elicit its value and potential. In this work, the potential of a storage is determined by its size ( $C_s$ ) and its efficiencies. For all practical purposes, energy transaction with storage results in certain conversion losses due to limited storage efficiencies ( $\eta < 1$ ). In situations when instantaneous generation exceeds the instantaneous load, a part of the positive mismatch is lost during storage interaction. Similarly, to balance the negative mismatch during the hours of need, more energy is drawn out of the storage to compensate for the storage losses. These conversion losses in the storage is mathematically expressed as:

$$\tilde{\Delta}(t) = \eta_{in}\Delta_+(t) + \eta_{out}^{-1}\Delta_-(t) \quad (2.13)$$

where  $\eta_{in}$  is the efficiency to put energy in the storage and  $\eta_{out}$  is the efficiency to take energy out of storage. A simple dispatch strategy is used here to model to storage interactions. Any deficit is first covered by the storage unless it runs empty and any excess generation is first stored in the storage until the storage gets full. In order to deal with the remaining power mismatches, dispatchable resources are used as *backup* while all overproduction in power is discarded as *curtailment*.

How storages are filled depends on the mismatch. For an unconstrained storage, the storage filling ( $F$ ) is expressed through the equation:

$$F(t) = F(t-1) + \tilde{\Delta}(t) \quad (2.14)$$

For a constrained storage, however, the upper (and the lower) boundary of the storage must be pre-fixed. Hence, a more general form of Eq. 2.14 is presented:

$$F(t) = \begin{cases} C_s & \text{for } F(t-1) + \tilde{\Delta}(t) > C_s \\ 0 & \text{for } F(t-1) + \tilde{\Delta}(t) < 0 \\ F(t-1) + \tilde{\Delta}(t) & \text{otherwise} \end{cases} \quad (2.15)$$

When the storage level goes beyond storage capacity, the excess power is discarded and if it falls below zero, the remaining unbalanced load is balanced with backup from dispatchable resources. The initial storage filling level is determined by applying the procedure introduced in Ref. [69].

As long as the average power generation required after storage losses exactly matches the average load, the storage capacity can be simply computed from the storage filling time series as:

$$C_s = \max_t(F(t)) - \min_t(F(t)) \quad (2.16)$$

Depending on the parameter settings of  $\alpha, \eta_{in}, \eta_{out}$  the average generation after storage losses can surpass the average load. In that case, the storage filling exhibits a positive drift with time. Heide et al. [34] have pointed out that this requires an alternate definition of the storage capacity. Also, when the parameter settings  $(\alpha, \eta_{in}, \eta_{out})$  lead to a situation that the average generation after storage losses is outweighed the average demand, the storage filling displays a negative drift over time. Considering such situations, the following alternative definitions of storage capacity ( $C_s$ ) are derived:

$$C_s = \max_t \left( F(t) - \min_{t' \geq t} (F(t')) \right) \quad (2.17a)$$

$$C_s = \max_t \left( F(t) - \min_{t' \leq t} (F(t')) \right) \quad (2.17b)$$

Eq. 2.17a is used to compute storage capacity when storage is built up over time following the positive drift from the parameter settings. When parameter settings cause the storage to deplete over time, storage capacity is computed from Eq. 2.17b.





## Chapter 3

# Evaluation of regionally averaged PV power

Evaluation of simulated results against measurements is an integral and invaluable part of model development. Good agreement between simulated and measured datasets indicates that the model can reproduce the real world conditions quite accurately within the scope of its intended use and gives confidence to proceed further with the database. In this chapter, the PV power time series is validated to check the data quality and reliability prior to using it as input for Module-II.

Solar irradiance, and by extension PV power, derived from model simulations are often validated against measurements from single sites [15, 53, 61]. These site-specific studies use very precise information on the system designations, such as the tilt and the azimuth angles of the PV installations, the nameplate capacity of the system along with detailed environmental factors that might affect the power production (such as artefacts from shading by nearby objects [18]). However, these detailed information are not always available, specially when analyzing a much larger area. In such cases, comparison of regionally averaged data is more suitable and efficient than comparing individual PV systems. However, acquiring regionally averaged data requires monitoring a wide variety of representative PV power systems with different configurations and installed capacities. Among the 33 countries simulated in this work, only Germany provides enough PV power data to validate the spatially averaged simulation results with measurements. So, for this chapter, the analysis is restricted to Germany only.

The operation, monitoring, and maintenance of German power grid is controlled by four transmission system operators (TSOs): Tennet, Amprion, 50 Hertz, and TransnetBW. In 2009, these four German TSOs and the European Energy Exchange

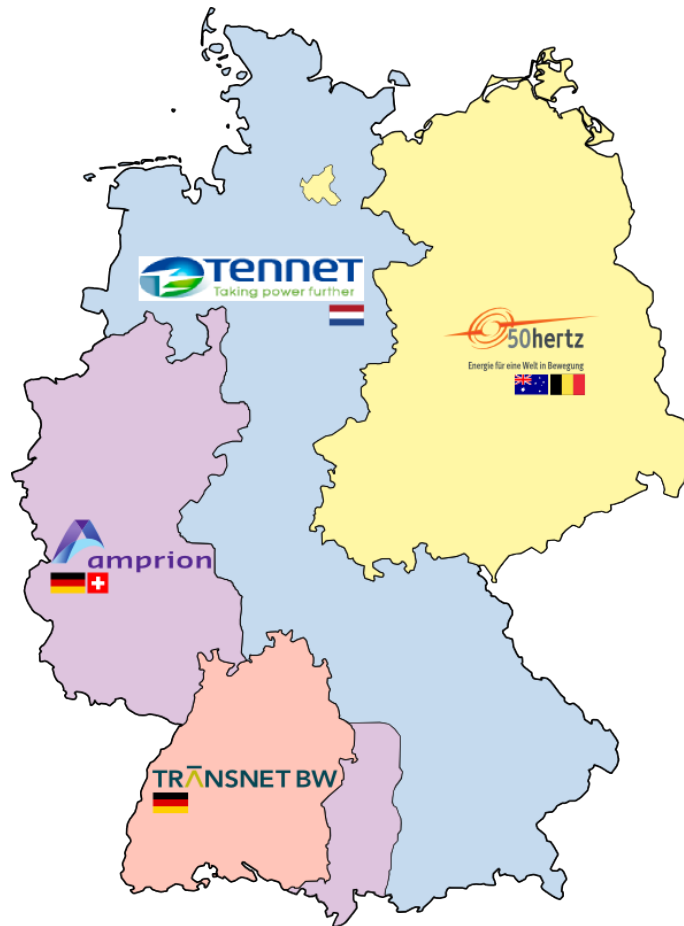


Fig. 3.1: Regional coverage of four TSOs from Germany © Wikipedia: Tennet ([https://de.wikipedia.org/wiki/Tennet\\_TSO](https://de.wikipedia.org/wiki/Tennet_TSO)), [accessed on: 24. 03. 2017]

(EEX) established a neutral platform (Transparency in Energy Markets) to allow transparency in energy markets by allowing access to comprehensive fundamental data and relevant information for wholesale energy trading. On this platform, each TSO publishes the power feed-in data from systems that fall under their respective control areas (Fig. 3.1) on a regular basis. It is to be noted that there are over 1.5 million photovoltaic systems installed all over Germany by the end of 2015 [92], ranging from small roof-top PV systems, to medium commercial and large utility-scale solar parks. Since continuous monitoring of all these systems is practically impossible, each provider performs their own upscaling procedure using a set of PV systems that can represent the spatial distribution of all sites (latitude and longitude), the distribution of installed capacity, and the module configurations (tilt and azimuth angles) of all systems in that control area. As a consequence, the PV feed-in time series provided by the TSOs does not necessarily reflect the actual power, but only a projection of PV power based

on different models. To emphasize this, the measurement data used in this work is referred to as the ‘upscaled measurements’ instead of just ‘measurements’.

Taking the liberty that four TSOs provide regionally averaged PV power data for their respective control zones, here the evaluations for each control zone as well as for Germany as a whole are included. Additionally, the TSO Tennet provides PV power data for all the federal states that fall within its domain. So, a multi-scale analysis of regionally averaged PV power data is provided as follows:

Country → Control zones → Federal states

The quarter-hourly measurement data are averaged to the hourly scale (rounding around the hours) for a reasonable comparison with the simulated PV data. Since only a few years from the simulation period overlap with the period for which measurement data is provided by the TSOs, the analysis in this chapter is focused only on one particular year: 2012. As the PV installed capacities used in the simulation of Germany are significantly larger than that of 2012, both simulated and measured PV power time series are normalized with their respective capacities. Unfortunately, detail information on the changes in installed capacities throughout 2012 was not available. As information on the capacity values were only known for the beginning and the end of 2012, a linear increase in capacity was assumed for the simulation. The information on the installed PV capacities for each control zone are taken from a database published by the TSOs as a mandatory regulation under the Renewable Energy Sources Act (RES), 2014 (or Erneuerbare Energien Gesetz (EEG) in German). The RES datasets are published by the TSOs [1, 2, 4, 5] on a regular basis by the Federal Network Agency (Bundesagentur). However, this database doesn’t include information on the tilt and the azimuth angles of the PV systems. To allow a legitimate comparison with measurements, the PV power for this particular chapter is derived using the capacity distribution and the PV module configurations as of the real world in 2012. The latter is deduced from the analysis of the *Meteocontrol GmbH* [48].

### 3.1 Evaluation on country level

This section comprises of the comparison between regionally averaged simulated and measured PV power data for Germany. According to [21], the installed capacity of PV in Germany increased from 24.28 to 32.44 GW during 2012. To normalize the upscaled measurements, a linear increase in capacity is assumed and applied.

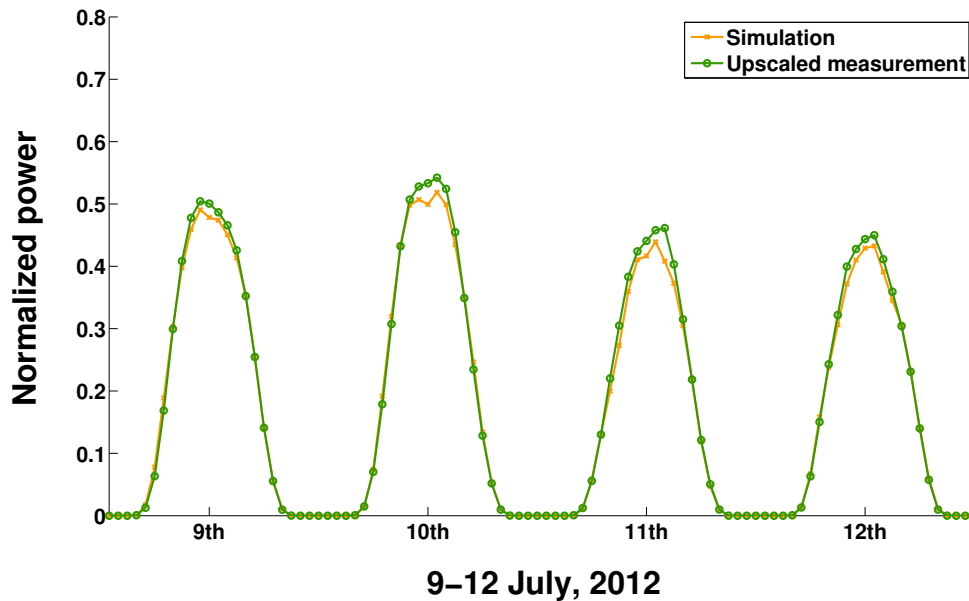


Fig. 3.2: Comparison of simulated and upscaled measured regionally averaged normalized PV power for Germany.

Here the comparison between simulated and measured PV power is presented on multiple scales to verify their behaviors on diurnal and seasonal changes. Fig. 3.2 shows the diurnal patterns of normalized PV power during four summer days. Due to the averaging of the data over a very large area (entire Germany), the diurnal shapes in Fig. 3.2 appear quite smooth. In spite of this smoothing effect, the simulation results also indicate the partial coverage of clouds on 10<sup>th</sup> of July, 2012.

Fig. 3.3 summarizes the comparison of simulated and measured data for the complete year on two different temporal resolutions (hourly and daily). It shows that the results of this comparison are in good agreement with each other, except for a few days in winter and in spring. This difference results from the assumption of linear increase in capacity and from snow covered modules that are not corrected in the model. Some statistical measures to compare simulated and upscaled measured data of normalized PV power are given in Table 3.1. It shows that the Bias and the RMSE values are quite low, specially on daily resolutions, whereas they have very high linear correlation coefficients. The capacity factor<sup>1</sup> values calculated are also very close to one another (11.30% for simulation and 11.29% for upscaled measurements). Overall,

<sup>1</sup>Capacity factor is the ratio of net electricity generated for the time considered to the energy that could have been generated at continuous full-power operation during the same period (<https://www.nrc.gov/reading-rm/basic-ref/glossary/capacity-factor-net.html>).

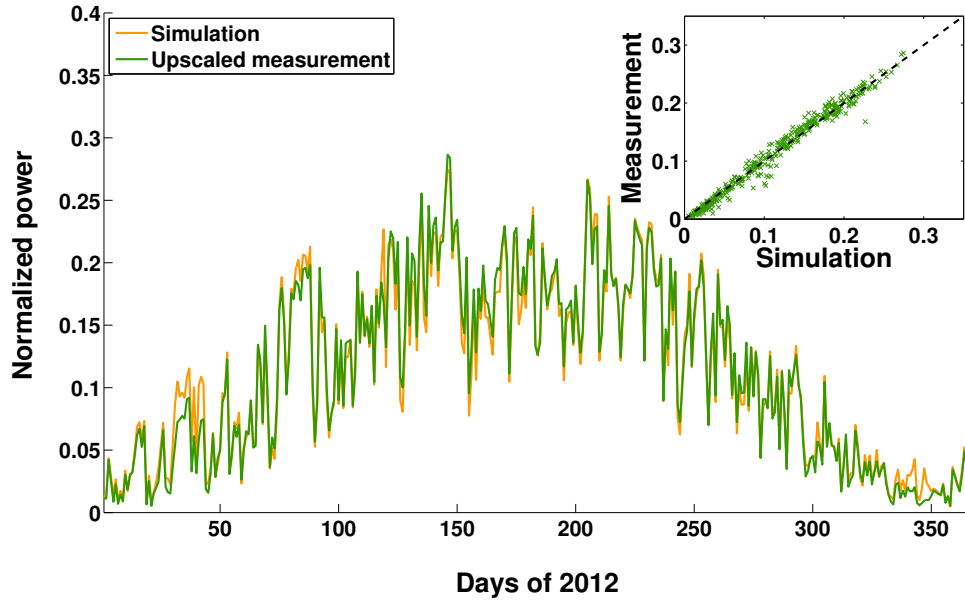


Fig. 3.3: Comparison of simulated and upscaled measured normalized PV power for Germany, 2012. The time series is shown for daily mean values while the scatter plot in the inset is given on the hourly scale.

these quantitative estimates strongly assert good agreement between simulated and upscaled measured regionally averaged PV power data for Germany.

	RMSE	RMSE <sub>rel</sub>	Bias	STDERR	Correlation coefficient
Hourly	0.029	0.136	0.000	0.029	0.988
Daily	0.010	0.090	0.000	0.010	0.990

Table 3.1: Comparison of statistical measures of normalized PV power time series of Germany for 2012 (rounded to 3 digits after decimal).

## 3.2 Evaluation of control zones

This section covers the validation of simulated PV power averaged over each control zone against upscaled measurements of the same. Under the RES act, it is mandatory for all PV sites in Germany to be registered. The RES database includes site-specific information on the installed capacity with the initial date of operation. In order to

achieve the highest possible transparency while at the same time ensuring the protection of personal data (in accordance to the provisions of the Federal Data Protection Act or the German Bundesdatenschutzgesetz (BDSG)), this data is published with location information restricted only to the postal code resolution. In order to identify these control areas inside the model domain, the postal codes are converted<sup>2</sup> to the latitude and longitude values [3] to simulate regionally averaged PV power data for each control zone.

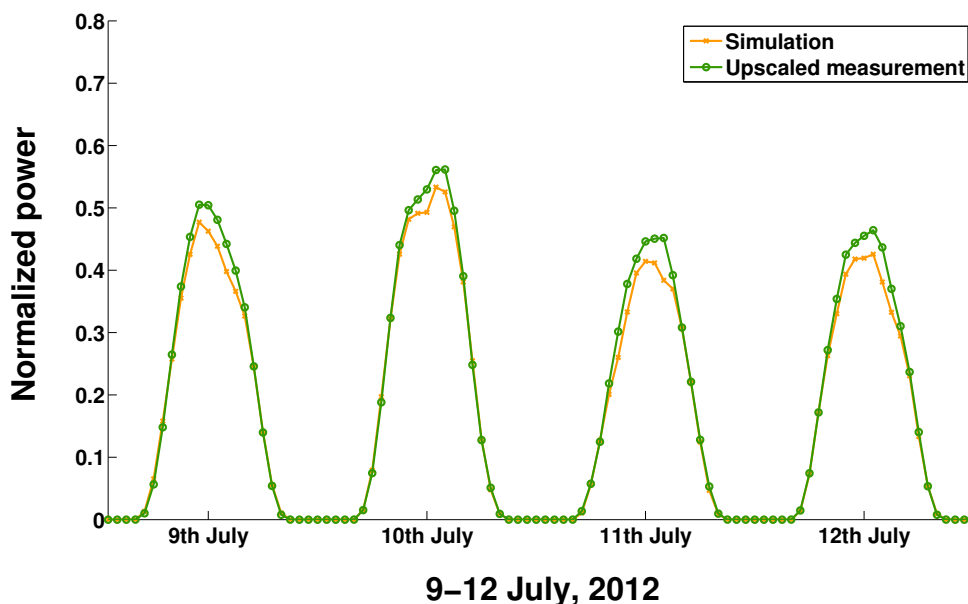


Fig. 3.4: Comparison of simulated and upscaled measured regionally averaged normalized PV power for the control zone of Tennet.

The hourly time series of normalized power averaged over the control area of Tennet is shown in Fig. 3.4 for four summer days. These diurnal curves are less smoother than those shown in Fig. 3.2, since the averaging is applied here over a much smaller domain. Overall, the simulated data agrees well with the upscaled measurements.

A further analysis includes the complete year on hourly and daily resolutions (Fig. 3.5). The corresponding statistical measures are given in Table. 3.2. 50Hertz exhibits the highest spread with large RMSE and Bias. This is also in accordance to Fig. 3.5. This is partially due to the assumption of linear increase in capacity

---

<sup>2</sup>It is to be noted that in this conversion process, a very small fraction of capacity is lost (for example, only  $\sim 0.78\%$  capacity is lost for Tennet) due to technical issues such as unidentified postal codes, spurious data, the converted coordinate falling outside the German border used for the model domain etc.

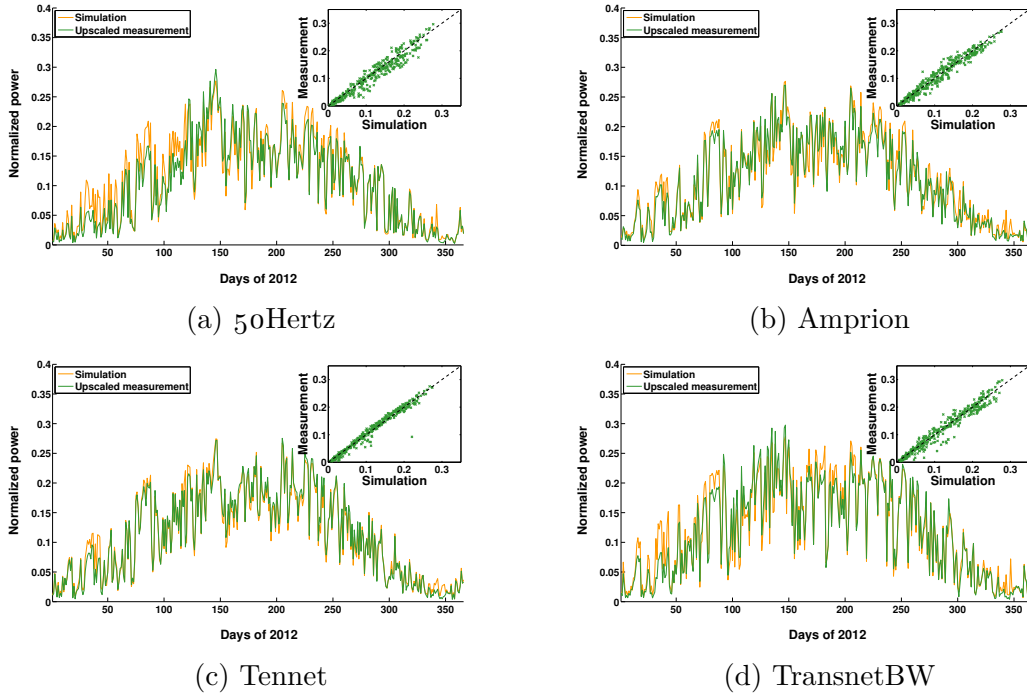


Fig. 3.5: Comparison of simulated daily PV power with upscaled measurements for four TSOs in Germany, 2012. All time series are normalized to their respective installed capacities. In the inset is the scatter plot of normalized hourly time series.

used in the simulation. It is discussed in [48] that the increase in capacity through 2012 for different control zones are not quite linear. It is discussed in [48] that this non-linearity is most prominent for the 50Hertz, specially in the beginning of the year. This effect is reflected in the comparisons shown in Fig. 3.5 which also shows that highest discrepancy is exhibited by 50Hertz (Fig. 3.5a). Another practical problem with network operators' reports is that, for technical reasons, their network areas are usually not directly covered by the administrative boundaries of municipalities or counties. While converting the postal codes to the latitude and longitude values, sometimes the converted coordinate falls outside the country border used by the model and are usually discarded. As a consequence, the model domain selected for simulating each control zone is not strictly the same as the real world. Apart from these issues, there are also the effects of snow covered modules discussed in Sec. 3.1.

In spite of all these constraints, the simulated data shows overall good agreement with the upscaled measurements. The capacity factor values calculated for each TSO are also pretty close to each other (Table. 3.3). Other statistical measures for quantitative comparison are given in Table. 3.2. The correlation coefficients of all four TSOs are

	Control Zones	RMSE	RMSE <sub>rel</sub>	Bias	STDERR	Correlation coefficient
Hourly	50Hertz	0.045	0.226	0.012	0.043	0.973
	Amprion	0.038	0.181	0.004	0.038	0.978
	Tennet	0.030	0.140	0.001	0.030	0.987
	TransnetBW	0.045	0.194	0.006	0.045	0.976
Daily	50Hertz	0.018	0.178	0.006	0.017	0.971
	Amprion	0.015	0.136	0.002	0.015	0.977
	Tennet	0.012	0.105	0.000	0.012	0.987
	TransnetBW	0.017	0.142	0.003	0.017	0.977

Table 3.2: Comparison of statistical measures of normalized PV power time series for four TSO controlled zones for 2012 (rounded to 3 digits after decimal).

Control Zones	Upscaled measurements (%)	Simulation (%)
50Hertz	10.3	11.0
Amprion	10.9	11.1
Tennet	11.2	11.2
TransnetBW	11.9	12.2

Table 3.3: List of capacity factors (%) of each control zone calculated for simulations and upscaled measurements.

quite high ( $> 0.97$ ). Among them, Tennet shows best agreement in both hourly and daily scales.

### 3.3 Evaluation of selected German federal states

Among all the TSOs in Germany, only Tennet provides upscaled measurement data for six federal states that fall within its control area. These are Schleswig-Holstein, Bremen, Lower Saxony, North Rhine-Westphalia, Hesse, and Bavaria. In this section, a comparison of simulated and upscaled measured data of two selected federal states (Schleswig-Holstein and Bavaria) is presented. The installed capacities at the begin and the end of 2012 for these two federal states are taken from the annual statistical



reports produced by the ‘Bundesnetzagentur’ of Germany (EEG-Statistikbericht [10] and [12], respectively).

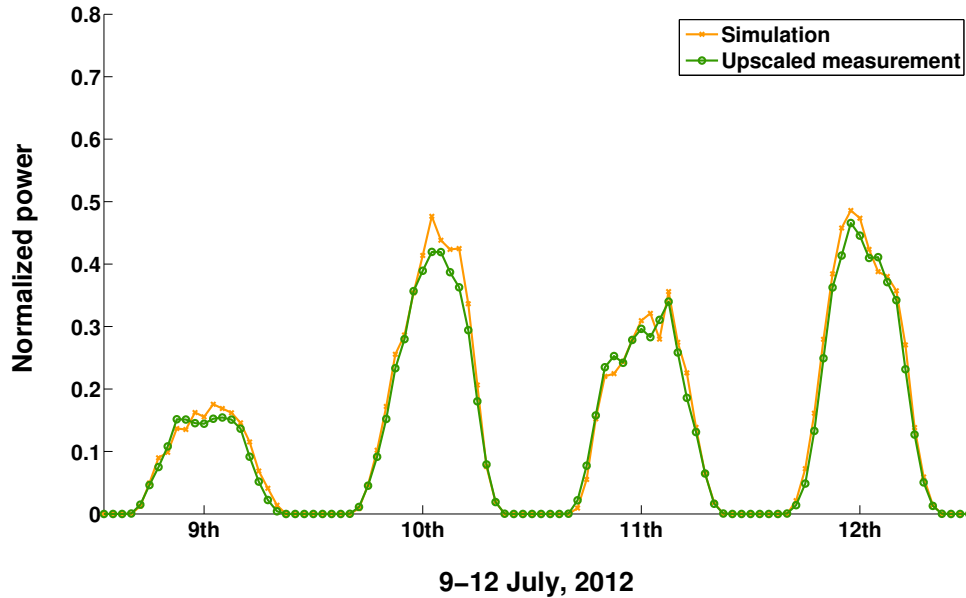
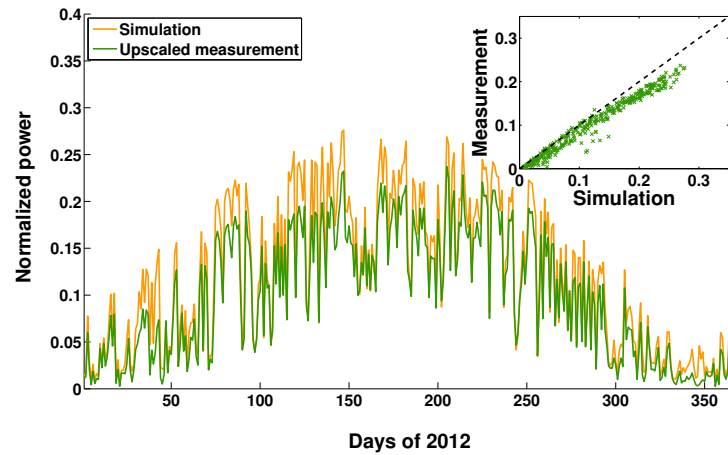


Fig. 3.6: Comparison of simulated and upscaled measured regionally averaged normalized PV power for the German federal state of Schleswig-Holstein.

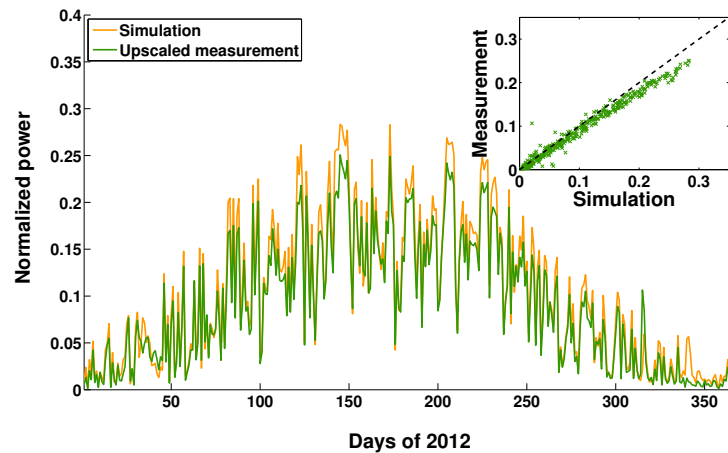
The hourly time series of four summer days is shown in Fig. 3.6 for Schleswig-Holstein. In this figure, days with different cloud conditions (clear-sky, broken-clouds, and overcast) are nicely discernible. Similar figures shown earlier (Fig. 3.2 and 3.4) for the same days lack this information on cloud conditions due to averaging over much larger surface areas. In Fig. 3.6, the simulated results are seen to follow the upscale measurements very closely, with only some minute differences in the details.

Fig. 3.7 shows the comparisons of normalized PV power from simulation and upscaled measurements for Bavaria and Schleswig-Holstein. The results of Bavaria are in less agreement with the upscaled measurement compared to Schleswig-Holstein. The quantitative estimates of their comparison are given in Table. 3.4.

There are several factors that contribute to the low correlation between simulated and upscaled measurements for Bavaria. First of all, Schleswig-Holstein is the only state that is fully covered by Tennet. For the remaining five states, Tennet offers only partial coverage (Fig. 3.8). However, exact latitude-longitude information on the regional coverage of Tennet was not available. Hence, all simulations were performed for the complete federal states. As a consequence, the total area used in the simulations of Bavaria are roughly one fifth times larger than the true coverage of the state by



(a) Bavaria



(b) Schleswig-Holstein

Fig. 3.7: Comparison of simulated daily PV power with upscaled measurements for two federal states of Germany, 2012. All time series are normalized to their respective installed capacities. In the inset is the scatter plot of normalized hourly time series.

Tennet that corresponds to the measurement data (Fig. 3.8). Thus, the results of Schleswig-Holstein (Fig. 3.7b), are in better agreement than that for Bavaria (Fig. 3.7a).

Apart from the issue of spatial coverage, there is also the problem of the assumption of linear increase of PV installed capacity throughout 2012 (discussed in Sec. 3.1 and 3.2). In fact, it is not just the assumption of linearity, but also installed capacity values themselves that can significantly affect the normalized power comparison. Additionally, if either initial or the final PV capacity value is inferred poorly, the slope of increasing capacity can be significantly changed. This, in turn, can influence the time series of PV power when normalized with respect to their installed capacities.

	Federal States	RMSE	RMSE <sub>rel</sub>	Bias	STDERR	Correlation coefficient
Hourly	Bavaria	0.057	0.298	0.038	0.043	0.985
	Schleswig Holstein	0.041	0.231	0.021	0.035	0.986
Daily	Bavaria	0.025	0.252	0.020	0.016	0.987
	Schleswig Holstein	0.017	0.184	0.011	0.013	0.990

Table 3.4: Comparison of statistical measures of normalized PV power time series for two German federal states which are partly/fully covered by Tennet for 2012 (rounded to 3 digits after decimal).



Fig. 3.8: Regional coverage of the federal states by Tennet © Tennet (<https://www.tennetso.de/>), [accessed on: 24. 03. 2017]

It is to be noted here that this effect will be more prominent when analyzed over relatively smaller domains like the federal states as installed capacity values inferred from erroneous data or even unregistered small PV systems can significantly influence the end results.

With all these issues explained, the comparison between simulated and upscaled measured results of Bavaria and Schleswig-Holstein appear, in general, satisfactory. They have high correlation coefficients and low RMSE and Bias, specially Schleswig-Holstein. The capacity factor values calculated for Bavaria are 9.97% for upscaled

measurements and 11.93% for simulations. For Schleswig-Holstein, the capacity factor from the upscaled measurements is 9.10% while that from the simulations is 10.17%.

### 3.4 Summary

In the previous sections, a multi-scale evaluation of PV power is presented for Germany during 2012. Several factors have been pointed out and discussed in details to highlight any mismatch that remains between the simulated and upscaled measurement data. These include the issues of spatial coverage, assumption of linear increase in capacity, the corrections for the snow covered modules, the unidentified postal codes etc. The evaluation manifests that the agreements between simulated and upscaled measured normalized PV power data increase from the comparisons of the federal states to the control zones to that of the entire country. The spatial averaging over larger domain aids in the smoothing effect, resulting in improved agreement with increasing regional coverage. It is to be noted here that the measurement data used in this context are actually derived from a set of representative system, computed internally by each TSO. This data is often provided without any internal validation. As a result, most of the times this database includes erroneous values. Hence, these upscaled measured data, strictly speaking, do not necessarily reflect the reality. In spite of all these factors, the model is found to reproduce the upscaled measurements quite well. Not only the annual patterns are well matched but also the diurnal changes are nicely captured by the model. These results give confidence to the model and allows to proceed further with this data set.

# Chapter 4

## Variability analysis of VRE sources

The major challenge linked to the integration of renewable energy sources is the weather-driven nature of the most promising resources, namely solar PV and wind. The risks associated with high levels of PV and/or wind penetration to the power system are discussed in Chapter. 1. Understanding the variability will allow system planners and operators to develop effective measures such as reinforcement of cross-border transmission, demand flexibility, and usage of storage and backup systems to ensure satisfactory and reliable system standards. This particular chapter is dedicated to the analysis and quantification of the variable nature of solar and wind resources, along with the variability of the power demand wherever necessary.

Variability is a multi-faceted concept that is best described by a number of distinct parameters. Thus, variability has different characteristics and depend also on the scale of measurement. In a recent review on the variability characteristics of European wind and solar power resources [30], the authors have identified certain measures that are most widely used in the field to assess the characteristics of these variable resources. In this work, a subset of those recommended measures, which are best suitable in the context of the present research, have been used. These selected measures are spatial correlations, long term distributions, step changes, cross-correlations, and predictable patterns. Unpredictability is also often considered as a variability characteristic, but is not included here to limit the scope of this study.

This chapter consists of the following topics: A brief overview of the spatial distribution of resources is given in Sec. 4.1. The diurnal and seasonal patterns of solar, wind and power demand are discussed subsequently in Sec. 4.2 and Sec. 4.3, respectively. Any finer analysis on the intra-hour resolutions are beyond the scope of this work. For the time resolutions larger than the seasonal scales, such as the inter-annual variability, the reader is referred to the annual report of RESTORE

2050 [43]. For the most part of this chapter, the main focus will be on solar energy, specifically solar PV.

## 4.1 Spatial variability of resources

The geographic distribution of average solar irradiance and wind speed are highly inhomogeneous. Solar irradiance has a latitudinal gradient that gradually decreases from the equator towards the poles. Additionally, clouds (and atmospheric turbidity) also influence regional insolation. Hence, arid regions with mostly clear skies usually have high average solar irradiance compared to any other location along the same latitude. The spatial distribution of PV capacity factors in Europe is shown in Fig. 4.1. The average and the standard deviation of PV capacity factors are calculated for ten years of simulation and shown in Fig. 4.1a and Fig. 4.1b, respectively. In the Southern Europe, capacity factors can reach over 0.18 while for the Scandinavian countries it ranges between 0.07 - 0.11. These numbers are close to the findings in Ref. [35]<sup>1</sup>. While the latitudinal gradient of solar irradiance is clearly visible in Fig. 4.1a, the larger deviations over the mountainous regions of Europe is indicated in Fig. 4.1b. Suri et al. [81] have found similar increase in standard deviations of solar irradiance over central Europe and argued that stronger altitude gradients of these mountainous terrains cause this higher standard deviations. Just as solar irradiance, wind speed also has a characteristic spatial distribution with major influence by the surface roughness. Hence it strongly increase over smooth ocean surfaces while reducing significantly over the land, specially in urban regions with tall building structures. For the details of the spatial distribution of wind power, please see the annual report of RESTORE 2050 [43].

It is to be noted that integration of large amount of variable renewable resources require additional investments in terms of power transmission as high resource regions do not necessarily correlate with the high demand locations. In this study, unlimited transmission is assumed between neighboring countries and the power grid is assumed to cope with large shares of renewables ensuring reliable and stable operation.

Fig. 4.1a illustrates that PV power production follows markedly different patterns in different European countries. Table. 4.1 shows some descriptive statistics about

---

<sup>1</sup>According to Ref. [35], the full-load hours in Scandinavian countries for sites using optimally inclined modules range between 650 to 800 hours/annum. In terms of capacity factor, these values read 0.07 and 0.09, respectively. For Southern Europe, full-load hour values of greater than 1500 hours/annum are reported, which roughly translates to the capacity factor of 0.17.

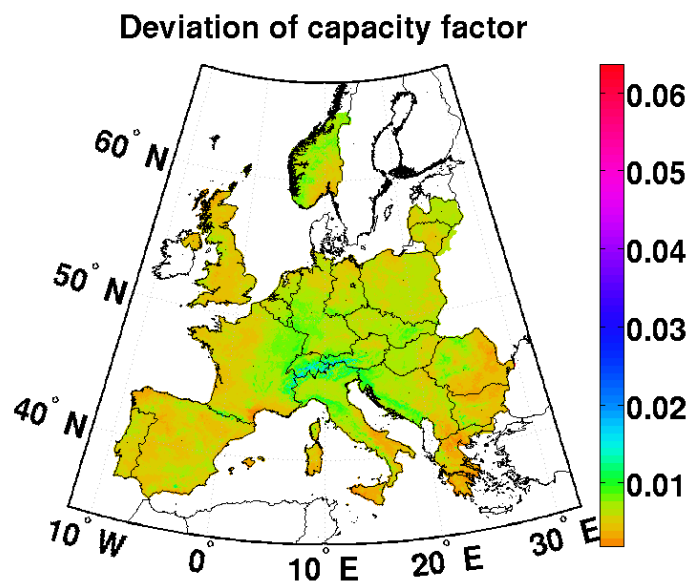
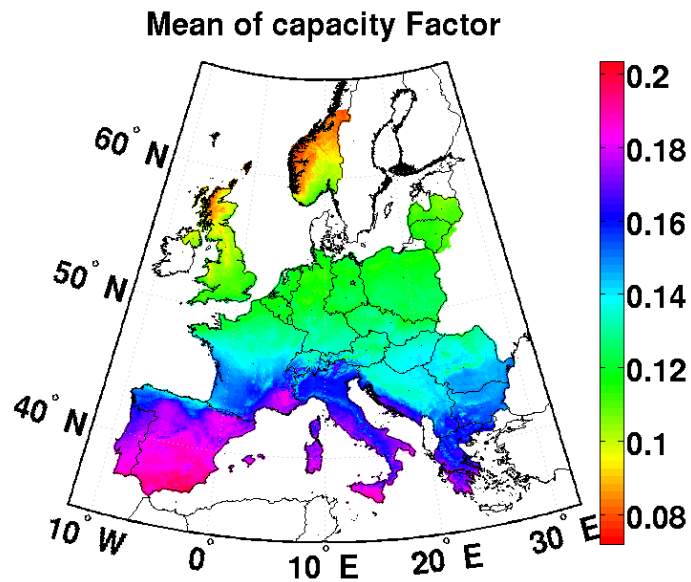


Fig. 4.1: Annual average (4.1a) and annual standard deviation (4.1b) maps of PV capacity factor for Europe calculated over ten years (2003-2012).

the mean value of PV capacity factor and its hourly variability based on ten years of simulation for the five selected countries. Countries in the South, such as Spain and Italy, receive high solar irradiance throughout the year and have highest mean values and lowest year-to-year deviations. Of all the 33 countries simulated in this work, the mean of annual capacity factors is highest for Spain (0.181), followed by Portugal (0.178) and lowest for Norway (0.093), followed by United Kingdom (0.106)<sup>2</sup>. For a detailed discussion on the inter-annual variability of capacity factors of different countries and their cross-correlations, the reader is referred to the annual report of RESTORE 2050 [43].

	Austria	Germany	Spain	France	Italy
Mean	0.135	0.124	0.181	0.148	0.168
Std.	0.007	0.006	0.004	0.005	0.004
Correlation					
Austria	1.000	0.947	0.491	0.881	0.892
Germany		1.000	0.248	0.898	0.862
Spain			1.000	0.405	0.399
France				1.000	0.726
Italy					1.000

Table 4.1: Mean, standard deviation (Std.), and correlation coefficients of PV capacity factors computed over the ten years of simulation period for five selected countries.

The power generation from VRE sources over a large geographic area can significantly balance the ramps from individual sites. This ‘smoothing effect’ is also mentioned in Chapter. 3 for multi-scale validation of PV power for Germany. The reduction of variability through spatial aggregation can be observed even on smaller scales, such as a PV plant or a wind park. This is because not all PV panels (or the wind turbines) in a park are affected by the moving clouds (or by the wind gust) at the same time. Mills et al. [73] have shown that although changes in insolation at a point due to passing clouds can exceed 60% of the peak insolation in a matter of seconds, the changes in overall insolation caused by the passing cloud to shade the entire plant, in contrast, is rather gradual and depend on the system size, cloud speed, cloud height, and other factors. In the past few years, a number of articles have been published which address this phenomenon of spatial smoothing for wind and solar

<sup>2</sup>This does not include those five countries with zero PV installed capacity assumed from the meta study [67], scenario-B. These countries are Estonia, Denmark, Finland, Ireland, and Sweden.



resources [46, 65, 89, 19, 14, 90, 13]. The smoothing of power variability via grid expansion aids in enhancing the quality and the reliability of the power generated by large grid-connected plants that are negatively affected by the source characteristic variability.

## 4.2 Diurnal variability

The Day-ahead market of European power system operates on hourly resolution [70]. Thus, grid operators and system planners are often interested in the assessment of solar (and wind) variability on the hourly scale. In this section, resource variability and their hourly ramp rates are analyzed and discussed.

Since the two solar technologies discussed in this thesis, namely solar PV and CSP, operate with different components of solar irradiance ( $I_{\text{POA}}$  and DNI, respectively), it is important to understand their response to atmospheric variabilities. Various studies have shown that DNI is much more sensitive to the changes in clouds and aerosols than GHI and  $I_{\text{POA}}$  [31, 58, 75, 76]. In absence of clouds and neglecting other sources of errors, the impact of aerosols in direct surface irradiance is about three to four times larger than it is for GHI [31]. This is because the changes in clouds (and aerosols) produce counteracting variations in the direct and diffuse components that largely cancel out for GHI. Fig. 4.2 shows the comparison between GHI and DNI for two example days in Spain with different cloud conditions. Due to high sensitivity of DNI to clouds, CSP plants are primarily constructed over deserts where the influence of clouds are minimal. For the rest of this chapter, the discussion will be constrained only to solar PV, allowing a deeper understanding of its characteristics fluctuations.

Fig. 4.2 shows that irrespective of the component, solar irradiance has a very prominent diurnal course primarily governed by the sun's position in the sky. This induces an inevitable constraint of no solar power generation at night. On clear days, the diurnal curve of PV power usually has a characteristics bell shape. However, the exact shape of the curve strongly depends on the module configurations. Fig. 4.3 displays the average diurnal PV power from different module configurations along with the wind and the load curves. While sun-rise and sun-set times are manifested differently on modules with different orientations, their relative differences become more prominent with increasing module inclinations. The daily course of wind, however, is much weaker than that of solar resources, specially when averaged over a large area and a long period of time. For most European countries, the load curve has a prominent diurnal variability, with a primary peak in the evening. This indicates that

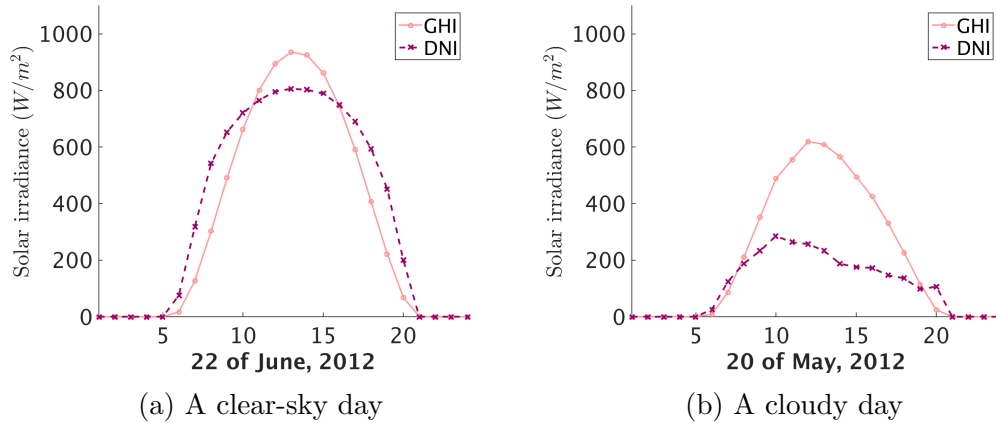


Fig. 4.2: Comparison between GHI and DNI in Spain for two days with different cloud cover.

highly inclined West facing modules may be very suitable to match the daily load curve, specially in scenarios with no other available measures to compensate for the strong diurnal variability of PV. This will be discussed in details in Chapter. 5.

Along with the qualitative comparison of PV power from different module configurations (shown in Fig. 4.3), it is also important to present a quantitative measure of their variabilities. Standard deviation is one of the most useful quantity to estimate fluctuations of VRE sources. Fig. 4.4 summarizes the standard deviations of PV power from each of the 55 configurations analyzed in this work, all normalized to their average power. On one hand, South facing modules have least hourly standard deviations, with lowest being the highly inclined ones. On the other hand, the East/West facing modules have high standard deviations, specially for highly inclined modules.

One of the major challenges for power systems with very high shares of variable resources is their ability to respond to changes in power demand and generation. Apart from the issues of forecast uncertainties, the variability of wind and solar power stresses system operations by causing balancing resources to cycle more frequently and by generating ramps of extreme steepness or duration [38]. To meet these challenges, the power system needs to be flexible. Ma et al. [56] defined flexibility as the power system's ability to cope with uncertainty and variability in demand and generation to maintain system reliability at reasonable additional costs. A quantitative estimation of flexibility requirement is often expressed with power ramps, i.e., the change of power over a given time interval of  $h$ :

$$\Delta_h P(t) = P(t) - P(t - h) \quad (4.1)$$

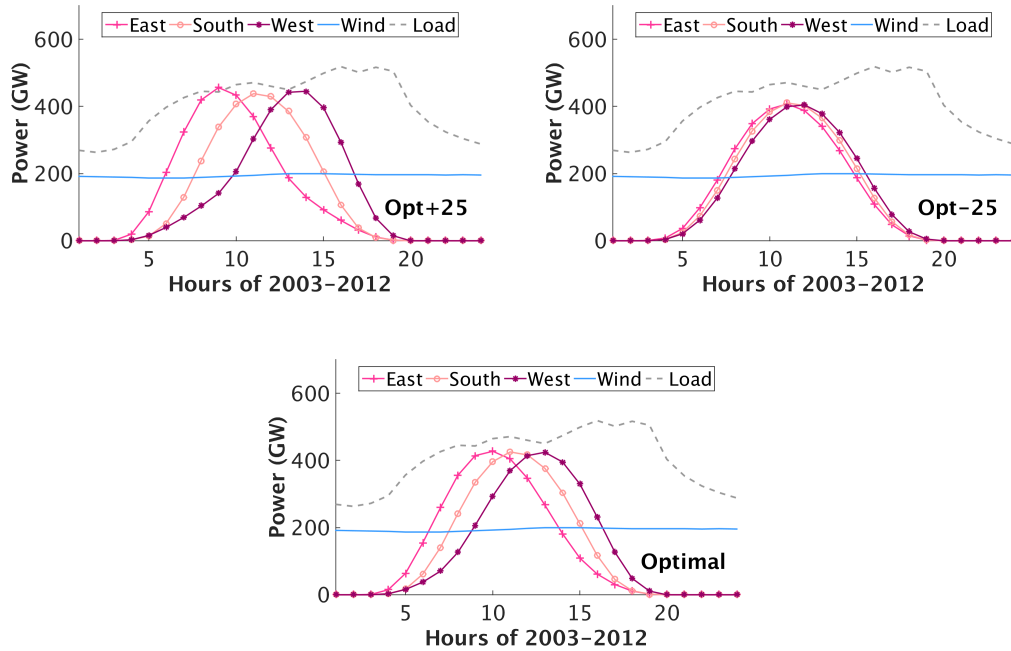


Fig. 4.3: The diurnal variation of European load, wind, and PV power from different module configurations averaged over the simulation period in a power system with  $\alpha = 1.0$  and  $\beta = 0.4$ .

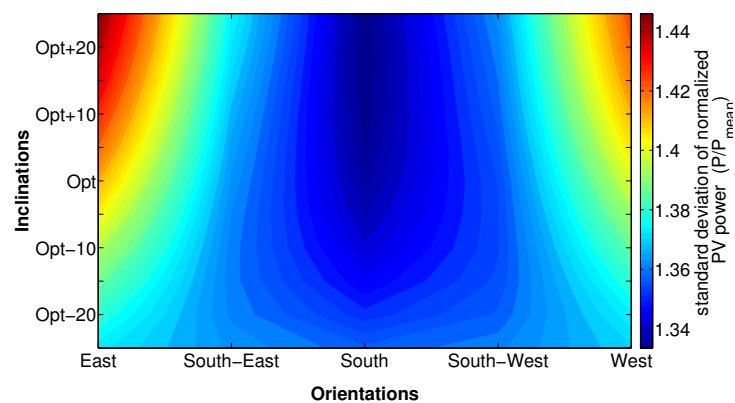


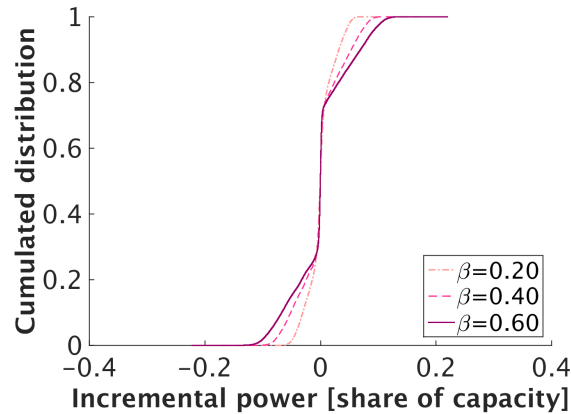
Fig. 4.4: Hourly standard deviation of 55 different module configurations. This standard deviation is normalized to the mean PV power.

where,  $P(t)$  is the power generation at time  $t$ . In a special report by North American Electric Reliability Corporation (NERC) [7], the authors have identified ramp magnitude, ramp frequency, and response time as the primary measures of flexibility requirements. Several studies have addressed these issues related to system flexibility focusing on finding metrics of flexibility [56, 49, 85, 57]. Huber et al. [38] have determined that flexibility requirements increase strongly in systems with combined wind and PV contribution of more than 30% of total energy ( $\alpha > 0.3$ ) and a share of PV in the renewables mix above 20 – 30% ( $\beta > 0.2-0.3$ ). A summary on the statistical measures of the variability of power generation and power ramps is presented in Table. 4.2 for different shares of solar PV and wind for Europe. While standard deviation of power ramps steadily increases with increasing solar shares, deviation of power generation is lowest around  $\beta = 0.1-0.2$ . It is noteworthy here that Heide et al. [34] have found that this is also the optimal mix of solar and wind resources in terms of minimum balancing requirements.

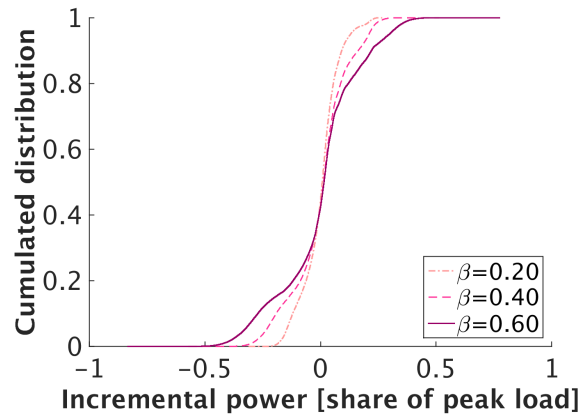
Solar share ( $\beta$ )	Power			Ramp		
	Mean	Max.	Std.	Mean	Max.	Std.
1.00	0.67	3.49	0.90	0.18	1.32	0.21
0.90	0.67	3.23	0.80	0.17	1.19	0.19
0.80	0.67	2.98	0.71	0.15	1.06	0.17
0.70	0.67	2.73	0.62	0.13	0.93	0.15
0.60	0.67	2.47	0.53	0.11	0.79	0.13
0.50	0.67	2.22	0.45	0.09	0.66	0.10
0.40	0.67	1.97	0.38	0.08	0.53	0.08
0.30	0.67	1.78	0.31	0.06	0.40	0.06
0.20	0.67	1.69	0.27	0.04	0.27	0.04
0.10	0.67	1.63	0.26	0.03	0.14	0.02
0.00	0.67	1.63	0.29	0.01	0.10	0.01

Table 4.2: Mean, maxima (Max.), and standard deviation (Std.) of hourly power ramps for different shares of PV and wind. All values are expressed as the share of peak load.

Fig. 4.5 exhibits the cumulated distribution of hourly ramps of power generation (Fig. 4.5a) and power mismatch (Fig. 4.5b). Each plot consists of three curves representing different solar shares of 20%, 40%, 60%. The figure shows that with increasing PV shares, the ramps increase on both positive and negative trails, indicating that systems with high solar shares can strongly ramp up on clear sunny afternoons.



(a) Cumulated distribution of generation.



(b) Cumulated distribution of mismatch.

Fig. 4.5: Cumulated distribution of hourly incremental power generation and mismatch.

Table. 4.3 shows hourly ramp of mismatch and their respective statistical dispersions for different degrees of renewable penetration ( $\alpha = 0.3$  and  $0.5$ ) and different mixes of solar PV and wind ( $\beta = 0.2, 0.4, 0.6$ ). As shown in Table. 4.3, normalized ramps increase with increasing  $\alpha$  and  $\beta$  values. Huber et al. [38] have shown that the frequency distribution profiles of mismatch ramps maintain the same shape as for 100% wind mix case up to a threshold PV contribution of 20%. They have also found that for some countries the threshold can be as high as 30%.

### 4.3 Seasonal variability

Both power demand and renewable energy resources exhibit characteristic seasonal fluctuations. The correlation between the demand side and the generation side on the seasonal scale not only indicates the storage capacity needed to smooth out monthly

$\alpha$	Solar share ( $\beta$ )	Mean	Min.	Max.	Std.
95 <sup>th</sup> percentile					
0.3	0.2	0.10	0.05	0.13	0.02
	0.4	0.10	0.06	0.14	0.02
	0.6	0.12	0.06	0.15	0.02
0.5	0.2	0.11	0.07	0.17	0.02
	0.4	0.13	0.06	0.17	0.03
	0.6	0.17	0.06	0.22	0.04
5 <sup>th</sup> percentile					
0.3	0.2	-0.10	-0.14	-0.06	0.02
	0.4	-0.11	-0.15	-0.07	0.02
	0.6	-0.13	-0.16	-0.06	0.02
0.5	0.2	-0.12	-0.15	-0.07	0.02
	0.4	-0.14	-0.18	-0.07	0.03
	0.6	-0.18	-0.23	-0.07	0.04

Table 4.3: Statistical dispersion of hourly mismatch ramps [share of peak load] calculated for different degrees of renewable penetration ( $\alpha$ ) and different shares of PV and wind ( $\beta$ ).

variations but also aids in deciding the optimal mix of PV and wind to minimize the balancing needs.

Seasonal variabilities of solar, wind, and load curves of Europe are shown in Fig. 4.6 in weekly time series of 2011. Solar power exhibits the strongest seasonal trend with maximum yield in summer and minimum yield in winter. Wind has a seemingly opposite and comparatively weaker seasonal pattern, with average wind over Europe being stronger in winter than in summer. The load curve of Europe has an even weaker seasonal trend with larger electricity demand in winter than in summer due to enhanced heating and lighting needs in these latitudes. Existing studies have further analyzed the seasonal patterns of power demand for different sectors and showed that the variations are highest in the residential sector, followed by the commercial sector, and least for the industrial sector [62]. In Fig. 4.6, wind and PV power are each scaled to the average load. This figure also exhibits the variability characteristics of different module configurations. East and West facing modules can best cover the early morning and late evening hours, respectively. Therefore, they yield low power in winter due to reduced day-light hours. East facing modules show a similar annual course as those

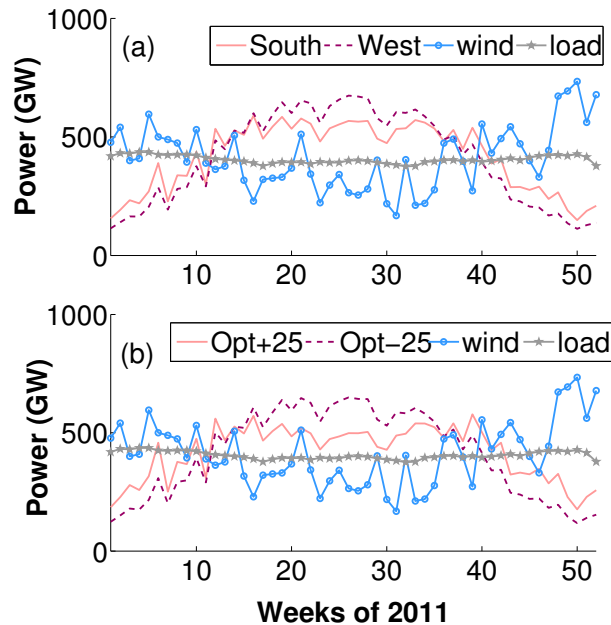


Fig. 4.6: Weekly time series depicting the annual course of load, wind, and different module configurations for 2011.

facing West and are not shown in Fig. 4.6 explicitly due to figure clarity. For the South facing and optimally inclined modules, the summer peak is apparently reduced due to the 2.2% lowering of their nominal capacity for leveled gross output. The low solar elevation in winter aids in larger power yield from highly inclined modules. However, in summer, these highly inclined modules appear less suitable in capturing solar irradiance as the sun mostly remains high during this period. Moreover, highly inclined modules seem to lose a substantial portion of solar irradiance behind the modules.

The lowly inclined, East and West facing modules have a steeper annual course. This effect induces larger seasonal fluctuations for these module configurations. Fig. 4.7 displays the weekly standard deviations of 55 PV module configurations. The highly inclined South facing modules, by virtue of their less steeper annual course, have lowest standard deviation on the seasonal scale. While diurnal patterns dominate over the hourly PV power variability and the seasonals on the weekly scale, the patterns of Fig. 4.4 and Fig. 4.7 differ significantly from each other, with relative differences in standard deviation between different configurations being much larger on the weekly compared to the hourly scale.

It is discussed above that wind power exhibits a positive correlation with European load curves while solar PV shows negative correlation on the seasonal scale. The

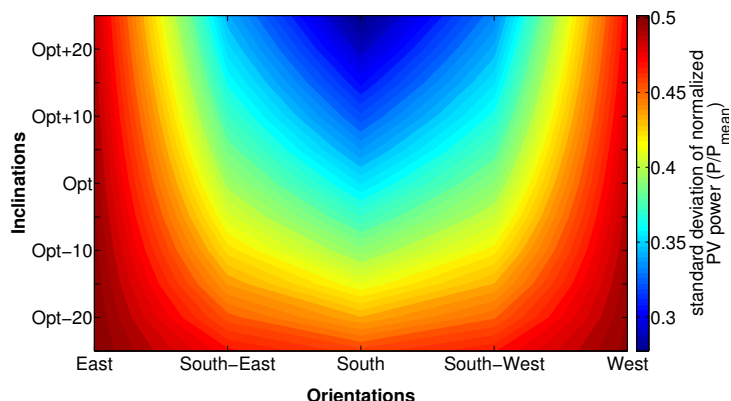


Fig. 4.7: Weekly standard deviation of 55 different module configurations. This standard deviation is normalized to the mean PV power.

systematic variability of PV with no generation at night and the seemingly opposite behavior to the annual load curve require seasonal storage to be filled in from the peak electricity generation periods. This effect is of particular importance in power systems with high shares of solar PV. In Chapter. 5, the minimum storage capacity requirement is calculated to maintain a stable grid without introducing any additional balancing. The corresponding discussion also covers the issues of optimal mix of PV and wind that can minimize the balancing needs. Heide et al. [33] have concluded that the seasonal optimal mix is 55% wind and 45% solar in a 100% solar and wind based scenario. This choice of integrating higher wind shares arrives due to its greater correlation with the demand profile than solar variations. It is to be noted here that seasonal load curve has a much weaker profile than does wind and further addition of wind power into the grid will result in much over-production in winter and under-production in summer. With the optimal mix of solar PV and wind, and using adequate storages, one can reduce the operational filling factors of the dispatchable power plants that require energy and time to ramp up and down and can improve the economic model of these facilities.

Table. 4.4 summarizes the findings on the statistical measures of time series and ramps of power demand and power generation on daily, weekly, and monthly resolutions. Here, the PV and wind generation are shown for PV-only and wind-only scenarios, respectively. This means, in the PV-only scenario, the average PV power has been scaled to match the average load on the respective time scale. The same is also true for wind power generation. That's why the mean values from each of the time series are the same (0.87 on daily, 0.92 on weekly, and 0.94 on monthly scales). The minima and the maxima of each time series indicates the range of possible variations, while standard deviation values give a quantitative insight on their variability characteristics.



		Demand		PV		Wind	
		Time series	Ramp	Time series	Ramp	Time series	Ramp
Daily	Mean	0.87	0.00 (0.05)	0.87	0.00 (0.07)	0.87	0.00 (0.18)
	Max	1.00	0.15 (0.15)	1.51	0.31 (0.36)	2.07	1.09 (1.09)
	Min	0.72	-0.11 (0.00)	0.19	-0.36 (0.00)	0.15	-0.76 (0.00)
	Std.	0.06	0.06 (0.04)	0.33	0.09 (0.06)	0.36	0.23 (0.14)
Weekly	Mean	0.92	0.00 (0.02)	0.92	0.00 (0.10)	0.92	0.00 (0.22)
	Max	1.00	0.09 (0.11)	1.52	0.53 (0.53)	1.83	0.78 (0.78)
	Min	0.85	-0.11 (0.00)	0.30	-0.43 (0.00)	0.25	-0.74 (0.00)
	Std.	0.04	0.02 (0.02)	0.34	0.12 (0.08)	0.31	0.27 (0.16)
Monthly	Mean	0.94	0.00 (0.02)	0.94	0.00 (0.16)	0.94	0.00 (0.17)
	Max	1.00	0.05 (0.05)	1.46	0.36 (0.41)	1.60	0.52 (0.55)
	Min	0.90	-0.05 (0.00)	0.36	-0.41 (0.00)	0.45	-0.55 (0.00)
	Std.	0.03	0.03 (0.02)	0.34	0.19 (0.10)	0.25	0.21 (0.12)

Table 4.4: Statistical measures of power and ramp of demand and generation. All values are expressed as the share of the peak load of the corresponding temporal resolution. The PV and wind generation are shown for PV-only and wind-only scenarios, respectively. Here, Std. stands for standard deviation. The values in the parenthesis denote the corresponding numbers of the absolute values of ramps.

Apart from the time series itself, Table. 4.4 also provides many interesting facts on the power ramps on daily, weekly, and monthly scales. As the positive and negative ramps cancel out each other over the complete simulation period, the mean values of the actual power ramps are always zero, irrespective of the temporal resolution. However, the means of the absolute values of power ramp are significantly different for demand, PV and wind generation and for each time scale. In Sec. 4.2 it is shown that the hourly standard deviation of PV is much higher than that of wind due to the strong diurnal pattern of solar power. This effect is removed on the daily resolution and one can find that the standard deviation of PV is lower than wind on the daily scale (0.33 for PV and 0.36 for wind). On the weekly and monthly scales, however, the annual course of the power sources play the most dominating role in determining their deviations. Since solar PV has a more pronounced annual course than wind, the standard deviations of PV are higher on weekly and monthly scales. For the power ramps, the standard deviations are lower for solar PV than they are for wind on all

temporal scales discussed here. This concludes that PV power changes slowly from one day to the next (or one week to the next or one month to the next) than does wind.

## 4.4 Summary

The variability characteristics of PV and wind are discussed above in the context of their large scale grid integration for a future European power system. Hence, the discussion is extended to include the variability of power demand as well. Existing studies have identified the importance of different solar and wind shares on system flexibility requirements [38] and have also proposed the optimal mix of these two resources in terms of minimum balancing needs [34]. The results presented in this thesis resemble these earlier findings. Additionally, the impact of different module configurations on balancing needs is included in this thesis alongside other factors like  $\alpha$  and  $\beta$ . The analysis presented in this chapter not only covers the variability issues of the power generation and demand, but also their incremental or ramp analysis on multiple scales relevant to grid stability issues. It is shown that the variable nature of PV and wind is not entirely arbitrary, rather a large part of their variability is highly systematic and therefore, predictable. Also, spatial aggregation is shown to have significant smoothing effect on the fluctuation of PV and wind power, not only on large continent scale, but also to some extent over smaller domains, such as over large solar or wind parks. On the hourly scale, the large variations in solar power is primarily governed by sun's position in the sky, resulting in the characteristic bell shape of its diurnal pattern. Although precisely predictable, this induces the inevitable constraint of no solar power generation at night. This prominent day-night variability of PV power can be largely smoothed by introducing a small storage (at least 6 hours of average load) that can store the excess power generation from the mid-day and utilize it when needed. As the average European load curve primarily peaks in the evening, West facing highly inclined PV modules are found to be best suitable to match with the diurnal load curve. On the seasonal scale, solar power exhibits seemingly opposite trend with the seasonal load curve. The highly inclined South facing modules, by virtue of their less steeper annual course, are most suitable to reduce balancing on the seasonal scale. It has also been pointed out that the seasonal load curve of Europe has a very weak pattern, thus introducing very large shares of wind power will cause over-production in winter and under-production in summer. These results and the corresponding analysis are further discussed in Chapter. 5 for multiple plausible scenarios.

# Chapter 5

## Impact of PV module configurations on European balancing needs

Power systems with high shares of variable renewable energy sources like solar PV and wind require additional balancing options like storage and backup from dispatchable resources to maintain stable, uninterrupted power supply. In this work, the entire investigation is carried out under the aspect of system-friendly renewable energy sources [36, 37]. The main idea behind system-friendly generation is to consider system integration effects, rather than minimizing only generation costs [37]. To ensure stable grid operation, system integration of solar PV and wind requires specific information, such as the optimal mix of these two resources. In this work, the optimal mix of PV and wind is investigated and the balancing needs are estimated for a future European power system with very high shares from these variable resources. Several factors influence the storage and other balancing needs, such as the overall VRE penetration to the power system, the mix of PV and wind etc. Additionally, the orientation and the angle of inclination of PV modules can have significant impact in determining the balancing needs. In this chapter, all these factors are discussed in details under various scenarios.

The major content of this chapter is presented in two sections: Sec. 5.1 comprises of the quantification of backup needs while Sec. 5.2 provides estimates of storage requirements. Each section contains several subsections that indicate specific system scenarios. Although some of these scenarios are quite extreme and less probable to be absolutely true for future European power system, they provide excellent boundaries to mathematically express system requirements. For the analysis in this chapter,

unlimited transmission is assumed among the neighboring countries. Although this is a major simplification of the network flow model, this assumption not only gives an upper bound to the balancing needs but also significantly speeds up the overall computational process.

## 5.1 Estimation of backup needs

In this section, backup requirements are discussed for scenarios with and without any storage. In this context backup is expressed with either the balancing parameter ( $E_b$ ) or the average additional balancing parameter ( $E_b^{add}$ ), defined in Eq. 2.11 and 2.12, respectively. Both of these are dimensionless parameters. Rasmussen et al. [69] have pointed out that these parameters are derived from average values and it is not a priori possible to assign them to a time series.

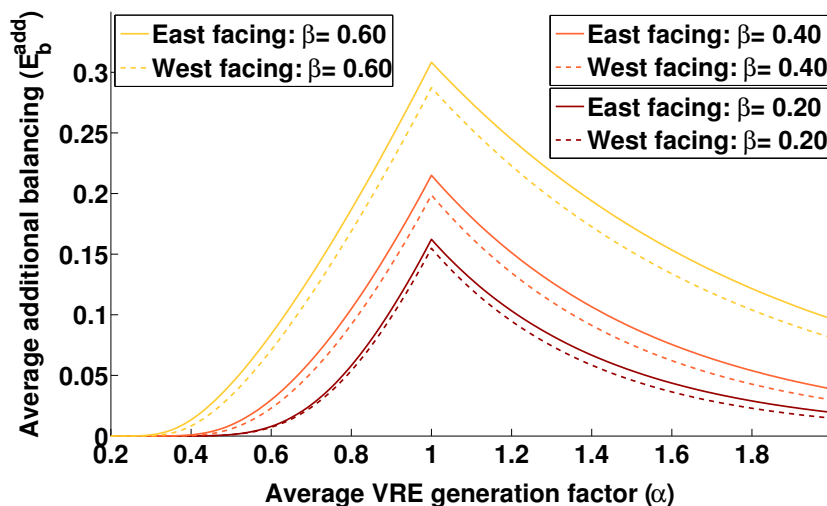


Fig. 5.1: Additional average balancing  $E_b^{add}$  as a function of average VRE generation factor  $\alpha$  in absence of any storage for highly (optimal+25°) inclined PV modules with different orientations for different shares of PV and wind.

### 5.1.1 Backup in absence of storage

In absence of storage, all residual load present in the system is covered by backup supply from dispatchable resources. Lack of storage also means that excess generation cannot be retained for later usage and is potentially lost from the system. Backup requirements in power systems with high shares of fluctuating energy sources are well

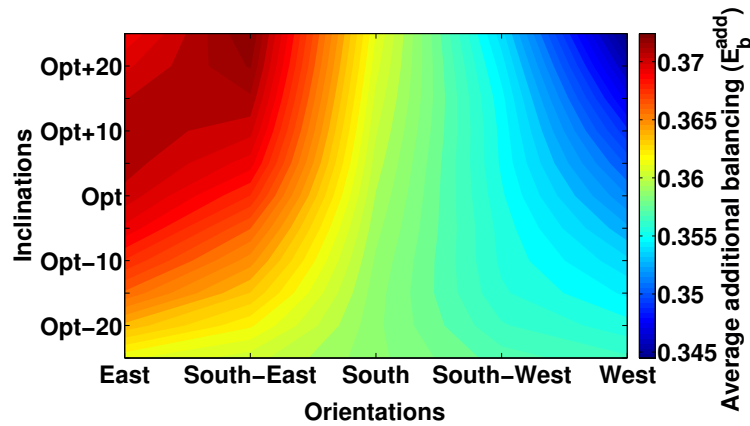
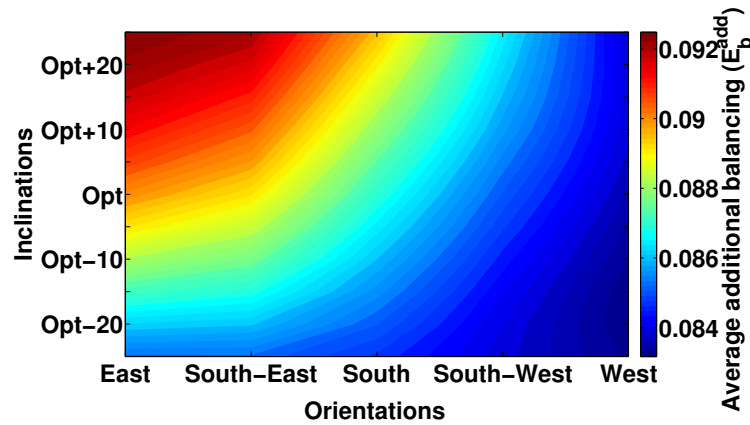
(a) PV-dominated scenario ( $\beta=0.8$ )(b) Wind dominated scenario ( $\beta=0.2$ )

Fig. 5.2: Average additional balancing needs ( $E_b^{add}$ ) for different module configurations for  $\alpha = 1.25$ .

discussed in literature. Lise et al. [52] have shown that in 2050, if  $\sim 5\%$  of demand is covered by some external means (such as, demand side management), the maximum amount of stable generation required will be below 400 GW. They estimated that this level of stable generation can be achieved by assuming installed capacity of 115 GW of nuclear and 450 GW of fossil fuel power plants. In a study on the Iberian peninsula, Kies et al. [45] have estimated that in absence of storage, the minimum backup energy required is 22.1% of the demand for an optimal mix of 77% wind and 23% PV. Heide et al. [34] have shown that in a scenario without any storage, the balancing needs can be very large even when average generation exceeds average load ( $\alpha > 1$ ). They have also highlighted the importance of PV and wind mix in determining balancing needs as the unavailability of solar irradiance during night makes it an inefficient choice to allow very large shares of PV power in the grid, if no storage is used to utilize

the surplus energy from mid-day to the hours of need. This analysis is expanded by Rasmussen et al. [69] to the domain  $\alpha < 1$  and they found a distinct peak of  $E_b^{add}$  at  $\alpha = 1$ . They have also shown that the size of this peak strongly depends on the mix of solar and wind. In this chapter, the balancing needs for Europe are further investigated to estimate the effects of different PV module configurations alongside other dominant factors like  $\alpha$  and  $\beta$ .

Solar share	South-facing optimal tilt	West-facing Opt-25°	West-facing Opt+25°
0.00	0.071	0.071	0.071
0.10	0.048	0.045	0.046
0.20	0.050	0.047	0.046
0.30	0.063	0.059	0.056
0.40	0.085	0.081	0.075
0.50	0.119	0.114	0.106
0.60	0.168	0.163	0.152
0.70	0.235	0.230	0.217
0.80	0.318	0.314	0.299
0.90	0.405	0.402	0.386
1.00	0.492	0.490	0.473

Table 5.1: Comparison of  $E_b^{add}$  between different module configurations with changing solar shares. These values are computed for  $\alpha = 1.5$  in the scenario without any storage.

The balancing parameters strongly vary with  $\alpha$  and  $\beta$ . This variation of  $E_b^{add}$  is shown in Fig. 5.1 for different module configurations. Rasmussen et al. [69] have reported that the integration of wind and solar power works up well up to around  $\alpha \approx 0.5$ , with no requirement of average additional balancing. However, it is shown in Fig. 5.1 that this threshold strongly depends on the PV and wind mix and shifts towards lower  $\alpha$  values with increasing PV shares. It is mentioned in Chapter. 2 that power time series from each PV module configuration is scaled such that their gross generation over the entire simulation period is the same. Hence, the relative differences in balancing needs estimated from different configurations result from their fluctuation characteristics, not their gross output. Fig. 5.1 also manifests that although the effect of PV and wind mix on the balancing requirements is more pronounced than that from different module configurations. Nevertheless, proper choice of PV module configurations can lower the balancing needs for any chosen values of  $\alpha$  and  $\beta$ . The

relative differences between different module configurations (Fig. 5.1) become more prominent with increasing solar shares. In absence of storage, West facing modules are most suitable to reduce balancing needs than modules with any other orientation as they best match the diurnal load curve of Europe that has its primary peak in the evening. The choice of proper module inclination is, however, also influenced by the share of PV and wind. In PV-dominated scenarios (Fig. 5.2a), power mismatch is primarily determined by the day-night cycle of PV and the highly inclined West facing modules, by virtue of their better productivity during the peak demand hours in the evening, are suitable to reduce balancing. This is discussed in details in Chapter. 4 and illustrated with Fig. 4.3. The effect of day-night cycle is, however, significantly diminished in scenarios with larger shares of wind (Fig. 5.2b) and lowly inclined West facing modules are more effective to reduce backup needs. This is also discussed in Chapter. 4 while analyzing the seasonal variability of different module configurations. Table. 5.1 summarizes the average additional balancing needs for different module configurations with changing solar shares. It shows that for low solar shares ( $\beta < 0.2$ ), lowly inclined West facing modules have balancing needs even lower than the popular South facing optimally inclined (SFOI) ones. With increasing solar shares, highly inclined West facing modules appear to have lowest need of backup supply. It is to be noted that when  $\alpha$  falls below a certain value ( $\alpha < 0.8$ ), the magnitudes of  $E_b^{add}$  for large solar shares become comparable for West and South facing modules and the optimum module configuration in terms of minimum backup needs shifts towards the South facing ones.

	Balancing reduction (%)	Capacity increase (%)
West, optimal	1.4	22.9
East+West, optimal	6.0	21.8
West, optimal+25°	1.8	41.9
East+West, optimal+25°	11.3	40.1

Table 5.2: Reduction in balancing potential with the accompanying capacity increase shown for different module configurations compared to the optimally inclined South facing ones in a scenario with  $\alpha = 1.0$  and  $\beta = 0.4$ . All values are given in %.

Since combined East and West facing modules better adapt the diurnal load curve due to their much flatter plateau, repowering some old South facing modules with combined East-West facing modules can be quite beneficial in long terms from the point of grid operations [84]. The balancing reduction potential of West facing and

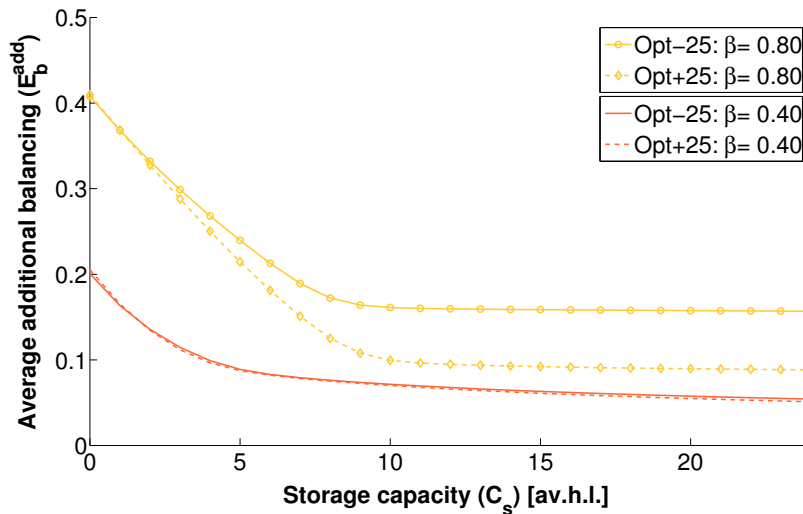


Fig. 5.3: Variation of average additional balancing  $E_b^{add}$  as a function of small storage size  $C_s$  for South facing modules with different inclinations for different solar and wind shares for  $\alpha = 1$ . No storage loss is considered here.

East-West combined modules are summarized in Table 5.2. It shows that combined configurations not only have much larger balancing reduction potential than the West facing modules, but also result in higher profit from the slightly less investment in installed capacity.

In absence of any storage, the optimal mix of solar PV and wind to minimize balancing energy depends on the  $\alpha$  values [69]. In this work, it is found that it also depends on the chosen module configuration. For all 55 module configurations analyzed here, the optimal solar share ( $\beta_{opt}$ ) varies between 0.18-0.21 for  $\alpha = 0.75$ , between 0.15-0.18 for  $\alpha = 1.0$  and between 0.09-0.14 for  $\alpha = 2.0$ . With increasing module inclinations, the optimal mix shifts towards the higher solar shares.

### 5.1.2 Backup in presence of storage

The backup needs are reduced when storages are included in power system operation. In a study of German power system, Weitemeyer et al. [88] have reported that in presence of flexible backup power plants, small but highly efficient storage devices are favorable over large but less efficient seasonal storage devices to reach a share of about 80% of electricity demand being met by VRE sources. For the isolated Iberian peninsula, Kies et al. [45] have shown that the backup energy need decreases from 22.1% of the consumption in a ‘no storage’ scenario to 16.1% in presence of a hydro storage for an optimal mix of 74% wind and 26% PV. The decrease in backup needs

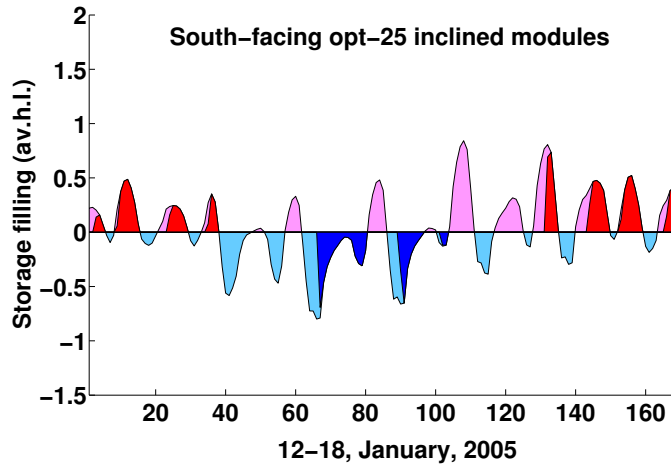


Storage capacity ( $C_s$ av.h.l.)	$\alpha$	South facing Opt-25°	South facing Optimal tilt	South facing Opt+25°
6	0.75	0.065	0.048	0.037
	1.00	0.213	0.192	0.181
	1.50	0.088	0.079	0.077
12	0.75	0.022	0.005	0.001
	1.00	0.160	0.123	0.095
	1.50	0.044	0.021	0.011
24	0.75	0.018	0.001	0.000
	1.00	0.157	0.118	0.088
	1.50	0.041	0.017	0.007

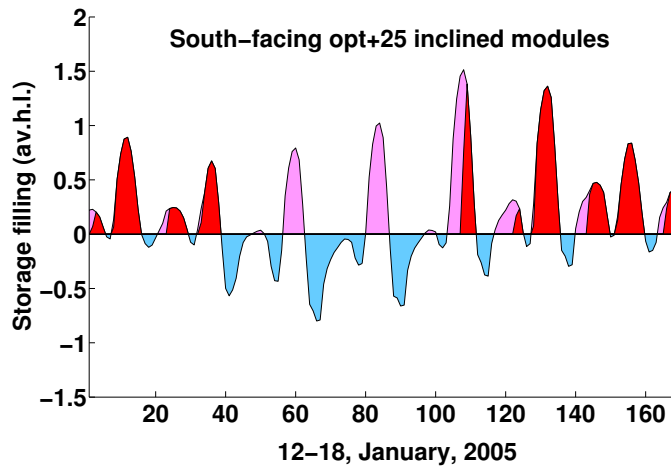
Table 5.3: Average additional balancing needs in presence of lossless storages for South facing modules with different inclinations. All values are calculated for high solar shares ( $\beta = 0.8$ ) to distinguish between different configurations.

with increasing storage capacity is almost exponential up to a certain threshold, and beyond that, it follows a linear trend [69]. Inclusion of a small storage ( $\sim 6$  average hourly load or 6 av.h.l.) can strongly diminish the balancing needs as this storage capacity is ideal to smooth out the intra-day cycle of PV. Beyond this limit, the balancing needs are no longer governed by the diurnal behavior, but rather influenced by their annual variability. In this section, the balancing reduction potential due to the addition of a storage is discussed for various shares of PV and wind and for different module configurations.

Fig. 5.3 shows how  $E_b^{add}$  is reduced with increasing storage capacities for different  $\beta$  values. For very large solar shares, a storage of  $\sim 6$  av.h.l. becomes inadequate to smoothen the intra-day solar cycle (Fig. 5.3) and the threshold shifts towards higher  $C_s$  values. For storage capacities below this threshold, highly inclined West facing modules best reduce the balancing needs. Above this threshold, the reduction potential is much higher and highly inclined South facing modules are most suitable in reducing balancing needs. Depending on the  $\beta$  values,  $E_b^{add}$  in presence of a lossless 12 av.h.l. storage can be reduced up to 22.9% (for  $\alpha = 1.0$ ) when SFOI modules are replaced with South facing optimal+25° inclined modules. Table. 5.3 shows the reduced balancing needs in presence of storages with different capacities and for different  $\alpha$  values. The storage capacities in this table are expressed in hourly average load. The  $E_b^{add}$  values given in this table indicates a peak at  $\alpha = 1$  (discussed for Fig. 5.1). The balancing needs also decrease with increasing storage capacity and from lower to higher



(a) Winter days: South-facing optimal-25° inclined modules.



(b) Winter days: South-facing optimal+25° inclined modules.

Fig. 5.4: Excerpt of storage filling with charging (pink), discharging (light blue), curtailment (red) and balancing needs (dark blue) for a few days in winter. This example compares different module configurations for  $\alpha = 1.0$ ,  $\beta = 0.4$ , and  $C_s = 6$  av.h.l.

module inclinations. For different module orientations, the potential for balancing reduction using a constrained storage is rather low (for optimally inclined modules, 4.7% balancing reduction is possible by changing orientations from South to West).

In Fig. 5.4, the influence of module inclinations on *backup* and *curtailment* is shown for a few winter days in 2005. Modules with higher inclinations have enough excess generation in winter (Fig. 5.4b) due to their less pronounced annual course. With a leveled average power generation from all module configurations, highly inclined

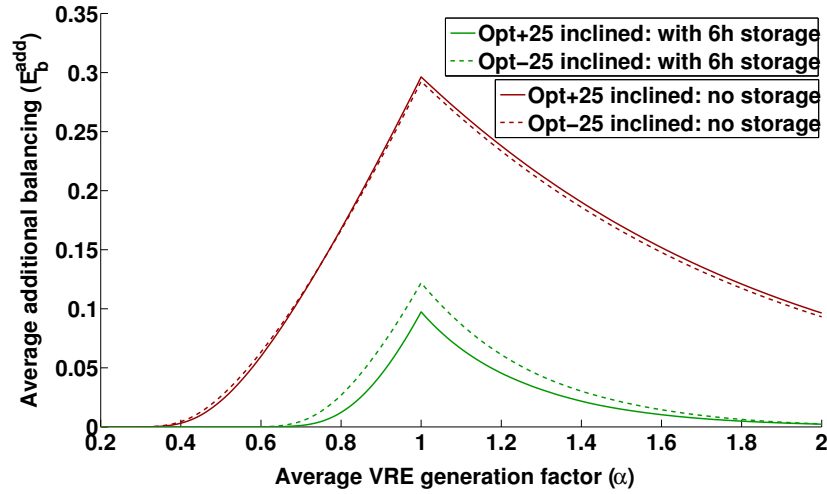


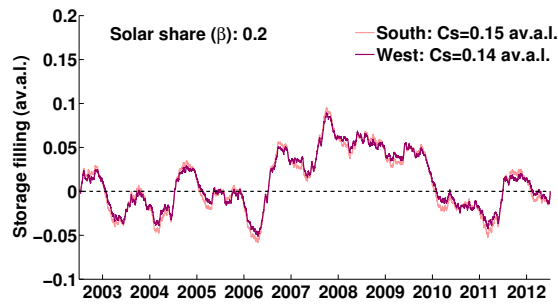
Fig. 5.5: Reduction in average additional balancing  $E_b^{add}$  up on using a lossless storage shown for South facing modules with different inclinations over a wide range of  $\alpha$  values. Example shown for  $\beta = 0.6$ .

modules have relatively higher backup needs in summer, specially in a wind-dominated scenario. The opposite trend is exhibited by lowly inclined modules (Fig. 5.4a).

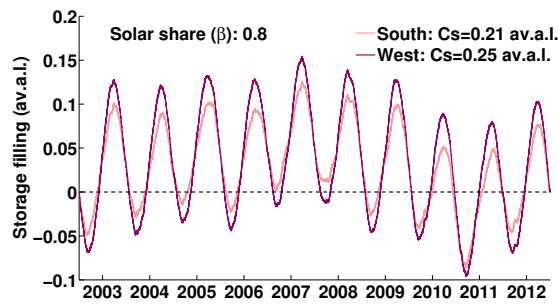
It is discussed above how a small storage can strongly reduce the huge balancing needs estimated in a ‘no storage’ scenario (Fig. 5.3). By including a small storage, the governing factors of balancing needs are moved from the diurnal to seasonal changes. This effect is shown in Fig. 5.5 where inclusion of a small storage not only aids in largely reducing the balancing needs but also changes preference from lowly inclined to largely inclined South facing modules.

## 5.2 Estimation of storage needs

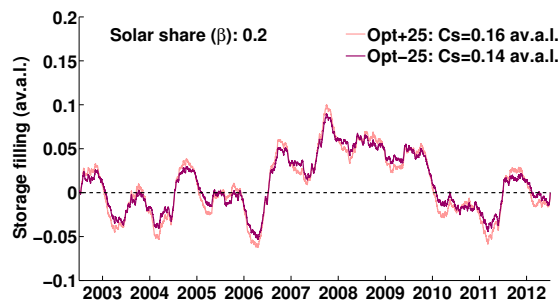
Effective integration of VRE sources in an electric power grid usually relies on storages. If storage is present, not only can it provide energy when needed, but also part of the otherwise curtailed energy can be fed into the system. The amount of reusable energy depends on storage capacity and its efficiency. This study is not focused to any particular type of storage technology like battery, flywheel, pumped hydro etc. Here the generic term ‘storage’ is used to indicate a system with specific efficiency that can store excess energy as well as provide power when needed. Two main variables are used here, namely storage efficiency and storage capacity, to model storage instead of choosing any particular technology. This gives large flexibility to the model as it can represent a wide variety of storage systems with different efficiencies and capacities.



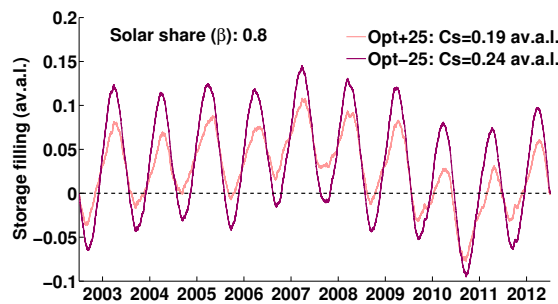
(a)



(b)



(c)

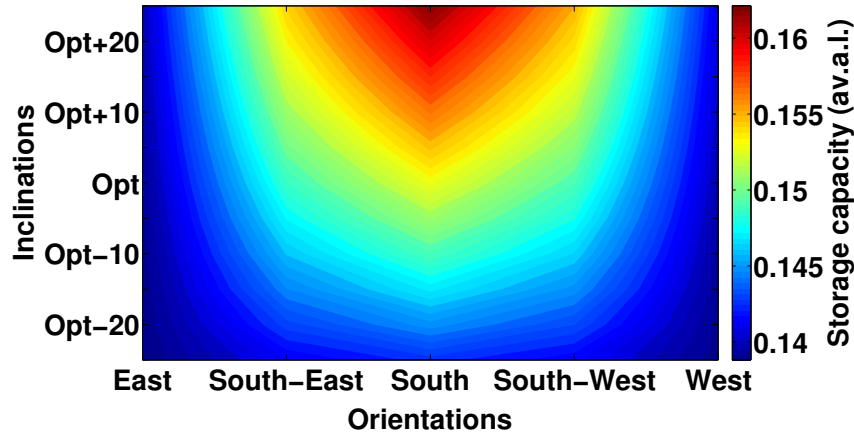


(d)

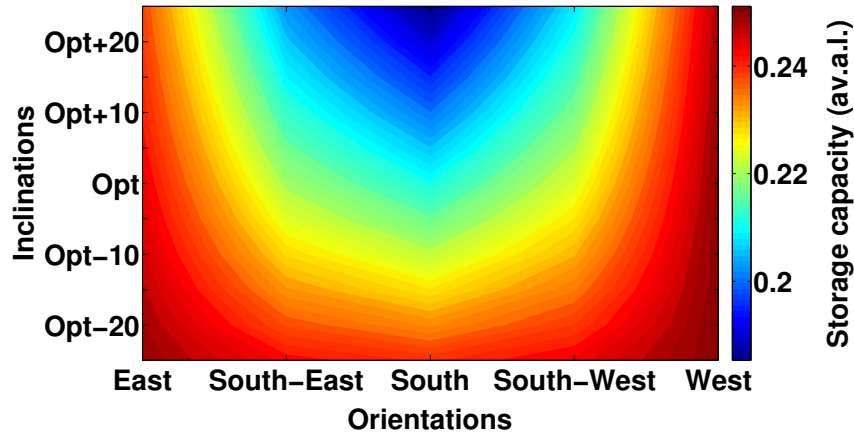
Fig. 5.6: Lossless storage filling for different shares of solar (and wind) and for different module configurations at  $\alpha = 1$ . (a)-(b) compare optimally inclined modules with different orientations while (c)-(d) compare South-facing modules with different inclinations.

In this section, different scenarios are analyzed to quantify the effect of different shares of PV and wind and different module configurations on storage needs. For simplicity and clarity, no storage loss is considered in Sec. 5.2.1. A more realistic storage scenario with specific storage losses is presented in Sec. 5.2.2.

### 5.2.1 Unconstrained lossless storage



(a) wind dominated scenario ( $\beta = 0.2$ )



(b) PV dominated scenario ( $\beta = 0.8$ )

Fig. 5.7: Storage capacity ( $C_s$ ) in average annual load (av.a.l.) at  $\alpha = 1$  for different module configurations for (a) solar share ( $\beta$ ) 0.2 and for (b) solar share ( $\beta$ ) 0.8.

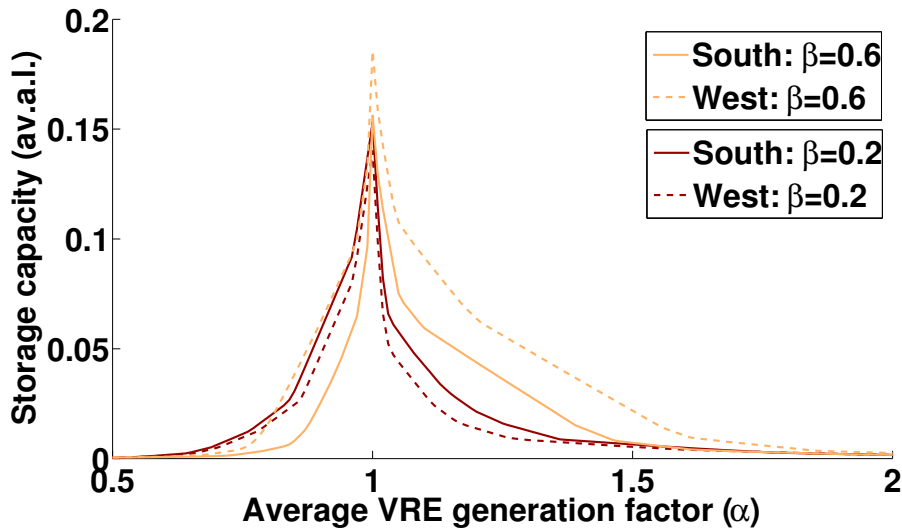
This section covers scenarios that allow storages to save enough excess generation to completely avoid any  $E_b^{add}$ . Over the past few years, researchers have extensively studied this scenario of unlimited storage capacity. In a study of German power

system [88], the authors have shown that with a wind share of 60% and an average renewable generation factor of  $\alpha = 1.0$ , a lossless storage device would need to have a storage size of the order of 80 TWh. This is orders of magnitude higher than today's storage capacities in Germany [8], and even higher than Europe's total hydrogen storage potential in salt caverns [66]. For a 100% wind-plus-solar-only scenario of future Europe, Heide et al. [34] have investigated how the storage capacities are influenced by the choice of  $\alpha$  and  $\beta$ . For a range of  $\alpha$  values from 1.0 - 2.0, they found that storage needs are extremely high at  $\alpha = 1$ , specially for very high and very low  $\beta$  values. They have also shown that the optimal mix of solar and wind in terms of minimum storage capacity is  $\alpha$ -dependent. For  $1.1 \leq \alpha \leq 1.4$ ,  $\beta_{opt}$  equals 0.25 and for  $1.6 \leq \alpha \leq 1.9$ , it is around 0.55. In this work, PV module configurations are identified as additional factors to determine storage needs.

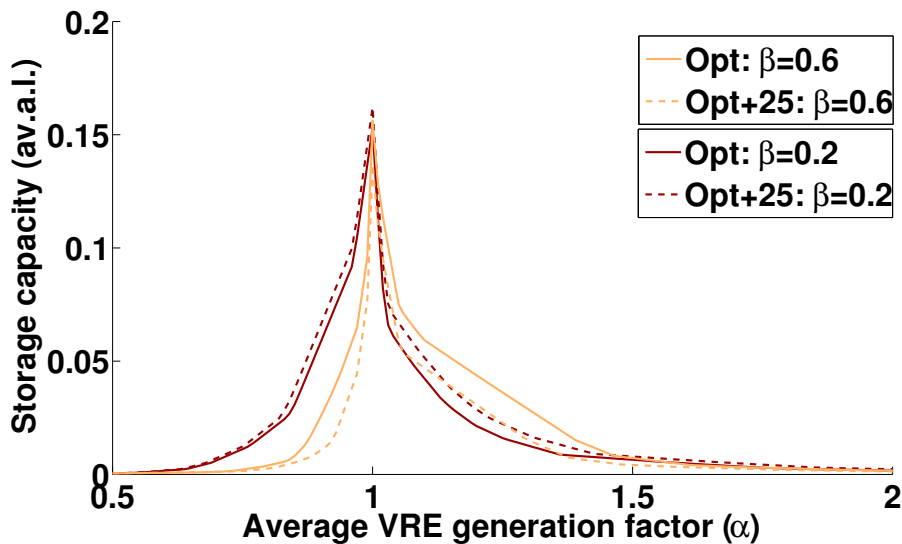
The filling levels of an unconstrained storage are shown in Fig. 5.6 for different solar shares and for different module configurations. With increasing PV share, the seasonal (and by extension, inter-annual) variations of VRE generation become more prominent and distinct. Since PV has seemingly opposite pattern to the power demand on the seasonal scale, larger storage capacities are required in PV-dominated scenarios. However, very low solar share is also not an optimal choice since such scenarios usually have over-production in winter and under-production in summer due to comparatively weaker seasonal variability of load than that of wind (Fig. 4.6).

Around  $\beta = 0.4$ , the seasonal generation curves change their shapes (seasonal maxima and minima) creating two separate regimes of wind-dominated and PV-dominated scenarios. The examples of storage needs in these two regimes are shown in Fig. 5.7 for different module configurations. On one hand, lowly inclined East/West facing modules best match the seasonal load curve for  $\beta = 0.2$  and are least storage demanding (Fig. 5.7a). On the other hand, highly inclined South facing modules with less steeper annual course are best suitable to minimize storage needs in PV-dominated scenarios (Fig. 5.7b). Storage needs are reduced to  $C_s = 0.19$  av.a.l. for South facing optimal+25° inclined modules compared to  $C_s = 0.21$  av.a.l. for SFOI in a PV-dominated scenario (Fig. 5.6b, 5.6d). For large wind shares, optimal-25° inclined South facing modules require  $C_s = 0.14$  av.a.l. while SFOI modules result in storage need of  $C_s = 0.15$  av.a.l. (Fig. 5.6a, 5.6c). Additional results of storage requirements are tabulated in Table. 5.4 to compare between module configurations for different values of  $\alpha$  and  $\beta$ .

Besides the mix of solar and wind, storage needs are also affected by changes in  $\alpha$ . Rasmussen et al. [69] have found that storage needs exhibit a pronounced peak at  $\alpha =$



(a) Comparing optimally inclined modules



(b) Comparing South facing modules

Fig. 5.8: Storage capacity ( $C_s$ ) for unconstrained lossless storage shown for different module configurations and for different shares of PV and wind. (a) compares optimally inclined modules with different orientations while (b) compares South-facing modules with different inclinations.

1.0. In Fig. 5.8, storage need is plotted as a function of  $\alpha$  for a lossless unconstrained storage scenario. This figure shows that proper choice of module configurations can remarkably change the storage needs. For sufficiently large solar share ( $\beta = 0.6$  in Fig. 5.8), storage capacity  $C_s$  can be reduced  $\sim 52\%$  by orienting West facing modules

$\alpha$	$\beta$	South facing Optimal tilt	South facing Opt+25°	West facing Opt+25°
0.75	0.1	0.021	0.022	0.020
	0.2	0.011	0.012	0.010
	0.3	0.005	0.007	0.004
	0.4	0.002	0.003	0.002
	0.5	0.002	0.002	0.003
1.00	0.1	0.191	0.196	0.185
	0.2	0.153	0.162	0.141
	0.3	0.121	0.137	0.107
	0.4	0.111	0.117	0.130
	0.5	0.132	0.117	0.155
1.50	0.1	0.015	0.018	0.012
	0.2	0.006	0.008	0.005
	0.3	0.004	0.003	0.005
	0.4	0.003	0.003	0.005
	0.5	0.004	0.003	0.008

Table 5.4: Storage capacity needs ( $C_s$ ) for different values of  $\alpha$  and  $\beta$  shown for different module configurations.  $C_s$  is expressed as average annual load (av.a.l.).

to South at  $\alpha = 0.92$  and  $\sim 74\%$  by changing optimal-25° to optimal+25° at  $\alpha = 0.93$ . It is to be noted that for very large values of  $\alpha$ , all curves in Fig. 5.8 overlap with each other indicating that regardless of the PV and wind mix, overly excess generation ensures less frequent deficits as the storage mostly remains full in such conditions.

In Ref. [69], it is shown that the optimal mix ( $\beta_{opt}$ ) to minimize storage needs very closely follows the  $\beta = 0.4$  for most of the  $\alpha$  values. Carefully analyzing its dependence on module configurations, it is inferred that  $\beta_{opt}$  is more sensitive to module orientations than inclinations and significantly varies between 0.15-0.65. Fig. 5.9 illustrates the variation of  $\beta_{opt}$  with  $\alpha$  for four module configurations. Depending on  $\alpha$ ,  $\beta_{opt}$  varies between 0.20 - 0.40 for lowly inclined West facing modules and between 0.30 - 0.65 for highly inclined South facing modules.

### 5.2.2 Using a two-storage system

In this section, a combined usage of a high efficiency 6 hour storage and a large seasonal storage with a round-trip efficiency of 0.36 is discussed. The parameter settings for this section are maintained to ensure that average power generation after storage losses



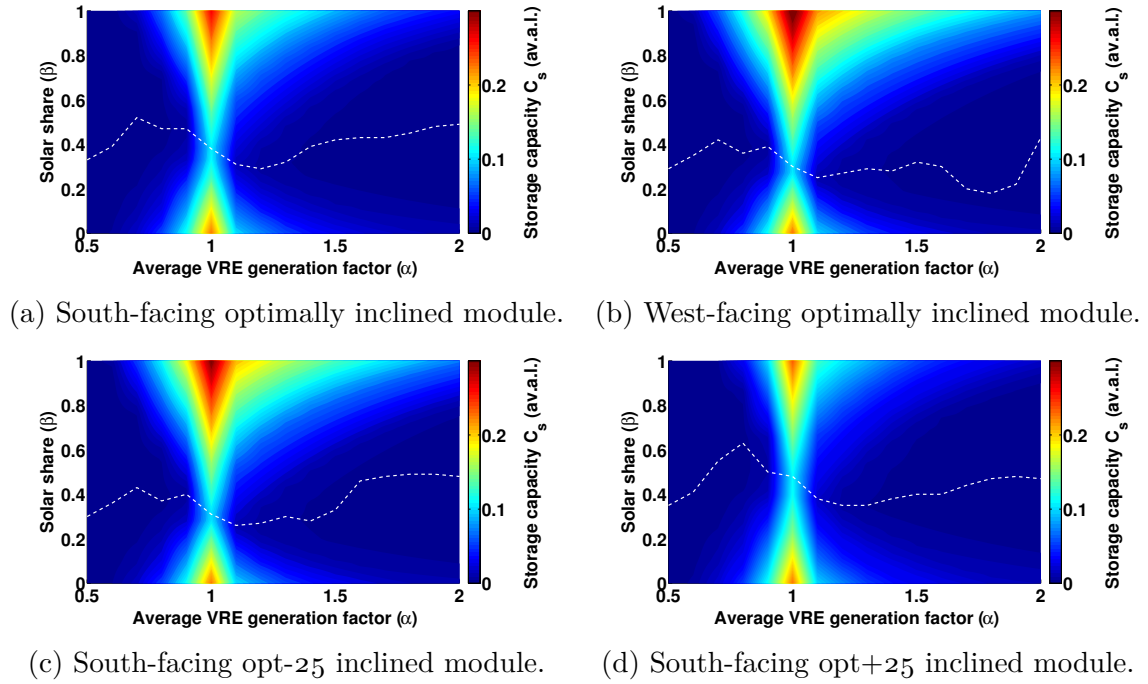
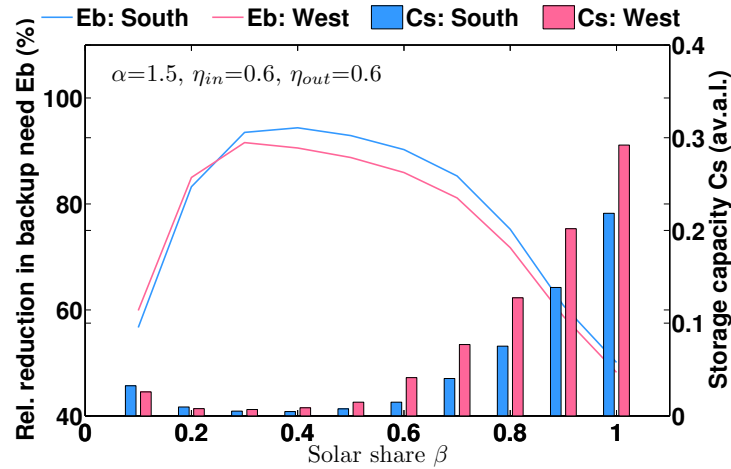


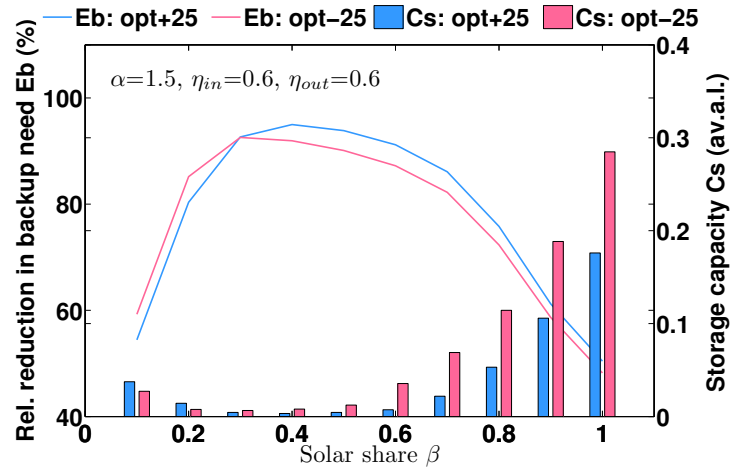
Fig. 5.9: Storage capacity as a function of  $\alpha$  and solar shares  $\beta$ . The dashed line indicates the optimal mix ( $\beta_{opt}$ ) that minimizes the storage capacity without introducing any average additional balancing.

is larger than the average demand so that storage losses are compensated by the excess generation ( $\alpha = 1.5$ ). The reduction of balancing needs up on introducing a small storage is discussed in Sec. 5.1.2. While Fig. 5.5 illustrates this effect for different  $\alpha$  values, in this section the analysis is focus on the reduction potential of different PV and wind shares (Fig. 5.10). The potential of a 6 hour storage to smoothen the intra-day cycle strongly depends on how much solar share is assumed in the model. In case of very large solar shares, the 6 hour storage appears inadequate and must be replaced with 12 hour storage in the extreme case of  $\beta = 1$  [69]. Fig. 5.10b shows that a 6 hour storage can reduce  $E_b^{add}$  by  $\sim 80 - 95\%$  in the range  $0.2 \leq \beta \leq 0.8$ .

The remaining mismatch after interaction with the small storage is directed to a seasonal hydrogen storage ( $\eta_{in} = \eta_{out} = 0.6$ ). It is discussed in Sec. 5.2.1 that very large solar shares, and to some extent very large wind shares, result in increased storage needs. For intermediate  $\beta$  values ( $0.2 \leq \beta \leq 0.8$ ), the opposite seasonal trend of solar and wind compensate each other leading to a much lower storage requirement. Unless solar share falls below 0.2, highly inclined South facing modules require least storage capacities. For very large wind shares, the annual course of lowly inclined East/West



(a) Optimally inclined differently oriented modules.



(b) South facing differently inclined modules.

Fig. 5.10: Changes in relative reduction in backup needs for different shares of PV and wind up on introducing a lossless 6 hour storage. The remaining mismatch is then used to quantify the storage needs for a seasonal storage ( $\eta_{in} = \eta_{out} = 0.6$ ) for different shares of PV and wind and for different module configurations.

facing modules better match the seasonal load curve and storage requirement gets minimized.

## 5.3 Summary

The primary idea behind the analysis in this chapter is the quantification of the impact of different module configurations on the balancing needs of European countries. Since different configurations have different power generation potential, their installed capacities are adjusted to ensure they have the same gross power output over the complete simulation period to avoid any unwanted change in PV and wind share. Multiple scenarios with different degrees of renewable penetration and different PV and wind shares are analyzed and the most suitable module configuration that minimizes balancing needs in each of these scenarios is identified. The balancing reduction potential are found to be largely dependent on the relationship between power generation and demand on diurnal and seasonal scales.

When no storage is included, balancing needs are covered entirely by backup supplies and are mainly steered by the diurnal patterns of generation and load. Since West facing modules peak around the same hours as the European load curves, they are best suitable in a ‘no storage’ scenario. Still, the reduction in balancing needs of 1.8% for optimal+25° inclined West facing modules compared to SFOI for  $\alpha = 1.0$  and  $\beta = 0.4$  is comparatively small. A further enhancement in balancing reduction potential can be achieved by combining East and West facing modules as long as solar share is high enough to maintain the bell-shape of the diurnal generation curve. A combination of equal shares of optimal+25° inclined East and West facing modules can reduce  $E_b^{add}$  by 11.3% compared to SFOI, although the price of such configurations in terms of increased installed capacity (40.1%) can be considerably large.

A small storage of at least 6 av.h.l. can strongly smoothen the day-night variability of PV, thereby making diurnal changes no longer the key controlling factor. In presence of a storage, balancing needs are rather governed by the seasonal patterns of generation and load. For large wind shares, East/West facing optimal-25° inclined modules reduce balancing needs by ~4.9% compared to SFOI in presence of a lossless 12 av.h.l. storage ( $\alpha = 1.0, \beta = 0.2$ ). They can also reduce storage needs by ~9.2% to completely avoid additional balancing for the same parameter settings. For the same solar share, the highest reduction of 38.1% appears at  $\alpha = 1.2$ . These balancing reductions are possible for ~13% increase in capacity. In a PV-dominated scenario, South facing optimal+25° inclined modules are most suitable to reduce balancing (~22.6% reduction in presence of a lossless 12 av.h.l. storage and ~12.3% reduction in storage need to completely avoid additional balancing for  $\alpha = 1.0, \beta = 0.8$ ). These configurations require a capacity increase of ~7.3%. These results suggest that a proper choice of module configurations can significantly lower the balancing needs compared to the SFOI modules that are most

widely used now-a-days. Although such configurations require additional investment in terms of installed capacities, re-powering old PV systems with suitable configuration can be highly advantageous in the long run.

# Chapter 6

## CSP import from North Africa

Concentrated solar power (CSP) is one of the renewable energy technologies capable of harnessing the immense solar energy sources available in Southern Europe and North Africa. Researchers have shown growing interest in Europe-North Africa electricity grid interconnections because of the huge solar resources in North Africa with less seasonal variations, significant improvement in CSP and transmission technologies over the past few decades, and European Union's target to urgently reduce carbon emissions to combat climate change. Recent studies, such as DESERTEC [6], TRANS-CSP [25], MedGrid [9], have analyzed the possible solar electricity import corridors from North Africa to Europe.

In this chapter, CSP is modelled over North Africa and the impact of the electricity import on European balancing needs is quantified for different scenarios. An overview of the meteorological data sources and the capacity distribution of CSP in North Africa is presented in Sec. 6.1. Sec. 6.2 outlines the measures undertaken to improve the solar irradiance retrieval from satellites in order to guarantee good quality of the input data to compute the changes in European balancing needs presented in Sec. 6.3.

### 6.1 Data set for North Africa

#### 6.1.1 Meteorological data

Accurate measurements of direct normal irradiance (DNI) are essential to the design and implementation of CSP projects. For this work, solar irradiance is retrieved from the Meteosat satellite images. Of the ten years of simulation (2003-2012), solar irradiance for the first two years are derived from the visible channel of Meteosat First Generation (MFG) satellites with spectral range between 0.5-0.9  $\mu\text{m}$ . This channel has

a spatial resolution of  $2.5 \times 2.5$  km and a temporal resolution of 30 minutes. For the remaining eight years, Meteosat Second Generation (MSG) satellites are used. It has been mentioned in Chapter. 2 that for the model domain of Europe, high resolution visible (HRV) channel of MSG was used. However, this broadband channel of MSG (channel 12) has only partial coverage over North Africa and is not archived for this region at University of Oldenburg. So, a narrowband visible channel (VIS008) of MSG was selected to retrieve solar irradiance over North Africa. This channel has a spectral coverage of  $0.74\text{-}0.88 \mu\text{m}$ . This channel is capable of supplying satellite images of the hemisphere at  $3 \times 3$  km spatial and 15 minutes of temporal resolutions. For uniformity, the satellite derived solar irradiance is interpolated to a coarser grid of  $0.5^\circ \times 0.5^\circ$  over North Africa with a temporal resolution of one hour for all simulated years.

### 6.1.2 CSP capacity

In this work, CSP is modelled with a homogeneous distribution over North Africa as the abundant solar irradiance ensures that the average annual DNI well exceed the technical and economic thresholds ( $1800$  and  $2000 \text{ kWh/m}^2/\text{y}$ , respectively, [83]) for CSP plants to operate successfully. Since CSP is more a centralized rather than a distributed technology, a homogeneous distribution over a reduced spatial resolution of  $0.5^\circ \times 0.5^\circ$  is reasonable. Considering the technological advancements of Europe and the abundant solar resources in North Africa, similar CSP capacities are crudely assumed for Europe and North Africa. Existing studies of a future European power system with high shares of renewable sources have projected CSP capacities of Europe [67, 82, 28]. For the year 2050, the energy [r]evolution scenario of [82] has estimated 81 GW of CSP capacity for Europe. For the same year, the [67] study projects 18 GW of European CSP capacity (scenario B). In Sec. 6.3, CSP capacities from both of these studies are used as their underlying differences (such as solar and wind shares, projected differences in power generation and power demand sectors etc) allow analysis of a variety of scenarios.

## 6.2 Cloud index data base

Ensuring high quality solar irradiance data is extremely important prior to the calculations of CSP itself. To model CSP over North Africa a cloud index data base is derived from the satellite images which includes quality control of those images and an adaptation of the model to better account for Bidirectional reflectance in spring and autumn which is found to be necessary when using the narrowband channel. In the

following section, the improvement up on quality control and removal of the effects of Bidirectional reflectance is discussed in details. Since an atmospheric correction term was included in the algorithm of MFG and the selected channel from MFG is less sensitive to the Bidirectional reflectance, the results derived from MSG are free from these effects. Hence, the preliminary and the revised results from MSG are compared with that from MFG for 2005 which is an overlapping year between MFG and MSG satellites.

### **6.2.1 Quality control (QC)**

To improve the quality of the time series, satellite images with unusual artefacts (e.g., data loss at specific image segment or along image pixels, recurring unusual patterns in images, images shifted to a few pixels, corrupted header etc.) are detected and removed. The result is shown in Fig. 6.1 which indicates significant improvement of the data quality.

### **6.2.2 Removing the effects of Bidirectional reflection**

The surface reflectance has a directional property and as such depends upon the incident solar and the receiving satellite detector angles. Therefore, the geometric differences among detectors can affect the reflected solar irradiance. This Bidirectional reflectance is caused by the anisotropic reflectance of the surface below and under certain geometric conditions of the sun and the satellite, the reflected radiation recorded by the satellite sensors can increase significantly. To maintain standard data quality, removal of these effects of Bidirectional reflectance is required.

When using the narrowband channel, rapid changes in ground reflectivity are observed. Usually, ground albedo is calculated for each time slot (quarter hourly) over a complete month. For this, it is assumed that the changes in solar elevations are small enough so that the influence of bidirectional reflectance remains negligible. However, solar elevation changes rapidly during Spring and Fall seasons and hence, calculating ground albedo over thirty days turn out to be inappropriate. To overcome this, ground albedo for Spring and Fall seasons was recalculated using shorter time periods. As North Africa has much less cloudy days than Europe, ten images (for Europe, it is usually thirty) turned out to be enough to find cloudless pixels to compute ground reference values for this region. This significantly improved the results, removing the mid-day dips that appeared in these seasons (Fig. 6.2). The improvements are checked

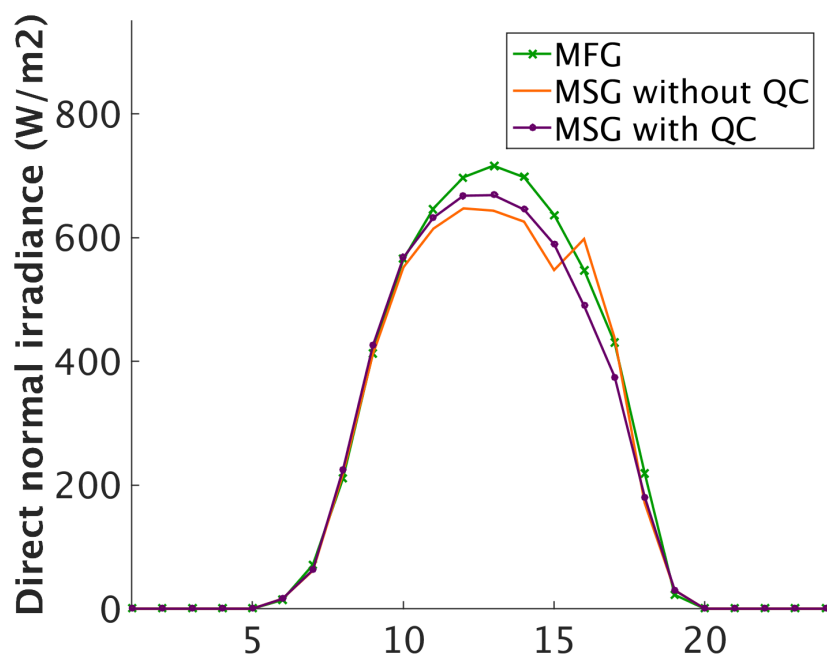
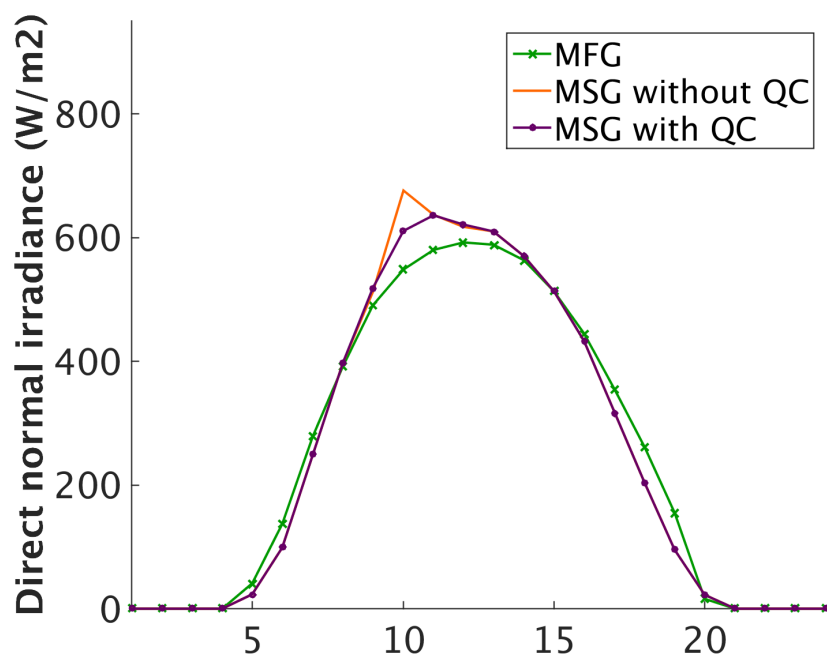
(a) 15<sup>th</sup> February, 2005(b) 13<sup>th</sup> May, 2005

Fig. 6.1: Improvement of DNI time series upon quality control.



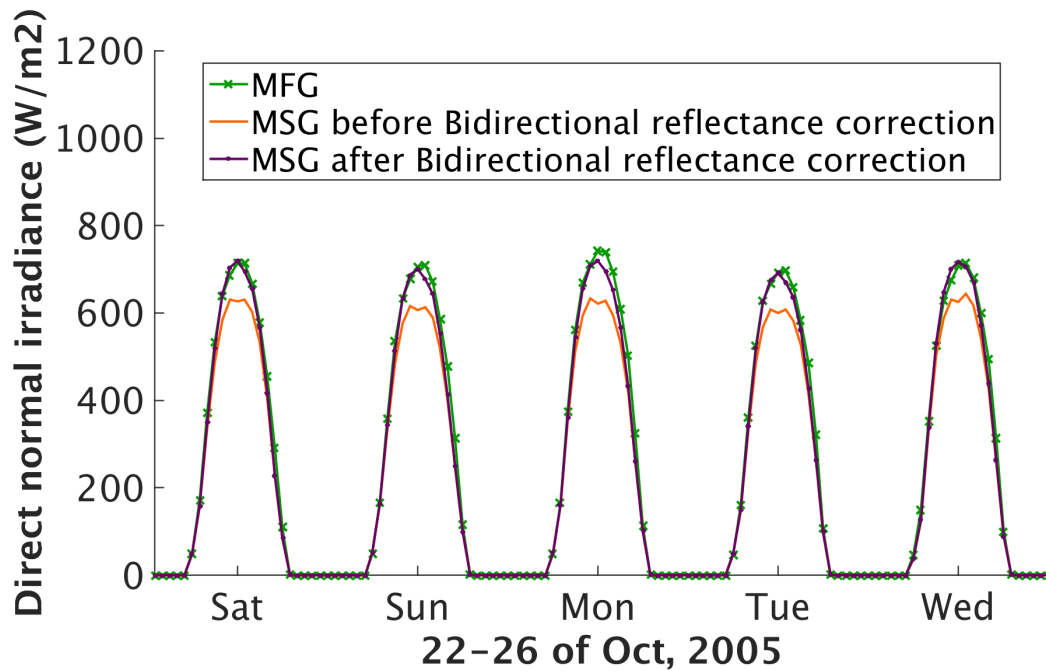


Fig. 6.2: Removing the effects of Bidirectional reflection shown for a few days in Fall.

against the solar irradiance retrieved from the MFG satellites during the overlapping year 2005 and are summarized in Table. 6.1.

Additional statistical comparison of the CSP time series from MFG satellites, preliminary and the revised MSG retrievals are given in Table. 6.2.

### 6.3 Impact of CSP import on European balancing needs

North Africa offers a vast potential of electricity production from CSP due to higher levels of solar irradiance throughout the year. Technically, this power generation potential far exceeds its local demand. Exporting the surplus electricity produced from CSP to Europe would open up new opportunities for economic and technical cooperation between these two regions and in turn, help Europe in its long term  $CO_2$  reduction targets. In fact, the opportunity of exporting electricity from CSP to Europe is one of the major drivers for CSP growth in North Africa. In the following section, the impact of CSP import on European balancing needs is discussed. No transmission loss is considered here.

The quantification of the balancing needs is derived from two existing studies [82, 67] mentioned in Sec. 6.1. Up on selecting the 33 countries including the Balkans, the chosen

	Bias	RMSE	RMSE <sub>rel</sub>	Correlation coefficient
Before removing effects of Bidirectional reflectance	-10.49	30.42	0.12	0.990
After removing effects of Bidirectional reflectance	-7.00	27.12	0.10	0.991

Table 6.1: Statistical measures of DNI time series of 2005 from MSG satellite against the same retrieved from MFG. For the correlation coefficient, the night time values are filtered out.

	Aggregated production (TWh)	Standard deviation (GW)	Capacity factor (%)
MFG	46.0	5.8	29.2
MSG before removing effects of Bidirectional reflectance	43.8	5.7	27.8
MSG after removing effects of Bidirectional reflectance	44.5	5.8	28.2

Table 6.2: Statistical measures of CSP time series of North Africa for 2005.

scenario of [82] gives PV and wind capacities of 612.3 and 523.7 GW, respectively for 2050 (here after called Scenario-1). Over the ten years of simulation, the total PV and wind power generated in this scenario are 8038.2 and 14094.7 TWh, respectively. The other scenario, designated as Scenario-2, is based on [67] and projects 339.4 and 831.0 GW of PV and wind capacities, respectively for Europe in 2050. The total power generation over the ten years of simulation in this scenario are 4455.7 and 20607.1 TWh for PV and wind, respectively. It is to be noted here that the two scenarios not only differ in solar and wind shares ( $\beta$  is 0.36 for Scenario-1 and 0.18 for Scenario-2), but also in the average renewable penetration to the power system ( $\alpha$  is 0.62 for Scenario-1 and 0.71 for Scenario-2). For both scenarios, the model is simulated with the same power demand.

### Characteristics of CSP in Europe and North Africa

It is to be noted that the characteristics of DNI, and by extension CSP, are quite different for Europe and North Africa. One general remark is that North Africa being much closer to the equator experiences less seasonal variations than Europe. Moreover, the sensitivity of DNI on clouds and aerosol particles makes the contrast even more prominent. A major part of the model domain North Africa encompasses the Sahara desert. Although the dust particles of the desert can disperse the incoming solar radiation, the lack of water bodies in this region strongly diminishes the chances of optically thick cloud formation. This, in turn, further aids in the performance of CSP plants. For the same installed capacity, lack of clouds over North Africa results in higher average power production from CSP (Table. 6.3), although there may be some losses due to the soiling effects caused by the dust storms in Sahara.

	'03	'04	'05	'06	'07	'08	'09	'10	'11	'12
Europe	23.4	23.6	24.3	23.1	23.6	23.1	23.3	21.8	23.9	24.9
N. Africa	29.2	28.7	27.8	27.5	28.6	27.9	28.2	27.7	28.4	28.6

Table 6.3: Annual CSP capacity factors (%) of Europe and North Africa for each simulated year.

#### 6.3.1 Balancing in absence of storage

In absence of any storage, all balancing needs are covered by backup from dispatchable resources. When no import is considered in the model, the balancing parameter ( $E_b$ ) computed from Scenario-1 equals 0.39 while the same from Scenario-2 is 0.32. It is discussed in Chapter. 5 that when no storage is present, the lack of sunlight at night becomes a dominating factor in determining balancing needs. As a result, Scenario-2 with lower solar share (and also slightly higher  $\alpha$ ) has lower balancing needs than Scenario-1. When all CSP produced in North Africa is transferred to Europe, the imported power covers  $\sim 5.7\%$  of European load in Scenario-1 and  $\sim 1.3\%$  load in Scenario-2. This CSP import reduces  $E_b$  by 9.6% in Scenario-1 and 3.2% in Scenario-2.

Next, it is assumed that only a certain fraction of the total CSP generated in North Africa is imported to Europe. This is a more realistic assumption given that North African power demand is projected to increase in future with its increasing population growth and a reasonable fraction of CSP must first be allowed to cover the

	CSP imported (%)	Load coverage (%)	$E_b$ before import	$E_b$ after import	$E_b$ reduction (%)
Scenario-1	20	1.13	0.392	0.384	2.11
Scenario-1	40	2.27	0.392	0.376	4.13
Scenario-1	60	3.40	0.392	0.368	6.05
Scenario-1	80	4.53	0.392	0.361	7.88
Scenario-1	100	5.66	0.392	0.354	9.61
Scenario-2	20	0.25	0.322	0.320	0.65
Scenario-2	40	0.50	0.322	0.318	1.30
Scenario-2	60	0.76	0.322	0.316	1.94
Scenario-2	80	1.01	0.322	0.314	2.58
Scenario-2	100	1.26	0.322	0.311	3.21

Table 6.4: A table summarizing the impact of CSP import from North Africa on European balancing needs in absence of any storage. The first column states the chosen scenario, the second column gives the percentage of total CSP that is imported to Europe. As CSP generation capacity is very different in the two scenarios, their respective shares on load coverage is also significantly different (column four), even for the same share of CSP import. The remaining columns show the changes in the balancing parameter due to CSP import.

local demand. For such cases, the impact of certain shares of CSP import on European balancing needs is summarized in Table. 6.4.

### 6.3.2 Balancing combined with storage

In this section, balancing needs are estimated in presence of a small (6 av.h.l.) storage. A simple dispatch strategy is applied here: Any positive mismatch is first put in the storage until it gets full while all negative mismatches are balanced by taking energy out of the storage until it runs empty. After this storage interaction, if any positive mismatch remains is simply discarded and all negative mismatches are balanced with the dispatchable backup generation.

It is discussed in Chapter. 5 that a small storage can significantly smoothen the day-night cycle of PV, and the balancing needs are determined from the annual course of power generation. The seasonal European load curve with maximum demand in winter and least in summer exhibits the opposite trend as the seasonal PV power. As a consequence, scenarios with higher solar shares would have increased balancing needs than wind-dominated scenarios. Scenario-1 with relatively higher solar share has  $E_b$  of

	CSP imported (%)	Load coverage (%)	$E_b$ before import	$E_b$ after import	$E_b$ reduction (%)
Scenario-1	20	1.13	0.643	0.628	2.43
Scenario-1	40	2.27	0.643	0.612	4.79
Scenario-1	60	3.40	0.643	0.598	7.10
Scenario-1	80	4.53	0.643	0.583	9.35
Scenario-1	100	5.66	0.643	0.569	11.53
Scenario-2	20	0.25	0.521	0.518	0.70
Scenario-2	40	0.50	0.521	0.514	1.41
Scenario-2	60	0.75	0.521	0.510	2.11
Scenario-2	80	1.01	0.521	0.507	2.80
Scenario-2	100	1.26	0.521	0.503	3.49

Table 6.5: A table summarizing the impact of CSP import from North Africa on European balancing needs in presence of a storage with efficiency ( $\eta_{in}=\eta_{out}=0.6$ ). For the detailed description of each column, please see the caption of Table. 6.4 that has the same structure as this one.

0.37 while that from Scenario-2 is 0.30, before any CSP import from North Africa. These values of  $E_b$  correspond to an ideal condition with no storage loss included. In such condition, importing all electricity generated from CSP in North Africa decreases the balancing need by 15.05% and 3.82% in Scenario-1 and Scenario-2, respectively. This large difference between the scenarios on their balancing reduction potential reflects from the fact that Scenario-1 allows a much higher CSP generation capacity than Scenario-2. A more realistic measure with certain storage losses ( $\eta_{in}=\eta_{out}=0.6$ ) is presented in Table. 6.5.

## 6.4 Summary

Importing concentrated solar power from North Africa can have significant influence on European balancing needs. In this chapter, this possibility is analyzed for two different scenarios with different shares of solar and wind. Considering no transmission losses, the scenario with high solar shares gives  $\sim 11.5\%$  balancing reduction in presence of a small hydrogen storage for full import of CSP generated in North Africa. For the scenario with low solar share, the reduction can be up to  $\sim 3.5\%$ . Even for a scheme with import of only 40% of total CSP generated in North Africa, almost 2.3% of the average European load can be covered in Scenario-1 with a balancing reduction of

~ 4.5%. This indicates that by carefully choosing the optimal share of solar and wind, and by further extending the grid to import CSP from North Africa, the balancing needs of Europe can be significantly reduced in future.

# Chapter 7

## Summary and conclusion

The investigation presented in this thesis spans over a wide range of possible scenarios of a future European power system with high shares of VRE generation. The baseline scenario is formulated with power generation from solar and wind, two of the most promising and technologically mature renewable sources, with any existing residual load being covered either by storage systems and/or backup supply from flexible resources. Quantifying these balancing needs in relation to the weather-dependent variable nature of the VRE sources is the primary aim of this work. Additionally, a substantial portion of this investigation is directed towards the understanding of the relative differences between different PV module configurations in terms of variability and balancing requirements.

In this work, wind power is derived from the numerical weather prediction (NWP) model while solar power is calculated from Meteosat satellite images as part of the project RESTORE 2050. Subsequently, this satellite-derived solar power is evaluated against the regionally averaged PV power data provided by the German TSOs. The results indicate that the agreement between simulated and upscaled measured data increases from the federal states to the control zones to that of the whole country. On the hourly scale, the RMSE of the normalized PV power decreases from 0.041 – 0.057 for the federal states to 0.030 – 0.045 for the control zones to 0.029 for the entire country. This does not exclusively result from the smoothing effect of spatial aggregation, rather it indicates on the quality of the measurement data and its sensitivity over smaller spatial coverage. The PV power data provided by the TSOs are not direct measurements, rather derived from a representative set of PV modules. Moreover, these data are often provided without any internal validation. There are several other factors that can impede good agreement between simulated and measured upscaled data. These include the assumption of linear increase of capacity, the issues of incoherent

spatial coverage, unidentified postal codes, corrections for snow covered modules etc. In spite of all these factors, the comparison indicates overall good agreement not only on the seasonal scale, but also on the diurnal patterns with different sky conditions.

After gaining confidence on the quality of the PV power data, the next step is to proceed to the computation of balancing needs for different shares of PV and wind, and for different module configurations. Since different configurations have different power generation potential, their installed capacities are adjusted to ensure they have the same gross power output over the complete simulation period. This equalization helps to avoid any misinterpretation of increased (or decreased) balancing need as a consequence of low (or high) power generation and allows to investigate several other factors that might influence the balancing needs as well. One such factor is the mix of solar and wind power generation. The investigation presented in this thesis indicates that a favorable choice of module configuration with respect to balancing reduction is very sensitive to the shares of PV and wind. For high solar shares, highly inclined modules with a less pronounced annual course are favorable, if a storage with a capacity to cover at least 6 hours of average hourly load (6 hour storage) is available to compensate for the day-night cycle of PV. In a wind-dominated scenario, lowly inclined East/West facing modules are most suitable to reduce balancing needs. In absence of storage, a combination of highly inclined East and West facing modules reduces balancing needs as long as the solar share is high enough to distinguish between the contributions from different module configurations.

Another important factor that determines the balancing needs is the average VRE generation factor ( $\alpha$ ). It is shown in this thesis that the balancing needs can be significant even when generation on an average exceeds power demand (scenario  $\alpha > 1$ ) since it is unlikely that generation from weather-dependent resources can be sufficient at all times. In a ‘storage only’ scenario, storage capacity  $C_s$  can be reduced  $\sim 52\%$  for  $\beta$  of 0.6 by orienting optimally inclined West facing modules to South at  $\alpha = 0.92$  and  $\sim 74\%$  by changing optimal- $25^\circ$  to optimal+ $25^\circ$  at  $\alpha = 0.93$ . This is a very large reduction of potential, and can be of immense value given the high prices of storage systems.

The optimal mix of solar and wind power in terms of minimum balancing needs is also investigated in this thesis. In absence of any storage,  $\beta_{opt}$  values appear around 0.2. However, storages of  $\sim 6$  av.h.l. can largely smoothen the day-night cycle of PV, thereby raising the  $\beta_{opt}$  values to 0.4 in presence of such a storage. The  $\beta_{opt}$  values are more sensitive to module orientations than module inclinations. Depending on



---

$\alpha$ ,  $\beta_{opt}$  varies between 0.20-0.40 for lowly inclined West facing modules and between 0.30-0.65 for highly inclined South facing ones.

Another balancing option investigated in this work is the grid extension to North Africa to import CSP to Europe. The focus is made on how much the balancing needs are reduced up on importing a certain fraction of CSP generated in North Africa. Two scenarios are analyzed here, one with high (81 GW) and the other with relatively low (18 GW) CSP installed capacity of North Africa. Considering no transmission losses, the first scenario gives  $\sim 9.6\%$  and  $\sim 11.5\%$  reduction in balancing needs in cases of 100% CSP import in absence and in presence of a hydrogen storage, respectively. For the other scenario, the corresponding values are  $\sim 3.2\%$  and  $\sim 3.5\%$ , respectively. As it is more likely that of the total amount of CSP generated in North Africa, a certain fraction will first be used to meet local power demand and the rest to be imported to Europe, such possibilities with varied fraction of power import are also simulated and summarized in Tables. 6.4 and 6.5.

The entire analysis gives an insight into the impact of different module configurations on balancing needs and how this may change for varying values of  $\alpha$  and  $\beta$ . The model encompasses a number of scenarios for a possible future European power system with high shares of renewables. Needless to say, there is always scope of improvement. In this work, the model is based on an assumption of unlimited transmission between neighboring countries. In future, a more realistic power transmission grid is planned to be implemented in the model. Other renewable sources, such as hydro, can also be included alongside PV and wind. More balancing options, like DSM, can also be quantified in the model. So far, the economic aspects are not explicitly investigated in this work. In future, an investigation is planned to study the effect of renewable excess generation on levelized cost of electricity. With increasing penetration of VRE in the power system, it becomes more important to pick the correct solar and wind mix, not only with respect to installation costs, but also for the technical considerations, such as minimizing curtailment or balancing needs, in order to reduce final system costs. These tasks are planned to be implemented soon in the near future to further improve the results for a more realistic future European power system.



# References

- [1] 50hertz Transmission GmbH. EEG-Anlagendaten. <http://www.50hertz.com/de/EEG/Veroeffentlichung-EEG-Daten/EEG-Anlagenstammdaten>. Online; accessed: November-2013.
- [2] www.amprion.net. Aktuelle EEG-Anlagendaten. <http://www.amprion.net/eeg-anlagenstammdaten-aktuell>. Online; accessed: November-2013.
- [3] PLZ Postleitzahl. <http://www.plz-postleitzahl.com/de/>. [Online; accessed 27-September-2015].
- [4] Tennet. Einspeisung und Anlagenregister. <http://www.tennet.eu/de/kunden/eegkwkg/erneuerbare-energien-gesetz/eeg-daten-nach-52/einspeisung-und-anlagenregister.html>. Online; accessed: November-2013.
- [5] Transnetbw. EEG-Anlagendaten. <https://www.transnetbw.de/de/eeg-kwkg/eeg/eeg-anlagendaten>. Online; accessed: November-2013.
- [6] Desertec. <http://www.desertec.org>, 2009. [Online; accessed 10-March-2017].
- [7] Flexibility requirements and metrics for variable generation: Implications for system planning studies. Technical report, NERC, Princeton, August 2010.
- [8] Hydro in Europe: Powering renewables. Technical report, Eurelectric - Union of the electricity industry, 2011.
- [9] Medgrid. <http://www.medgrid-psm.com>, 2011. [Online; accessed 10-March-2017].
- [10] Bundesnetzagentur: EEG-Statistikbericht, 2011. Technical report, August 2013. URL [https://www.bundesnetzagentur.de/SharedDocs/Downloads/DE/Sachgebiete/Energie/Unternehmen\\_Institutionen/ErneuerbareEnergien/ZahlenDatenInformationen/StatistikberichtEEG2011pdf.pdf?\\_\\_blob=publicationFile&v=1](https://www.bundesnetzagentur.de/SharedDocs/Downloads/DE/Sachgebiete/Energie/Unternehmen_Institutionen/ErneuerbareEnergien/ZahlenDatenInformationen/StatistikberichtEEG2011pdf.pdf?__blob=publicationFile&v=1). [Online; accessed 13-January-2017].
- [11] Regenerative Stromversorgung und Speicherbedarf in 2050. Technical Report 03SFF0439A, Fortschrittsbericht des BMBF-Forschungsvorhabens, 2014. URL [http://forschung-energiespeicher.info/fileadmin/user\\_upload/projektassets/RESTORE\\_2050/RESTORE2050-Jahresbericht\\_No2.pdf](http://forschung-energiespeicher.info/fileadmin/user_upload/projektassets/RESTORE_2050/RESTORE2050-Jahresbericht_No2.pdf).
- [12] Bundesnetzagentur: EEG-Statistikbericht, 2012. Technical report, July 2015. URL [www.bundesnetzagentur.de/SharedDocs/Downloads/DE/Sachgebiete/Energie/Unternehmen\\_Institutionen/ErneuerbareEnergien/ZahlenDatenInformationen/](http://www.bundesnetzagentur.de/SharedDocs/Downloads/DE/Sachgebiete/Energie/Unternehmen_Institutionen/ErneuerbareEnergien/ZahlenDatenInformationen/)

- EEGinZahlen\_2012.xls?\_\_blob=publicationFile&v=2. [Online; accessed 13-January-2017].
- [13] M.H. Albadi and E.F. El-Saadany. Overview of wind power intermittency impacts on power systems. *Electric Power Systems Research*, 80:627 – 632, 2010.
- [14] M. Asari, T. Nanahara, T. Maejima, K. Yamaguchi, and T. Sato. A study on smoothing effect on output fluctuation of distributed wind power generation. In *IEEE/PES Transmission and Distribution Conference and Exhibition*, pages 938–943, Oct 2002. doi: 10.1109/TDC.2002.1177602.
- [15] O. Bartholomy, T. Vargas, M. Simone, C. Hansen, S. Fitchett, and A. Pohl. Benchmarking solar power and irradiance forecasting accuracy at Sacramento municipal utility district. In *2014 IEEE 40th Photovoltaic Specialist Conference (PVSC)*, pages 0063–0068, June 2014. doi: 10.1109/PVSC.2014.6925196.
- [16] S. Becker, R.A. Rodriguez, G.B. Andresen, S. Schramm, and M. Greiner. Transmission grid extensions during the build-up of a fully renewable pan-European electricity supply. *Energy*, 64:404 – 418, 2014.
- [17] H. G. Beyer, C. Costanzo, and D. Heinemann. Modifications of the Heliosat procedure for irradiance estimates from satellite images. *Solar Energy*, 56:207 – 212, 1996.
- [18] J. Bing, O. Bartholomy, and P. Krishnani. Validation of solar PV power forecasting methods for high penetration grid integration. In *2012 IEEE Power and Energy Society General Meeting*, pages 1–6, July 2012. doi: 10.1109/PESGM.2012.6345562.
- [19] C. Biyun, W. Suifeng, Z. Yongjun, and H. Ping. Wind power prediction model considering smoothing effects. In *2013 IEEE PES Asia-Pacific Power and Energy Engineering Conference (APPEEC)*, pages 1–4, Dec 2013. doi: 10.1109/APPEEC.2013.6837186.
- [20] Tom Brown, David Schlachtberger, Alexander Kies, and Martin Greiner. Sector coupling in a highly renewable European energy system. In *15th Wind Integration Workshop*, 2017.
- [21] Prof. Dr. Bruno Burger. Fraunhofer institute for solar energy systems ISE: Electricity production from solar and wind in Germany in 2012, February 08, 2013. [Online; accessed 08-June-2016].
- [22] S. Chatzivasileiadis, D. Ernst, and G. Andersson. The global grid. *Renewable Energy*, 57:372 – 383, 2013.
- [23] B. Dudley. BP Statistical review of world energy. <https://www.bp.com/content/dam/bp/pdf/energy-economics/statistical-review-2016/bp-statistical-review-of-world-energy-2016-full-report.pdf>, June 2016.
- [24] D. Dumortier. The Satelight model of turbidity variations in Europe. Technical report, Ecole Nationale des Travaux Publics de l’Etat, Vaulx-en-Velin, France, sixth SATELLIGHT meeting, September 1998.

- [25] F. Trieb et al. Trans-mediterranean interconnection for concentrating solar power. Technical report, June 2006. URL <http://www.dlr.de/tt/trans-csp/>.
- [26] D. Founda, D. Melas, S. Lykoudis, I. Lisaridis, E. Gerasopoulos, G. Kouvarakis, M. Petrakis, and C. Zerefos. The effect of the total solar eclipse of 29 march 2006 on meteorological variables in greece. *Atmospheric Chemistry and Physics*, 7(21): 5543 – 5553, 2007.
- [27] B. François, B. Hingray, D. Raynaud, M. Borga, and J.D. Creutin. Increasing climate-related-energy penetration by integrating run-of-the river hydropower to wind/solar mix. *Renewable Energy*, 87, Part 1:686 – 696, 2016.
- [28] M. Fuersch, S. Hagspiel, C. Jägemann, S. Nagl, D. Lindenberger, L. Glotzbach, E. Tröster, and T. Ackermann. Roadmap 2050 - a closer look: Cost-efficient RES-E penetration and the role of grid extensions. Technical report, EWI, Energynautics, October 2011.
- [29] S. Gottwalt, W. Ketter, C. Block, J. Collins, and C. Weinhardt. Demand side management—a simulation of household behavior under variable prices. *Energy Policy*, 39:8163 – 8174, 2011.
- [30] I. Graabak and M. Korpås. Variability characteristics of European wind and solar power resources—a review. *Energies*, 9:449, 2016.
- [31] C. A. Gueymard. Temporal variability in direct and global irradiance at various time scales as affected by aerosols. *Solar Energy*, 86:3544 – 3553, 2012.
- [32] A. Hammer, D. Heinemann, C. Hoyer, R. Kuhlemann, E. Lorenz, R. Müller, and H. G. Beyer. Solar energy assessment using remote sensing technologies. *Remote Sensing of Environment*, 86:423 – 432, 2003.
- [33] D. Heide, L. von Bremen, M. Greiner, C. Hoffmann, M. Speckmann, and S. Bofinger. Seasonal optimal mix of wind and solar power in a future, highly renewable Europe. *Renewable Energy*, 35:2483 – 2489, 2010.
- [34] D. Heide, M. Greiner, L. von Bremen, and C. Hoffmann. Reduced storage and balancing needs in a fully renewable European power system with excess wind and solar power generation. *Renewable Energy*, 36:2515 – 2523, 2011.
- [35] A. M. Held. *Modelling the future development of renewable energy technologies in the European electricity sector using agent-based simulation*. PhD thesis, Karlsruhe Institute for Technology (KIT), Karlsruhe, Germany, 2010.
- [36] L. Hirth and S. Müller. System-friendly wind and solar power. IEWT conference, 2015.
- [37] L. Hirth and S. Müller. System-friendly wind power: How advanced wind turbine design can increase the economic value of electricity generated through wind power. *Energy Economics*, 56:51 – 63, 2016.
- [38] M. Huber, D. Dimkova, and T. Hamacher. Integration of wind and solar power in Europe: Assessment of flexibility requirements. *Energy*, 69:236 – 246, 2014.

- [39] T. Huld, R. Gottschalg, H. G. Beyer, and M. Topič. Mapping the performance of PV modules, effects of module type and data averaging. *Solar Energy*, 84:324 – 338, 2010.
- [40] M. Z. Jacobson and M. A. Delucchi. Providing all global energy with wind, water, and solar power, part i: Technologies, energy resources, quantities and areas of infrastructure, and materials. *Energy Policy*, 39:1154 – 1169, 2011.
- [41] D. Kearney and H. Price. Recent advances in parabolic trough solar power plant technology. 2004.
- [42] A. Kies, K. Nag, L. von Bremen, E. Lorenz, and D. Heinemann. Investigation of balancing effects in long term renewable energy feed-in with respect to the transmission grid. *Advances in Science and Research*, 12:91–95, 2015.
- [43] A. Kies, K. Chattopadhyay, E. Lorenz, L. von Bremen, and D. Heinemann. RESTORE 2050 work package report D12: Simulation of renewable feed-in for power system studies. Technical report, Institute of Physics, University of Oldenburg, April 2016.
- [44] A. Kies, B. U. Schyska, and L. von Bremen. The demand side management potential to balance a highly renewable European power system. *Energies*, 9(11), 2016.
- [45] A. Kies, B. U. Schyska, and L. von Bremen. The optimal share of wave power in a highly renewable power system on the Iberian Peninsula. *Energy Reports*, 2:221 – 228, 2016.
- [46] K. Kikuchi and T. Nanahara. Study on smoothing effects of pv outputs—method with autocorrelation function. In *2014 49th International Universities Power Engineering Conference (UPEC)*, pages 1–5, Sept 2014. doi: 10.1109/UPEC.2014.6934659.
- [47] T.M. Klucher. Evaluation of models to predict insolation on tilted surfaces. *Solar Energy*, 23:111–114, 1979.
- [48] J. Kühnert. *Development of a photovoltaic power prediction system for forecast horizons of several hours*. PhD thesis, Fakultät für Mathematik und Naturwissenschaften der Carl von Ossietzky Universität, Oldenburg, 2016.
- [49] E. Lannoye, D. Flynn, and M. O’Malley. Power system flexibility assessment - state of the art. In *2012 IEEE Power and Energy Society General Meeting*, pages 1–6, July 2012.
- [50] F. Li, W. Qiao, H. Sun, H. Wan, J. Wang, Y. Xia, Z. Xu, and P. Zhang. Smart transmission grid: Vision and framework. *IEEE Transactions on Smart Grid*, 1(2):168–177, Sept 2010.
- [51] C. Linnemann, D. Echternacht, C. Breuer, and A. Moser. Modeling optimal redispatch for the European transmission grid. In *2011 IEEE Trondheim PowerTech*, pages 1–8, June 2011.

- [52] W. Lise, J. van der Laan, F. Nieuwenhout, and K. Rademaekers. Assessment of the required share for a stable EU electricity supply until 2050. *Energy Policy*, 59:904 – 913, 2013.
- [53] E. Lorenz, J. Remund, S.C. Müller, W. Traunmüller, G. Steinmaurer, D. Pozo, J.A. Ruiz-Arias, V.L. Fanego, L. Ramirez, M.G. Romeo, C. Kurz, L.M. Pomares, and C.G. Guerrero. Benchmarking of different approaches to forecast solar irradiance. 2009.
- [54] E. Lorenz, T. Scheidsteger, J. Hurka, D. Heinemann, and C. Kurz. Regional PV power prediction for improved grid integration. *Progress in Photovoltaics: Research and Applications*, 19:757 – 771, 2011.
- [55] H. Lund. Large-scale integration of optimal combinations of PV, wind and wave power into the electricity supply. *Renewable Energy*, 31:503 – 515, 2006.
- [56] J. Ma, V. Silva, R. Belhomme, D. S. Kirschen, and L. F. Ochoa. Evaluating and planning flexibility in sustainable power systems. *IEEE Transactions on Sustainable Energy*, 4:200–209, Jan 2013.
- [57] H. Mangesius, S. Hirche, M. Huber, and T. Hamacher. A framework to quantify technical flexibility in power systems based on reliability certificates. In *IEEE PES ISGT Europe 2013*, pages 1–5, Oct 2013.
- [58] D. Mateos, M. Antón, A. Valenzuela, A. Cazorla, F. Olmo, and L. Alados-Arboledas. Short-wave radiative forcing at the surface for cloudy systems at a midlatitude site. *Tellus B*, 65, 2013.
- [59] P. S. Moura and A. T. De Almeida. The role of demand-side management in the grid integration of wind power. *Applied Energy*, 87:2581 – 2588, 2010.
- [60] R.W. Mueller, K.F. Dagestad, P. Ineichen, M. Schroedter-Homscheidt, S. Cros, D. Dumortier, R. Kuhlemann, J.A. Olseth, G. Piernavieja, C. Reise, L. Wald, and D. Heinemann. Rethinking satellite-based solar irradiance modelling: The SOLIS clear-sky module. *Remote Sensing of Environment*, 91:160 – 174, 2004.
- [61] E. M. Natsheh and A. Albarbar. Solar power plant performance evaluation: simulation and experimental validation. *Journal of Physics: Conference Series*, 364:012122, 2012.
- [62] R. L. Nersesian. *Energy Economics: Markets, History and Policy*. Routledge; 1 edition, 2016.
- [63] T. S. Nielsen, H. Nielsen, H. Madsen, P. Pinson, G. Kariniotakis, N. Siebert, I. Marti, M. Lange, U. Focken, L. von Bremen, P. Louka, G. Kallos, and G. Galanis. *Advanced statistical modeling and uncertainty assessment for wind power forecasting*. 2006.
- [64] G. Notton, V. Lazarov, and L. Stoyanov. Optimal sizing of a grid-connected PV system for various PV module technologies and inclinations, inverter efficiency characteristics and locations. *Renewable Energy*, 35:541 – 554, 2010.

- [65] T. Oozeki, K. Otani, T. Takashima, Y. Hishikawa, G. Koshimizu, Y. Uchida, and K. Ogimoto. An evaluation method for smoothing effect on photovoltaic systems dispersed in a large area, June 2009.
- [66] A. A. Pérez and T. Vogt. Life cycle assessment of conversion processes for the large-scale underground storage of electricity from renewables in Europe. In *European Physical Journal Web of Conferences*, volume 79 of *European Physical Journal Web of Conferences*, page 03006, Dec 2014.
- [67] B. Pfluger, F. Sensfuß, G. Schubert, and J. Leisentritt. Tangible ways towards climate protection in the European Union (EU long-term scenarios 2050). Technical report, Karlsruhe, September 2011.
- [68] G. Pleßmann, M. Erdmann, M. Hlusiak, and C. Breyer. Global energy storage demand for a 100% renewable electricity supply. *Energy Procedia*, 46:22 – 31, 2014.
- [69] M. G. Rasmussen, G. B. Andresen, and M. Greiner. Storage and balancing synergies in a fully or highly renewable pan-European power system. *Energy Policy*, 51:642 – 651, 2012.
- [70] E. Raviv, K. E. Bouwman, and D. van Dijk. Forecasting day-ahead electricity prices: Utilizing hourly prices. *Energy Economics*, 50:227 – 239, 2015.
- [71] J. Remund and D. Domeisen. Aerosol optical depth and linke turbidity climatology: Description for final report of IEA SHC task 36. Technical report, Solar heating and cooling programme, International Energy Agency, Meteotest, Bern, 2010.
- [72] M. M. Rienecker, M. J. Suarez, R. Gelaro, R. Todling, J. Bacmeister, E. Liu, M. G. Bosilovich, S. D. Schubert, L. Takacs, G. Kim, et al. MERRA: NASA’s modern-era retrospective analysis for research and applications. *Journal of Climate*, 24: 3624–3648, 2011.
- [73] A. Mills et. al. Understanding variability and uncertainty of photovoltaics for integration with the electric power system. <http://escholarship.org/uc/item/58z9s527>, 2010.
- [74] R. A. Rodríguez, S. Becker, G. B. Andresen, D. Heide, and M. Greiner. Transmission needs across a fully renewable European power system. *Renewable Energy*, 63:467 – 476, 2014.
- [75] J. A. Ruiz-Arias, J. Dudhia, C. A. Gueymard, and D. Pozo-Vázquez. Assessment of the level-3 MODIS daily aerosol optical depth in the context of surface solar radiation and numerical weather modeling. *Atmospheric Chemistry and Physics*, 13:675–692, 2013.
- [76] J. A. Ruiz-Arias, J. Dudhia, F. J. Santos-Alamillos, and D. Pozo-Vázquez. Surface clear-sky shortwave radiative closure intercomparisons in the weather research and forecasting model. *Journal of geophysical research: Atmospheres*, 118:9901–9913, 2013.



- [77] K. Schaber, F. Steinke, and T. Hamacher. Transmission grid extensions for the integration of variable renewable energies in Europe: Who benefits where? *Energy Policy*, 43:123 – 135, 2012.
- [78] K. Schaber, F. Steinke, P. Mühlich, and T. Hamacher. Parametric study of variable renewable energy integration in Europe: Advantages and costs of transmission grid extensions. *Energy Policy*, 42:498 – 508, 2012.
- [79] D.P. Schlachtberger, S. Becker, S. Schramm, and M. Greiner. Backup flexibility classes in emerging large-scale renewable electricity systems. *Energy Conversion and Management*, 125:336 – 346, 2016.
- [80] S. Shafiee and E. Topal. When will fossil fuel reserves be diminished? *Energy Policy*, 37:181 – 189, 2009.
- [81] M. Suri, T. Huld, E. Dunlop, M. Albuissou, M. Lefèvre, and L. Wald. Uncertainties in solar electricity yield prediction from fluctuation of solar radiation. In *22nd European Photovoltaic Solar Energy Conference, Milan, Italy*, Sep 2007.
- [82] Sven Teske. Energy [r]evolution - a sustainable EU 27 energy outlook. Technical report, EREC, October 2012.
- [83] Dr. Franz Trieb. Concentrating solar power for the Mediterranean region, final report. Technical report, German Aerospace Center (DLR), April 2005.
- [84] E. Tröster and J.D. Schmidt. Evaluating the impact of PV module orientation on grid operation. 2nd International Workshop on Integration of Solar Power into Power Systems, Lisbon, Portugal, 2012.
- [85] A. Ulbig and G. Andersson. On operational flexibility in power systems. In *2012 IEEE Power and Energy Society General Meeting*, pages 1–8, July 2012.
- [86] M. Šuri, T. A. Huld, E. D. Dunlop, and H. A. Ossenbrink. Potential of solar electricity generation in the European Union member states and candidate countries. *Solar Energy*, 81:1295 – 1305, 2007.
- [87] M.J. Wagner and P. Gilman. Technical manual for the SAM physical trough model. Technical report, NREL/TP-5500-51825, 1617 Cole Boulevard Golden, Colorado 80401, June 2011.
- [88] S. Weitemeyer, D. Kleinhans, T. Vogt, and C. Agert. Integration of renewable energy sources in future power systems: The role of storage. *Renewable Energy*, 75:14 – 20, 2015.
- [89] P. L. Wevita, R. Matsushashi, and T. Yoshioka. Smoothing effect of distributed wind farms and its impact on output fluctuation. In *2013 International Conference on Renewable Energy Research and Applications (ICRERA)*, pages 938–943, Oct 2013. doi: 10.1109/ICRERA.2013.6749886.

- 
- [90] J. Widèn, N. Carpman, V. Castellucci, D. Lingfors, J. Olauson, F. Remouit, M. Bergkvist, M. Grabbe, and R. Waters. Variability assessment and forecasting of renewables: A review for solar, wind, wave and tidal resources. *Renewable and Sustainable Energy Reviews*, 44:356 – 375, 2015.
- [91] Wikipedia. List of solar thermal power stations — Wikipedia, the free Encyclopedia, 2015. URL [https://en.wikipedia.org/wiki/List\\_of\\_solar\\_thermal\\_power\\_stations](https://en.wikipedia.org/wiki/List_of_solar_thermal_power_stations). [Online; accessed 19-July-2015].
- [92] H. Wirth. Recent facts about photovoltaics in Germany. Technical report, Fraunhofer ISE, 2016.
- [93] A. Zani, G. Migliavacca, and A. Grassi. A scenario analysis for an optimal RES integration into the european transmission grid up to 2050. In *2011 8th International Conference on the European Energy Market (EEM)*, pages 401–406, May 2011. doi: 10.1109/EEM.2011.5953045.
- [94] Y. Zhang and S.J. Smith. Long-term modeling of solar energy: analysis of concentrating solar power (CSP) and PV technologies. Technical report, Pacific Northwest, National Laboratory, August 2008.
- [95] A. Zipp. Revenue prospects of photovoltaic in Germany- influence opportunities by variation of the plant orientation. *Energy Policy*, 81:86 – 97, 2015.

# Appendix A

## Overview of simulated European countries

The research work presented in this thesis encompasses a 33 European countries. The projected installed capacities of different solar and wind technologies substantially differ from one country to another. These differences result from the availability of resources, projected economic development, and on public interests. Existing studies for a future pan-European power system with high shares of renewables have accounted for such issues and provided possible installed capacities for each country [67]. Other studies, such as the Greenpeace report of 2012 [82] projects installed capacities cumulated to Europe, instead of individual country. In this thesis, the share of projected capacities of each country is maintained from the Scenario-B of [67]. Table. A.1 summarizes the names of all the countries simulated here along with their capacity factors for different technologies computed over 2003-2012.

Countries	ISO	Optimal angle	PV	CSP	Onshore wind	Offshore wind
Austria	AT	38	0.14	-	0.11	-
Belgium	BE	32	0.12	-	0.27	0.43
Bulgaria	BG	30	0.15	-	0.09	0.22
Bosnia & Herzegovina	BS	35	0.15	-	0.09	-
Switzerland	CH	37	0.15	-	0.07	-
Czech Republic	CZ	34	0.13	-	0.17	-
Germany	DE	34	0.12	-	0.25	0.45
Denmark	DK	38	-	-	0.38	0.45
Estonia	EE	40	-	-	0.26	0.38
Spain	ES	32	0.18	0.24	0.14	0.28
Finland	FI	46	-	-	0.24	0.39
France	FR	35	0.15	-	0.23	0.37
United Kingdom	GB	38	0.11	-	0.36	0.47
Greece	GR	28	0.17	0.23	0.07	0.23
Croatia	HR	33	0.15	-	0.12	-
Hungary	HU	36	0.14	-	0.14	-
Ireland	IE	38	-	-	0.40	0.39
Italy	IT	32	0.17	0.23	0.12	0.22
Kosovo	XK <sup>a</sup>	32	0.15	-	0.06	-
Lithuania	LT	38	0.11	-	0.27	0.40
Luxembourg	LU	33	0.12	-	0.21	-
Latvia	LV	39	0.11	-	0.27	0.39
Montenegro	ME	35	0.16	-	0.08	-
Republic of Macedonia	MK	31	0.16	-	0.05	-
Netherlands	NL	37	0.12	-	0.35	0.46
Norway	NO	42	0.09	-	0.13	0.47
Poland	PL	36	0.12	-	0.23	0.40
Portugal	PT	30	0.18	-	0.16	0.28
Romania	RO	35	0.14	-	0.05	0.23
Serbia	RS	32	0.14	-	0.10	-
Sweden	SE	45	-	-	0.22	0.34
Slovenia	SI	34	0.14	-	0.08	-
Slovakia	SK	37	0.13	-	0.14	-

<sup>a</sup> Kosovo is *not* listed as an ISO standard country. This unofficial code is used by the European Commission and others until Kosovo is assigned an ISO code.

Table A.1: List of capacity factors calculated over ten years (2003-2012) for each country simulated in this work. Additionally, the chosen optimal angle of PV module inclination to maximize average annual yield is included here. These angles are taken from Fig. 2.3 according to [86].

# Appendix B

## Additional investigation for PV modules with different configurations

The choice of orientation and inclination of PV modules can strongly influence their power production. Configurations of PV modules not only affect the gross output, but the variabilities on diurnal and seasonal scales can also be very different. As a consequence, changing PV module configurations can play important role in determining the balancing needs. One of the major goals of this work is to compare and analyze PV power production from modules with different configurations and to estimate their impact on storage and other balancing needs. Hence, a total of 55 (11 inclinations  $\times$  5 orientations) module configurations have been analyzed here (see Table B.1). It is to be noted that for all these configurations, the PV power is first computed at each model grid point and then aggregated together to Europe. Also, the optimal angles of inclination are different for each country and their values are taken from the work of Suri et al. [86]. They have deduced the optimal angles of inclination for South facing modules to maximize the average annual yield.

In order to avoid changes in PV and wind shares due to the use of modules with different configurations, their capacities are adjusted such that the average power production from all of these configurations are the same over the entire simulation period. The effect of capacity adjustment is shown in Fig. B.1. This adjustment is carried out by comparing PV power from each module configuration with a time series created with a realistic mix of different configurations shown in Table. 2.1. Since this reference time series combines a high ( $\geq 50\%$ ) shares of South facing optimally inclined (SFOI) modules, they need the least adjustment in capacity for leveled productivity

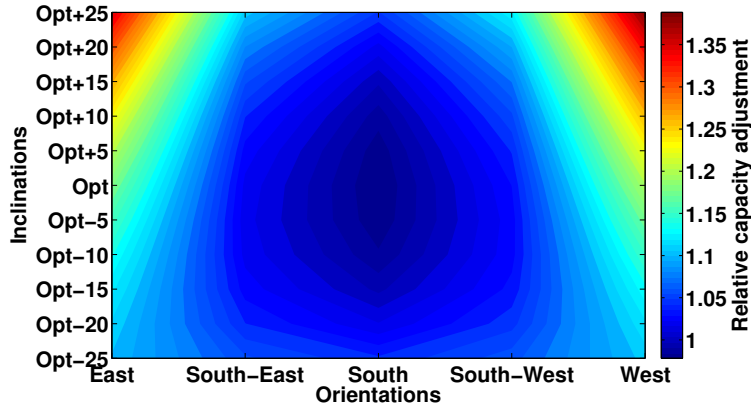


Fig. B.1: PV installed capacity adjustment with respect to a reference time series for different PV module configurations to have equal average yield.

and the degree of adjustment increases gradually towards highly inclined East and/or West facing modules (Fig. B.1). For South facing modules, change in module inclination does not require significant adjustment in the capacity (4.4% for South facing optimal-25° inclined and 5.0% for South facing optimal+25° inclined modules). For optimally inclined modules, East and West facing modules need comparatively higher capacity increase (18.1% for East facing optimally inclined modules and 20.2% for West facing optimally inclined modules). The highest capacity adjustments are required for highly inclined East and West facing modules (35.2% for East facing optimal+25° inclined and 38.8% for West facing optimal+25° inclined modules).

parameters	configurations
inclinations	opt±25°
	opt±20°
	opt±15°
	opt±10°
	opt±5°
	optimal
orientations	East
	South-East
	South
	South-West
	West

Table B.1: A list of module configurations analyzed in this work

# Appendix C

## Statistical error measures

Statistical error measures can give a quantitative description of the accuracy of the simulation results. In this thesis, a few measures of accuracy is applied that are considered most relevant for the intended application. In Chap. 3, the regionally averaged PV power data is evaluated against measurements. However, it is also possible to evaluate the model results against some other pre-validated or standardized data base. In Chap. 6, DNI time series from MFG satellite is used as a standard to evaluate the same from MSG satellite, to quantify the improvement achieved by removing the effects of bidirectional reflectance. Hence, in the context of this thesis, the term ‘reference’ time series is more appropriate than ‘measurement’ while discussing statistical error measures.

For the evaluation of solar and wind power, it is a common practice to use RMSE as the primary error measure [54, 63]. Following this convention, the RMSE of the simulation ( $X_s$ ) and the reference ( $X_r$ ) time series is used here as:

$$\text{RMSE} = \sqrt{\frac{1}{N} \sum_{i=1}^N (X_{s,i} - X_{r,i})^2} \quad (\text{C.1})$$

where  $N$  is the number of evaluated data pair. Another quantity,  $\text{RMSE}_{\text{rel}}$  is used in this work, which is the RMSE normalized to the mean of the reference time series:

$$\text{RMSE}_{\text{rel}} = \frac{\text{RMSE}}{\langle X_r \rangle} \quad (\text{C.2})$$

The RMSE can be further split into two components, related to the systematic and statistical errors. The Bias describes the difference between the mean values of simulated and reference values and correspond to the systematic part of the error:

$$\text{Bias} = \frac{1}{N} \sum_{i=1}^N (X_{s,i} - X_{r,i})^2 \quad (\text{C.3})$$

For the statistical part, the standard deviation of the error gives information on the fluctuation of the error around the mean value. Defining the error as:

$$\varepsilon_i = X_{s,i} - X_{r,i} \quad (\text{C.4})$$

the standard deviation of the error (STDERR) is given by:

$$\text{STDERR} = \sqrt{\frac{1}{N} \sum_{i=1}^N (\varepsilon_i - \langle \varepsilon \rangle)^2} \quad (\text{C.5})$$

The error measures are related to each other by:

$$\text{RMSE}^2 = \text{Bias}^2 + \text{STDERR}^2 \quad (\text{C.6})$$

Another important measure is the correlation coefficient. It is used to estimate how closely the simulation results follow the reference time series:

$$\text{Correlation coefficient} = \frac{\sum_{i=1}^N (X_{s,i} - \langle X_s \rangle)(X_{r,i} - \langle X_r \rangle)}{\sqrt{\sum_{i=1}^N (X_{s,i} - \langle X_s \rangle)^2 \sum_{i=1}^N (X_{r,i} - \langle X_r \rangle)^2}} \quad (\text{C.7})$$

All these measures together provide excellent measures on the accuracy of the simulated data base.